THÈSE

Pour obtenir le grade de

Docteur

Delivered by **UNIVERSITE de MONTPELLIER**
and **POTSDAM UNIVERSITY**

Prepared in the doctoral school of **ED 459**
and the **Institute of Chemistry - University of Potsdam**.

In the researcher units of **CEA Marcoule**
and **Max Planck Institute of Colloids and Interfaces**
Within the frameworks of : **L.I.A. Recycling CNRS-MPG**

Spéciality : **Chemistry and Physical Chemistry of Materials**

Presented by **Marie Jehannin**

About the role of physico-chemical properties and hydrodynamics on the progress of a precipitation reaction: the case of cerium oxalate particles produced during coalescence of drops.

Defended the 2nd of December 2015 in front of the jury composed of:

Mr.	Jean-François	DUFRECHE	Prof.	Uni. Montpellier	Jury President
Mr.	Hans-Jorg	BART	Prof.	TU Kaiserslautern	Examiner
Mr.	Thomas	ZEMB	Prof.	ICSM	Thesis Director
Mr.	Helmuth	MÖHWALD	Prof.	MPIKG	Thesis Director
Mrs.	Sophie	CHARTON	Dr.	CEA Marcoule	Supervisor
Mr.	Hans	RIEGLER	Dr.	MPIKG	Supervisor
Mr.	Jean-Christophe	VALMALETTE	Prof.	Uni. De Toulon	Reviewer
Mr.	Gerald	BREZESINSKI	Prof.	MPIKG	Reviewer
Mr.	Stéphane	GRANDJEAN	Dr.	CEA Marcoule	Guest

Published online at the
Institutional Repository of the University of Potsdam:
URN urn:nbn:de:kobv:517-opus4-88364
http://nbn-resolving.de/urn:nbn:de:kobv:517-opus4-88364

Abstract

The nucleation and growth of solid particles resulting from a precipitation process is an important topic both for fundamental science and industrial applications. In particular the sizes and morphologies of such precipitates are a major concern and their modification and control are relevant in separation chemistry, including nuclear fuel reprocessing.

In a precipitation process, different reactants, which are individually soluble in the same solvent, get in contact and react to form insoluble solid particles (the precipitate). The properties of the produced particles are the result of a strong coupling between the chemical reaction and the reactant feed and mixing rates. The latter are mainly provided by diffusive and convective transport processes through a reaction-diffusion-convection process. In the emulsion precipitation process considered here the reactants are enclosed into droplets. The local transport conditions can be modified in many ways by tuning the relevant parameters and thus be used to control the properties of the precipitated particles. The aim of this study is to investigate the impact of local flow and mixing conditions during the coalescence process on the precipitate properties, mainly its size, morphology and distribution. This is examined for two different systems, both composed of two coalescing droplets. In each case, one drop contains oxalic acid dissolved in an aqueous solution, while the other one contains cerium nitrate. Upon contact of the two miscible solutions a precipitate of cerium oxalate is formed. Besides, by adding chosen amounts of diols into the droplets, their surface tensions can be adjusted. Differences in surface tension cause a surface tension gradient in the section where both drops get in contact. This can lead to a Marangoni flow directed from the low surface tension interface to the high surface tension interface. This local convective flow will modify the local mixing conditions of the two solutions. This study focuses on how, where, when, which precipitate forms as function of the initial stoichiometry of the reactants and of the process conditions (e.g. the mixing conditions affected by the Marangoni flow). For this purpose, two configurations of coalescing drops are investigated experimentally.

The first configuration is motivated by a new operating conditions under development for the reprocessing of nuclear fuel, namely a water-in-oil emulsion with flowing drops. In our corresponding model system sessile drops of aqueous solutions are deposited on a hydrophobic substrate in an oil environment. Due to their high contact angles ($\geq 90^\circ$), the drops will get in contact with their liquid/liquid interface, thus representing the coalescence of flowing drops. The second configuration consists in bringing into contact two sessile drops of aqueous solutions on planar substrates with small contact angles ($\leq 25^\circ$). Here, the drops will contact each other at their three-phase contact line. The coalescence behavior of droplets in this configuration, in particular the influence of local Marangoni flows, had been analyzed recently for non-reactive liquids. In this study, the precipitate patterns are visualized by optical microscopy (reflection and confocal). The sizes and morphologies of the precipitated solid particles are characterized also by confocal optical microscopy and in addition by Scanning Electron Microscopy (SEM). Their structures are determined by X-Ray Diffraction (XRD) and Small Angle X-ray Scattering (SAXS).

Experiments with the “spherical" drop configuration in oil reveal that surface tension differences between both droplets barely affect the coalescence and the liquid mixing behavior. Precipitation mainly occurs in the contact area between the two drops, thus restricting the amount of mixing between both liquids and the precipitation reaction. This result is in agreement with previous studies on non-reactive liquids, which reveal that the influence of Marangoni flow is rather small compared to the capillary flow during the coalescence of high contact angle sessile drops. Moreover, at the water/oil interface Marangoni flows are weakened anyway due to the strong frictional/viscous dampening. The coalescence behavior of sessile droplets with low contact angles in air is very different. It was shown that Marangoni flow can dominate the droplet coalescence behavior of non-reactive drops and may even cause temporary “noncoalescence”. In the case of sessile drops containing reactive species, the local convective flow affects the liquid mixing and substantially changes the precipitation behavior. Location, size and morphology of the solid particles can be controlled independently by the surface tension difference between the two coalescing droplets and by the initial stoichiometry (both influencing the local supersaturation ratio). Without Marangoni flow the precipitation occurs in the contact area of the two drops, as in the case of “spherical" drops. With a strong Marangoni flow, a “non-coalescence” behavior is obtained like in the case of sessile drops without reactive species. With a Marangoni flow of intermediate strength three different precipitation patterns are observed depending on the supersaturation ratio. At low ratio, a uniform distribution of precipitate is obtained, spread out over the drop with the higher surface tension liquid. The solid particles exhibit needle-like morphology and scatter light strongly. At high supersaturation ratio, solid particles with “micro-flower”-like morphology are found. These are also covering the initially high surface tension drop surface. But the light scattering is very weak. XRD measurements reveal that both needles and micro-flowers have identical crystal structures. At intermediate supersaturation ratio, a periodic pattern of both particle morphologies is formed. The pattern consists of an alternation of the two cerium oxalate precipitate morphologies. Such periodic fringes can be explained by a feedback mechanism between convection, reaction and diffusion. The use of weakly structured ternary solutions, in the pre-Ouzo region of the phase diagram, allows access to two of these observed precipitation regimes, but for different supersaturation ratios. New precipitate morphologies have been achieved using this solvent.

Resume

La nucléation et la croissance de particules solides issues d'un procédé de précipitation est un sujet intéressant aussi bien du point de vue fondamental que vis-à-vis des applications industrielles. En particulier, le contrôle de la taille et de la morphologie des précipités est un enjeu majeur en chimie séparative, y compris pour le retraitement du combustible nucléaire irradié. Dans un procédé de précipitation, différentes espèces chimiques dissoutes dans un solvant sont mises en contact et réagissent pour former un composé insoluble, le précipité. Les caractéristiques de ce précipité résultent du couplage fort existant entre la réaction chimique et les vitesses d'apport et de mélange des réactifs, principalement assurées par la convection et la diffusion, à travers un véritable processus de réaction-diffusion-convection. Dans le procédé de précipitation en émulsion étudié ici, les réactifs sont contenus dans des gouttelettes. Il est en théorie possible de modifier de multiples façons l'apport en réactifs, y compris le transport local, et ainsi de contrôler les propriétés des précipités, en jouant sur les paramètres du procédé.

L'objectif de ces travaux est d'étudier et de comprendre les effets des différents flux de matière et des conditions de mélange sur le déroulement de la précipitation et la taille et la morphologie des particules obtenues. Pour cela, deux configurations reposant sur la coalescence de deux gouttes ont été investiguées. Dans chaque cas, l'une des gouttes contient de l'acide oxalique dissout en solution aqueuse et du nitrate de cérium est dissous dans la seconde goutte. Lorsque ces deux solutions aqueuses, totalement miscibles entre-elles, sont mises en contact, des précipités d'oxalate de cérium se forment. En outre, en ajoutant une quantité donnée de diols dans chaque goutte, il est possible de modifier et de contrôler leur tension de surface. Une différence de tension de surface entrainant un gradient lors de la mise en contact des gouttes, il peut en résulter un flux de Marangoni. Cet écoulement est dirigé de l'interface à faible tension de surface au-dessus de celle à forte tension de surface. Ce flux convectif va modifier localement les conditions de mélange. Les questions clés de cette étude sont comment, où, quand et sous quelle forme les précipités sont obtenus en fonction la concentration initiale des réactifs et des conditions de mélange, ou plus spécifiquement du flux de Marangoni. A cet effet, deux configurations de gouttes coalescentes ont été examinées expérimentalement en tant que système modèle. La première configuration est inspirée des nouvelles conditions opératoires proposées pour le retraitement du combustible nucléaire, à savoir une émulsion eau dans l'huile. Deux gouttes de solution aqueuse sont déposées sur un support hydrophobe dans une phase continue d'huile. En raison de leur fort angle de contact (angle de contact $\geq 90°$), les gouttes vont se toucher par leurs interfaces eau/huile. Il s'agit d'un système modèle typique pour la coalescence de gouttes en émulsion. La deuxième configuration consiste en deux gouttes de solution aqueuse posées sur un support avec de faibles angles de contact ($\leq 25°$). Dans ces conditions, les gouttes vont se contacter par leur ligne de contact triple (liquide/air/solide). La coalescence de telles gouttes, et plus particulièrement l'effet d'un flux de Marangoni, a été analysé récemment pour le cas de gouttes ne contenant pas d'espèces réactives (gouttes inertes). Dans cette étude, les motifs de précipitation sont suivis et observés à l'aide de techniques de microscopie optique (par réflexion et confocale). La taille et la mor-

phologie des précipités correspondants sont caractérisés par microscopie électronique à balayage (SEM) et microscopie confocale. Leurs structures sont déterminées par des mesures de Diffraction des Rayons X (DRX) et Diffusion des rayons-X aux Petits Angles (SAXS).

Les expériences représentatives des gouttes en émulsion révèlent que la coalescence et le mélange des liquides sont peu influencés par la différence de tension de surface entre les deux gouttes. La précipitation a lieu principalement dans la zone de contact entre les deux gouttes, limitant ainsi le mélange ultérieur et ralentissant en conséquence la réaction de précipitation. Ce résultat est en accord avec les conclusions d'une étude antérieure : lors de la coalescence de gouttes à fort angle de contact, le flux de Marangoni peut être négligé par rapport aux forces capillaires. En d'autres termes, la coalescence de gouttes posées à fort angle de contact est gouvernée par la minimisation de l'énergie interfaciale totale du système. De plus, dans ce cas, les forces de frottement visqueux à l'interface eau/huile contribuent également à affaiblir le flux de Marangoni. Les résultats concernant la coalescence de gouttes posées à faible angle de contact dans l'air sont très différents. Il a été montré que, dans cette configuration, le flux de Marangoni peut dominer la coalescence de gouttes inertes pouvant aller jusqu'à l'obtention d'un régime temporaire de non-coalescence. Dans le cas des gouttes contenant des espèces réactives, le flux convectif local impacte le mélange des liquides et modifie profondément la précipitation. La localisation, la taille et la morphologie des particules solides peuvent être contrôlées indépendamment via la différence de tension de surface des liquides des deux gouttes et la stœchiométrie initiale des réactifs (dont dépend le rapport de sursaturation). En l'absence de flux de Marangoni, la réaction de précipitation se déroule majoritairement dans la zone de contact des deux gouttes, menant à des résultats similaires à ceux observés dans la configuration en émulsion. En présence d'un fort flux de Marangoni, la coalescence des gouttes est retardée, comme dans le cas de gouttes inertes. En présence d'un flux de Marangoni modéré, trois motifs de précipitation sont observés en fonction du rapport de sursaturation. Lorsque ce dernier est faible, une distribution uniforme de précipités diffusant la lumière est obtenue au-dessus de la goutte de plus forte tension de surface. Ces particules solides ont une forme d'aiguilles. A fort rapport de sursaturation, des particules ne diffusant pas la lumière et présentant une forme plus complexe de type « micro-flower », précipitent majoritairement au-dessus de la goutte ayant initialement la plus forte tension de surface. Les mesures DRX ont révélé que les deux morphologies, aiguille et « micro-flower », présentent la même structure cristalline. Pour des rapports de sursaturation modérés, des motifs périodiques de domaines diffusant et ne diffusant pas la lumière se forment. Ces motifs correspondent à des domaines d'oxalate de cérium présentant des morphologies différentes, à savoir des aiguilles et des « micro-flowers ». L'obtention de telles franges peut s'expliquer par un mécanisme de rétroaction entre convection, réaction et diffusion. L'utilisation de solvants ternaires faiblement structurées, dans la zone pre-Ouzo du diagramme de phase, donne accès à deux de ces trois régimes mais pour des rapports de sursaturation différents. De nouvelles morphologies de précipité sont ainsi obtenues.

Zusammenfassung

Keimbildung und Wachstum von Partikeln als Resultat einer Fällungsreaktion sind wichtige Themen sowohl in der Grundlagenforschung als auch in industriellen Anwendungen. Insbesondere die Größe und Morphologie der Niederschlagspartikel sind wichtige Punkte und deren Änderung und Kontrolle sind relevant in der Separations-Chemie, beispielsweise im Fall der Wiederaufbereitung von Kernbrennstoffen. In einem Fällungsprozess kommen verschiedene Reaktionspartner, die einzeln im gleichen Lösungsmittel lösbar sind, miteinander in Kontakt, reagieren miteinander und bilden unlösliche Festkörperteilchen (einen Niederschlag). Die Eigenschaften der produzierten Teilchen sind das Resultat einer starken Kopplung zwischen der chemischen Reaktion, dem Zufluss der Reaktanten und den Mischungsraten, die hauptsächlich durch den diffusiven und konvektiven Transportprozess in diesem Reaktions-Diffusions-Konvektions-Prozesses bestimmt werden. In dem hier betrachteten Emulsions-Fällungs-Prozess sind die Reaktanten in Tröpfchen eingeschlossen. Die Transportbedingungen können auf viele Arten modifiziert werden indem die relevanten Parameter abgestimmt werden. Damit können sie benutzt werden, um die Eigenschaften der niedergeschlagenen Teilchen zu kontrollieren. Das Ziel der vorliegenden Arbeit ist die Untersuchung des Einflusses der lokalen Strömungen und Mischungsbedingungen während der Tropfenkoaleszenz auf die Eigenschaft des Niederschlags, insbesondere auf dessen Größe, Morphology und Verteilung. Dies wird untersucht anhand zweier verschiedener Systeme, die beide mit zwei koaleszierenden Tropfen arbeiten. In jedem Fall enthält ein Tropfen eine wässrige Lösung von Oxalsaeure während der andere Cer-Nitrat enthält. Bei Kontakt der beiden mischbaren Lösungen entsteht ein Niederschlag aus Cer-Oxalat. Daneben kann durch den Zusatz gewählter Mengen von Diolen in die Tropfen deren Oberflächenspannung eingestellt werden. Unterschiede in der Oberflächenspannung verursachen Oberflächenspannungsgradienten im Bereich, in dem beide Tropfen miteinander in Kontakt kommen. Dies kann zu einer Marangoni-Strömung von der Grenzfläche niedrigerer Oberflächenenergie zur Grenzfläche mit höherer Oberflächenenergie führen. Diese lokale Konvektionsströmung beeinflusst die lokalen Mischungsbedingungen der beiden Lösungen. Die vorliegende Studie befasst sich damit, wie, wo, wann sich als Funktion der ursprünglichen Stöchiometrie beider Reaktanten und der Prozessbedingungen welcher Niederschlag bildet (die Mischungsbedingungen werden durch die Marangoni-Strömung beeinflusst). Zu diesem Zweck wurden zwei Versuchsanordnungen mit koaleszierenden Tropfen experimentell untersucht. Die erste Konfiguration ist motiviert durch die industriellen Bedingungen zur Aufarbeitung nuklearen Brennstoffs, nämlich einer Wasser-in-Öl-Emulsion mit schwebenden Tropfen. In unserem entsprechenden Modellsystem sind liegende Tropfen einer wässrigen Lösung auf einem hydrophoben Substrat platziert, umgeben von einer Ölphase. Wegen ihrer großen Kontaktwinkel ($\geq 90^\circ$) kommen die Tropfen mit ihren Flüssigkeit/Flüssigkeits-Grenzflächen in Kontakt und repräsentieren damit frei schwebende Tropfen. Die zweite Konfiguration besteht darin, zwei liegende Tropfen aus wässrigen Lösungen auf ebenen Substraten mit kleinen Kontaktwinkeln ($\leq 25^\circ$) miteinander in Kontakt zu bringen. Dabei berühren sich die Tropfen an der Drei-Phasen-Kontaktlinie. Das Koaleszenzverhalten von Tropfen in dieser Anordnung, insbesondere der Einfluss lokaler Marangoni-Strömungen wurde

kürzlich für nicht-reagierende Flüssigkeiten analysiert. In dieser Untersuchung werden die Niederschlagsmuster mittels optischer Mikroskopie (in Reflexion und konfokal) visualisiert. Die Größe und Morphologie der niedergeschlagenen Festkörper-Partikel werden ebenfalls mittels konfokaler Mikroskopie und zusätzlich durch Raster-Elektronen-Mikroskopie untersucht. Die Struktur wird durch Röntgenbeugung und Roentgen-Kleinwinkel-Streuung bestimmt. Experimente mit der Versuchsanordnung "frei schwebender" Tropfen in Öl zeigen, dass Unterschiede in der Grenzflächenspannung der beiden Tröpfchen kaum das Koaleszenz- und Mischungs- Verhalten beeinflussen. Der Niederschlag findet vorwiegend in der Kontaktfläche zwischen den beiden Tropfen statt und begrenzt damit die Vermischung beider Flüssigkeiten und die Fällungsreaktion. Dieses Resultat ist in Übereinstimmung mit vorhergehenden Studien mit nicht-reaktiven Flüssigkeiten, die zeigen, dass bei liegenden Tropfen mit grossen Kontaktwinkeln der Einfluss von Marangoni-Strömungen im Vergleich zur Kapillar-Strömung recht klein ist. Zusätzlich sind Marangoni-Strömungen an Wasser/Öl Grenzflächen sowieso geschwächt wegen der starken Dämpfung infolge der Reibung/Viskosität. Das Koaleszenzverhalten liegender Tropfen in Luft mit kleinen Kontaktwinkeln ist sehr verschieden. Es wurde bereits gezeigt, dass Marangoni-Strömungen das TropfenKoaleszenzverhalten nicht-reaktiver Tropfen bestimmen können und sogar eine zeitweise "Nichtkoalezenz" bewirken können. Im Fall liegender Tropfen, die reaktive Komponenten enthalten, beeinflusst die lokale konvektive Strömung das Mischen der Flüssigkeiten und verändert das Niederschlagsverhalten beträchtlich. Ort, Größe und Morphologie der Festkörper-Teilchen können unabhängig voneinander durch den Unterschied der Oberflächenspannungen der beiden koaleszierenden Tröpfchen und durch die ursprüngliche Stöchiometrie (beide beeinflussen das lokale Übersättigungsverhältnis) kontrolliert werden. Ohne Marangoni-Strömung findet die Niederschlagsreaktion genau wie im Fall der "schwebenden Tropfen" in der Kontaktfläche der beiden Tropfen statt. Bei einer starken Marangoni-Strömung erhält man ein "Nicht-Koaleszenz-Verhalten" wie im Fall liegender Tropfen ohne reaktive Komponenten. Bei einer mittelstarken Marangoniströmung beobachtet man als Funktion des Übersättigungsverhältnisses drei verschiedende Niederschlagsmuster. Bei einem niedrigen Verhältnis erhält man eine gleichmäßige Verteilung des Niederschlags, der sich über den Tropfen mit der höheren Oberflächenspannung verteilt. Die Teilchen haben eine nadelförmige Gestalt und streuen das Licht stark. Bei einem hohen Übersättigungsverhältnis findet man feste Partikel mit einer blütenförmigen Morphologie. Diese bedecken ebenfalls die Oberfläche des Tropfens mit der ursprünglich hohen Oberflächenspannung, aber Licht wird nur schwach gestreut. Röntgenstreudaten zeigen, dass sowohl die Nadeln als auch die Blüten die gleiche Struktur haben. Bei mittleren Übersättigungsverhältnissen bildet sich ein periodisches Muster aus beiden Morphologien. Das Muster besteht aus einem Wechsel der beiden Cer-Oxalat-Morphologien. Solche periodischen Streifen können durch einen Rückkopplungsmechanismus zwischen Konvektion, Reaktion und Diffusion erklärt werden. Durch die Verwendung schwach strukturierter ternärer Mikroemulsionen erhält man zu zwei der beobachteten Niederschlagsmuster, jedoch für unterschiedliche Übersättigungsverhältnisse.

Contents

CHAPTER 1

INTRODUCTION

Crystal growth is an important issue in various fields including health, as in the case of kidney stones, and many industrial applications. Precipitation of solid particles with a controlled shape and structure is a challenging task. Indeed, the high supersaturation ratios involved in such processes lead to complex situations with mechanisms occurring rapidly and simultaneously[1]. Homogeneous and heterogeneous nucleation, growth, ripening and aggregation are the main mechanisms involved. This makes the precipitate shape and morphology difficult to predict also the later solid characteristics are usually of prime importance for the final applications[2]. For example, the physical properties of metallic particles are usually size-dependent[3, 4]. It is generally accepted that the precipitate features are strongly related to the mixing conditions applied during the precipitation process.

The precipitation of actinides is one of the key steps in nuclear industry, for the recovery of radioactive species from used nuclear fuel. The CEA (French Commission for Atomic and Alternative Energy) recently proposed a new process to enhance the productivity of the precipitation process[5, 6]. The process is based on a water in oil emulsion generated in a column apparatus. Two kinds of aqueous drops are present in the emulsion, some contain the oxalic acid and the others the radioactive species, which are aimed to be precipitated. In this process, precipitation occurs as a result of the coalescence of two drops with different composition.

Droplet coalescence is an important topic in many industrial processes such as petroleum industry [7], liquid-liquid extraction [8], ink jet printing [9], nanoparticle synthesis [10].

Drop coalescence is therefore an important field of researches, leading to numerous studies, in most of the cases involving identical liquids [11, 12, 13, 14, 15]. As we will detail in Chapter 2, the coalescence process is mainly driven by capillarity. However, it was recently shown that the situation can be very different during the coalescence of drops containing completely miscible but different liquids [16, 17, 18, 19, 20]. Indeed, in the case of sessile drops, a Marangoni flow, resulting from a surface tension gradient, may temporally delay the coalescence of the drops for some seconds up to minutes ('non-coalescence'). The coalescence and non-coalescence behaviour is quantitatively understood in the case of drops containing non-reactive liquids. The coalescence of drops containing chemical species that react with each other has not been investigated yet, although it is of major practical relevance for precipitation processes.

In this thesis, we study how the coalescence of drops is affected by a precipitation reaction. Moreover, the impact of the hydrodynamic conditions induced by the drops coalescence on a precipitation reaction is investigated. The reaction between oxalic acid and cerium nitrate has been chosen as a model system for the precipitation. The specific experimental set-up and characterization techniques applied to investigate these phenomena, are described in Chapter 3 Different coalescence configurations are implemented. In one case, "spherical" drops immersed in a viscous liquid contact each other by their liquid/liquid interfaces. In the other case, sessile drops on a planar substrate, in air, contact each other by their three phase lines (substrate/liquid/air). Results are discussed in Chapter 4 regarding either the coalescence behaviour (Sec: 4.1 to 4.3), or the solid characteristics (Sec: 4.4 and 4.5). Besides the hydrodynamic aspects, a new way of controlling the species reactivity, using structured solvent, is also investigated (Sec: 4.5).

Different precipitation behaviours, leading to different solid morphologies, have been observed depending on the coalescence regimes and initial conditions. Coalescence of "spherical" drops does not lead to a substantial mixing between the liquids of the two drops. In the case of sessile drops containing reactants, four coalescence behaviours (compared to only two cases for non-reacting liquids) were found. Under certain conditions, we observe the formation of intriguing periodic precipitation patterns composed of strongly and weakly light-scattering domains.
The precipitation conditions, morphologies and structures are analyzed in more details and open the way to a better control of industrial powders through the control of the

reactants transport and reactivity.

CHAPTER 2

FUNDAMENTALS

Crystallization refers to the formation of solid particles from liquid or gaseous phases. It is an ubiquitous process in nature, (*e.g.* ice crystallisation, shell, skeleton or diamond formation), and it is largely implemented at the industrial scale (e.g. metallurgy[], pharmaceutical industry[]). Regarding applications, particle characteristics are key parameters for the further material processing. These features (*e.g.* size, structure, morphology, particle density) are affected both by the hydrodynamic conditions (especially in the case of precipitation) and the chemical environment during the crystallisation elementary steps. In this chapter, first, the bases of crystallisation, precipitation and pattern formation will be introduced. A second part focuses on the hydrodynamics of coalescing drops. The last part concerns the surface tension of alcohol solutions and the properties of structured fluids.

2.1 Crystallization, precipitation and transport of reactants

In most natural and industrial processes, solid particles are produced by a phase transition induced either by a temperature, a pressure or a chemical concentration modification. Phase modifications are driven by thermodynamic laws, according to which the phase with the lower chemical potential is favoured at thermodynamic equilibrium. Moreover, the structure, morphologies and features of produced solid particles determine their applications or the viability of the next product processing step [2]. A chemical component may crystallize under different crystalline structures, which are named polymorphs[21]. According to the Ostwald rule of stage, it is the least dense species, *i.e.* the more soluble one, which precipitates first. The case of calcium carbonate, one

of the most abundant biominerals, has been extensively studied. In addition to amorphous calcium carbonate, $CaCO_3$ is known to be stable under various solid phases as calcite, aragonite or vaterite depending on the temperature and pressure conditions [22]. Although, crystallisation mechanisms have been studied for decades, they are still not fully understood. In the following, first a summary of the classic crystallisation theories is presented. Then a brief overlook on the recently emerging alternative theories is made. The third part deals with periodic and oscillation behaviours with a special focus on periodic precipitation patterns. The last part focuses on the particular case of a precipitation reaction, with the example of radioactive species recovery in the nuclear industry.

2.1.1 Nucleation and growth

Supersaturation

Supersaturation, S, is the driving force of every crystallisation process. Its value directly affects the relative importance of the basic steps occurring during crystallisation, *i.e.* nucleation, growth, aggregation and Ostwald ripening. Supersaturation is determined by the difference between the concentration of the crystallizing species and its solubility limit in a given solution. A saturated solution does not necessarily lead to a phase transformation due to the energy barrier necessary to form the first nuclei. Crystallization occurs only in supersaturated solutions. The supersaturation ratio is generally defined as the ratio of the activity of the crystallizing species in the solution, a_c, divided by the equilibrium molecular solubility product, K_{sp} (See Eq2.1):

$$S = \frac{a_c}{K_{sp}} \tag{2.1}$$

Crystallization occurs when $S \geq 1$. Moreover, at high S values, a high number of nuclei are formed simultaneously. This high nucleation rate leads to a fast decrease of the supersaturation in a closed system. The nuclei as produced do not grow extensively due to the restricted amount of building monomers available. In this case, numerous precipitates with restricted sizes are obtained. Conversely, at moderate S value, the nucleation rate is lower, only few nuclei are produced. The relative importance of nucleation and growth is well described in the literature only in the absence of other phenomena. As soon as other mechanisms operate, as aggregation or Ostwald ripening, the density and size of solid particles are much harder to estimate.

Classical nucleation theory

Nucleation corresponds to the birth of nuclei in a first order phase transition. Commonly, homogeneous nucleation, induced by stochastic fluctuations of the component concentration, is distinguished from heterogeneous nucleation, occurring at discontinuities as dust particle or other interfaces. The most famous description of a homogeneous nucleation process is probably the one arising from the work by Volmer and Weber [23] in 1926, and further developed by Becker and Döring [24], commonly called the classical nucleation theory (CNT). According to the CNT, nucleation is driven by the minimization of Gibbs free energy[25, 26], which corresponds to the minimisation of the chemical potential for a system kept at constant pressure and temperature (See Eq:2.2). At equilibrium, the phase of a chemical species with the lower chemical potential, μ, is favoured.

$$dG = -SdT + VdP + \sum \mu_i di \tag{2.2}$$

Stochastic fluctuations are at the origin of homogeneous nucleation. Furthermore, the nucleation rate J_i, which corresponds to the probability of forming a nucleus of i monomers, can be expressed by a Boltzmann approach as Eq:2.3.

$$J_i = A * \exp\left(\frac{-\Delta G_i}{k_b T}\right) \tag{2.3}$$

where k_b is the Boltzmann constant, A a constant prefactor and ΔG_i the change of Gibbs free energy implied by the formation of a group of i monomers. This change in the Gibbs free energy is composed of two parts (See Eq:2.4). The bulk energy part corresponds to the enthalpy difference between a molecule dissolved in a liquid and the same molecule inserted in a solid. This term is in favour of the crystal nucleation and varies with the volume of the nuclei. In other words, considering spherical nuclei of radius r, the bulk contribution is proportional to r^3. In contrary, the surface free enthalpy of a solid in a liquid prevents the formation of nuclei, this term varies with the nuclei surface (in case of spherical nuclei $\propto r^2$). The difference of these two terms leads to a maximum in the free energy as a function of the nuclei radius (See Fig:2.1).

$$\Delta G_i = \Delta \mu_i + \gamma A(i) \tag{2.4}$$

The abscissa of this maximum is called the critical radius, r^*. Below the critical radius, an assembly of components is thermodynamically unstable and destined to disappear. Above the critical size, the nuclei are stable and will grow into crystals. The CNT is

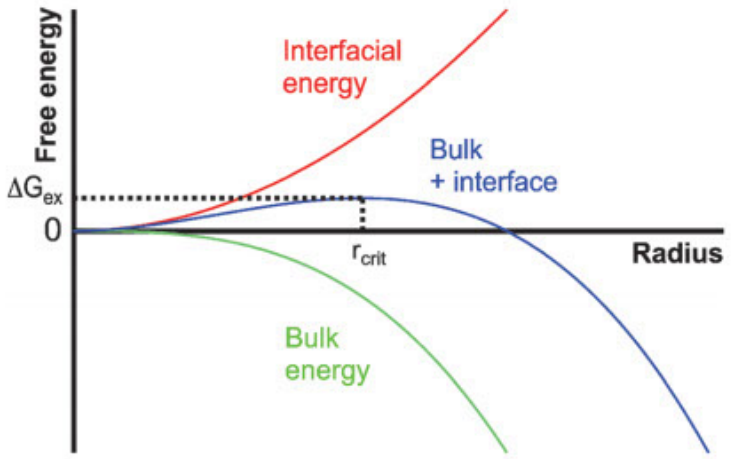

Figure 2.1: Evolution of the bulk energy and the surface free energy as a function of the nuclei radius. Reprinted from[27].

based on the hypothesis that the material properties at the microscopic scale, such as the phase surface tension, are identical to the macroscopic properties of this material. This hypothesis is known in the literature as the "capillarity assumption". However, the classical nucleation theory, which was initially developed by Gibbs, is valid only at moderate values of supersturation. For high supersaturation, the atomistic theory has to be considered [28].

Growth

Once a nucleus with a radius superior to the critical one has nucleated, it will probably grow into a crystal. According to Berthoud [29] and Valeton [30], the crystal growth is a two step process. First, the building monomers, *i.e.* ions, atoms or molecules, are transported to the crystal surface in most cases by diffusion. Once a monomer reaches the crystal surface, it is able to migrate along it. This forms the absorption layer. In a second step, the building monomer is integrated into the crystals at the position where the attraction of the monomer with the forming crystal is the highest, which means at a position enabling the largest number of bonds between them. The different positions, which may exist at the crystal surface, as step, kink and vacancies are summarized in Figure 2.2. In an ideal case, as expressed in [31], the crystal grows layer by layer, because the kink positions are always favoured compared to the steps or to the nucleation of a new island. In practice crystal growth is a dynamic process with continuous incorporation and detachment of building units. Moreover, other components, like solvent

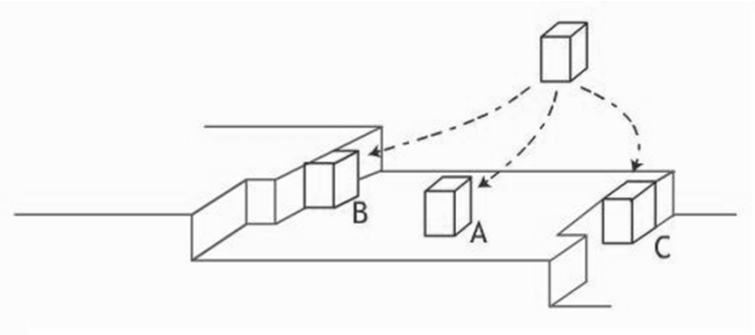

Figure 2.2: A monomer adsorbs at a crystal surface. It can integrate the crystal at different available positions. A)Island nucleation, B)Steps and C) Kink as represented by Mullin..

molecules or additives, may adsorb at the crystal surface, thus modifying the local surface energy of the crystal. These both facts result most of the time in a none idealistic growth of the crystal.
In most cases, the different faces of the crystal have different surface energies. This leads to different growth rates. The surfaces with the faster growth rate have tendency to disappear in favour of the slowly growing surfaces. These kinetic differences have a strong influence on the final crystal morphology[32]. Furthermore, the growth rate of the crystal surfaces can be modified by the presence of other components in the solution, *e. g.* solvent molecules, dust particles, organic and inorganic materials, which may adsorb on the crystal surface and act as surface poisoning agents. [33] have shown that the morphologies of cobalt and manganese oxide particles are greatly affected by the presence of polyols. For instance, an addition of 1,2-propanediol enables to change the morphology of cobalt oxalate particles from polyhedral shape in pure in 1,3-propanediol to spherical shape.

Aggregation

Agglomeration refers to the formation of a chemical bond between two crystals or a crystal and a nucleus. This mechanism is distinguished from aggregation and fluctuation by the nature of the chemical bond implied.

Ostwald ripening

For a dispersion of solid particles, the total Gibbs free energy decreases with the liquid/solid interface area. Such a thermodynamic principle leads to the dissolution of the

monomers from the smaller crystals, one by one, in favour of the bigger ones. This process is known as Ostwald ripening[34].

2.1.2 Mesocrystals and non-classical theory of crystallisation

The classical nucleation and the ion by ion growth model fail to explain quantitatively the original shape of some crystals, like biominerals. It was long thought that crystals exhibiting atypical curvatures could only arise from living systems and biological media. However, Garcia-Ruiz et al. [35] managed to synthesize inorganic materials exhibiting complex micro-structures identical to presumed microfossils. The crystals synthesized were self-assembled silica-carbonate solids. Some years later, Gebauer et al. [36] highlighted the gap between the classical nucleation theory and their experimental results during the crystallization of calcium carbonate in pH buffer solvent. Through precise electrochemistry based measurements, they highlighted the presence of prenucleation clusters, *i.e.* assembly of monomers, with a size below the critical radius r^*, in the solution during the calcium carbonate nucleation and growth steps. In the last decades, new theories have emerged aiming at filling part of the gap between the CNT predictions and experimental results. Glasner [37] suggested that nuclei could act, in some cases, as building blocks. In the last years, other alternative mechanisms have emerged from the formation of liquid precursors[27] to the assembly of oriented nanoparticles[21].

Recently, a lot of attention has been focused on mesocrystals or mesoscopically structured crystals[21]. This term describes crystals which grow by attachment of nanocrystals, with sizes ranging from 1 up to 1000 nm, oriented toward each other (See Fig:2.4). In a second step crystal bridges form between the oriented nano-blocks. The crystals resulting from this growth mechanism would lead to atypical microscopic geometry as sphere or pyramidal shapes. Examples of mesocrystals and other atypical crystals can be observed in figure 2.4. However, they are arranged at the atomic scale as crystals grown by monomer attachments. This spontaneous arrangement may be induced by the local electric field of the crystallized nanoblocks, by spherical repulsion effects or by absorbed additive species on the nanoblock surfaces, stabilizing them and orienting the attachment process. It can be difficult to differentiate between classical crystal growth and the mesocrystal mechanism due to the identical crystalline structures measured in both cases. Most of the mesocrystals described in the literature have been synthesized in presence of additives, like polymers, ions or organic components. However mesocrystal

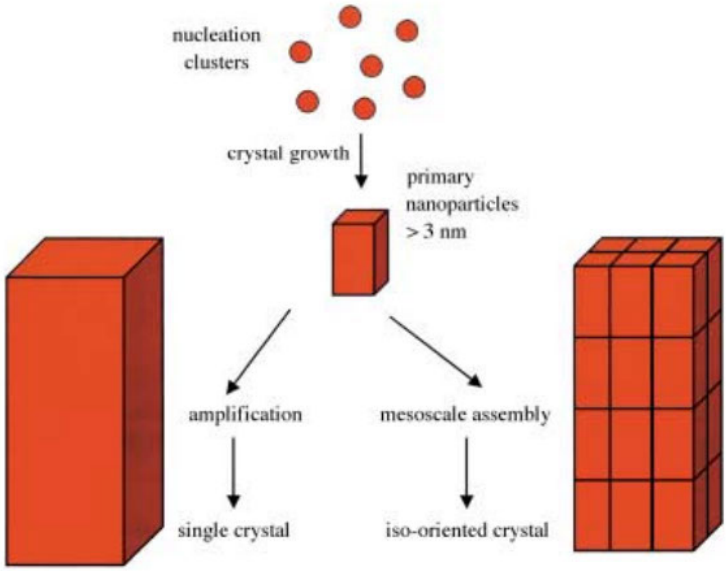

Figure 2.3: Growth mechanism proposed by Cölfen and Mann [38] from the formation of mesocrystals compared to the ion by ion attachment. Right: Mesocrystals would grow by attachment of nanoparticles, which orient spontaneously in the same direction. Left: Ion by ion growth of a crystal as expected according to the classical view of crystal growth.

formation may also occur without any additive. For example, $BaSO_4$ is known to form mesocrystals at high supersaturation (S$\geq$ 250) in pure water solvent[39].

Self-assembly should be distinguished from self-organised processes. Both terms refer to spontaneous ordered structured formation. However, self-assembly occurs in systems near-equilibrium, while self-organisation designed the arising of periodicity in systems far from equilibrium. In the first case, the crystallisation process is limited by the reaction, or more precisely the reaction kinetics, the building units move for some time along the adsorption layer. They are then integrated in the energetically more favourable position available, *i.e.*. the one for which the integration free energy is the lowest. The structures are single crystals with a characteristic length similar or smaller than the one of the building block. In the second case, the crystal growth is limited by the transport processes,*i.e.* most of the time by the diffusion of the building blocks to the growing crystal. The monomer is then integrated in the first available crystal position, leading to dendrites and fractal crystal shapes. The spacial periodicity of the system is larger than the dimension of the constituting units[44]. The formation of mesocrystal corresponds in most cases to a self-assembly processes, which occurs through specific interactions

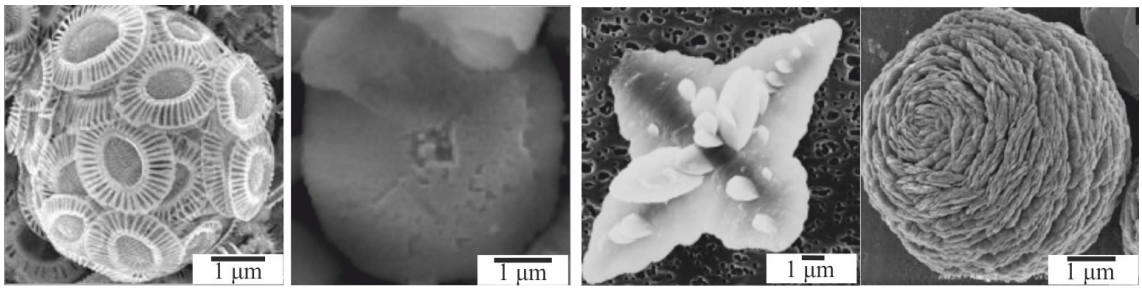

Figure 2.4: Various crystals with complex form a) Coccoliths a natural biomineral forms on calcite usually found in some exoskeleton of marine algae[40]. b) Copper oxalate supracrystals by [41] c)$BaSO_4$ crystal formed at high supersaturation ratio without additives, reprinted from[42] d)ZnO spherical particles presented as mesocrystal precipitated in presence of butanol from [43].

leading to a cascade of structural steps[21].

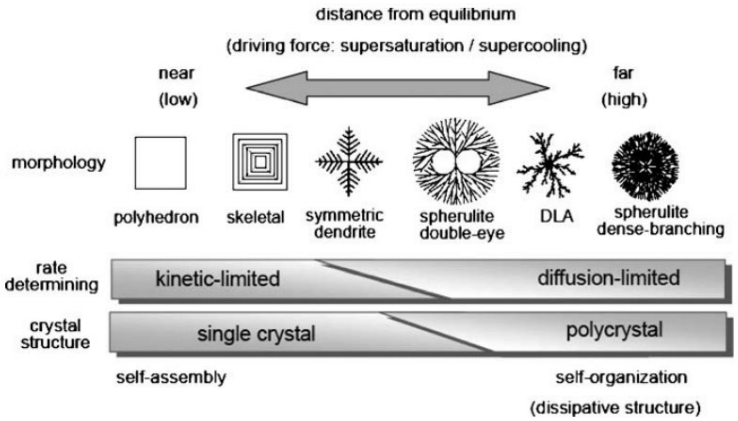

Figure 2.5: Morphology of the obtained precipitates reproduced from Imai [44]

The conditions leading to either self-assembly or self-organisation are summarized in Figure 2.5

2.1.3 Periodic precipitation and other oscillatory behaviours.

As mentioned above, self-organization results from the combination of reaction and transport processes. Moreover, periodicity in chemical systems appears only far from the thermodynamic equilibrium [45]. One of the most famous periodic patterns induced

by a precipitation reaction are the so-called Liesegang rings, named after the German chemist who first reported this phenomenon in 1896 [46]. One of the reactants is incorporated into a gel, either in a Petri-dish like vessel or in a test tube[47]. A drop of a solution containing the second reactive species is deposited above the gel and diffuses through it. In the case of the Petri-dish symmetry, circles of precipitates are soon observed which alternate with precipitate free domains. The circles are centred in the deposition point and appear one by one. In case of the test tube symmetry, layers of precipitates alternate with layers free of precipitates. In both cases, the wavelength increases with time[48].
Currently, the most accepted model for the formation of Liesegang rings is the so-called supersaturation theory, which was developed by Ostwald [49]. This theory relies on the fact that precipitation occurs only in a supersaturated solution regarding the reactant. Let's call A and B the reactive species dissolved in the gel and in the top solution respectively. B diffuses into the gel, close to the contact zone, consequently the local solubility product increases until the nucleation energy barrier is reached and even exceeded. Immediately, particles nucleate at this place and they growth rapidly. The growing particles deplete the surrounding zone in reactant A. Although B continuously diffuses through the gel, the low concentration in A restricts the solubility product to a low value. Thus the precipitation is prevented in the depletion zone. Soon the species B will reach the end of the depletion zone, the solubility will arise and a second circle/layer of precipitate will be created[47]. For the sake of this study, it is worth to precise that Liesgang patterns are formed only in systems free of convection flow.

Turing [50] was the first to propose a theoretical model for the formation of self-organised systems or patterns. He studied the morphogenesis and managed to model the formation of patterns in nature, as the skin of giraffe or zebra. This model methodology could be generalized to explain most periodic patterns formation. Considering a system with related concentration, *e.g.* due to auto-catalytic process, the variation of one of the components over time at position x is equal to the amount of this component produced or transported to x minus the one consumed or pushed away. This simple idea leads to the equations describing most of pattern formation processes.

The term oscillatory reactions gathers the chemical reactions exhibiting a periodic change in time of the reactants, intermediate species or product concentrations. The most famous example is the Belousov-Zhabotinski reaction (Or BZ reaction) [51] which was discovered in 1951 by the Russian chemist Boris Belousov and further investigated in

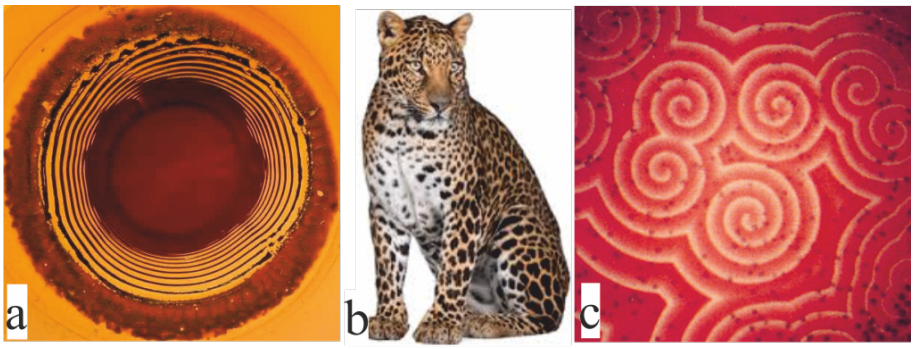

Figure 2.6: Example of periodic patterns in the case of a) Liesgang ring of silver-chromate in gelatine gel b)Turing patterns c) BZ reaction in a non-stirred reactors.

the 60s-70s by Zhabotinski, a student in biophysics [45]. A BZ reaction occurs by mixing bromide, organic acid and metal catalyst. In an unstirred vessel, multiple concentric blue circles are formed over a red background. The exact reaction mechanism of the BZ reaction remains unknown due to the numerous intermediate species involved. However, it is commonly accepted, that oscillatory reactions require that one of the chemical species acts as an auto-catalyst.

In the last decade, Rongy [52] investigated theoretically the effect of a surface tension gradient on an autocatalytic chemical front. They considered a thin liquid layer, in which a chemical reaction modified locally the reactant concentration, and thus the surface tension. The resulting surface tension gradient induces a Marangoni flow, which enhances the mixing and the chemical reaction (See Sec:2.2). They highlighted oscillatory deformations of the concentration field [53].

2.1.4 Precipitation: the recovery of radioactive species example

Precipitation, or reactive crystallization, is a particular case of crystallization with high local supersaturation values reached during precipitation processes. That way, a high amount of solid particles are created. In that case, the sudden increase of the supersaturation is generally generated by mixing two solutions, in which chemical reactants are dissolved. When the two solutions come into contact, the chemical species reacts into a sparingly soluble product. Processes based on precipitation are a key step in numerous industries going from pharmaceutical, water treatment or nuclear field[6]. The feature, as the morphology and size, of the outgoing particles are often of key importance either for the aimed application or the post-precipitation processing. Precipita-

tion is commonly less understood than crystallisation because the high supersaturation reached during this process generally implies a fast and simultaneous occurrence of mechanisms, which are difficult to decorrelate. The main mechanisms taking place in a precipitation process are nucleation, growth, agglomeration and Oswald ripening.

Precipitation reaction and supersaturation ratio

Precipitation is a common process in industry. It is largely used for the separation of chemical species. For example, the CEA patented in 2008 an emulsion based process for the recovery of used nuclear fuel[5]. A water in oil emulsion is created in a column. Two kinds of aqueous drops coexist in this column, in some of them is dissolved oxalic acid and in the other the radioactive species, which are aimed to be recovered[6, 54]. When two drops of different composition contact each other, they may coalesce. Then, the liquids of both drops mix, which leads to the formation of solid particles. The product features depend on the mixing condition, *i.e.* on the flow patterns induced by the drop coalescence and their movement in the column (See Fig:2.7).

This process is currently under development in research laboratories. Cerium or neodymium are often used to model the chemical species to recover. Hence, the constraints implied when working with radioactive species are avoided. In the case of cerium, it reacts with oxalic acid to produce a white solid, cerium oxalate2.5.

$$2Ce(NO_3)_3 + 3C_2H_2O_4 + 10H_2O \longrightarrow Ce_2(C_2O_4)_3, 10H_2O + 6HNO_3 \tag{2.5}$$

One of the key parameters of this system is the supersaturation ratio, S, expressed by [6]:

$$S = \bar{\gamma}\left(\frac{{C_{Ce}}^2 {C_{C_2O_4}}^3}{K_{SP}}\right)^{\frac{1}{5}} \tag{2.6}$$

where K_{SP} is the cerium oxalate solubility product and $\bar{\gamma}$ the mean activity coefficient. The activity coefficients can be calculated using the Davies model, valid at low and medium ionic strength. The supersaturation ratio S is the driving force for the precipitation and the underlying processes (nucleation, growth, Ostwald ripenning, aggregation.). It depends strongly on the local mixing.

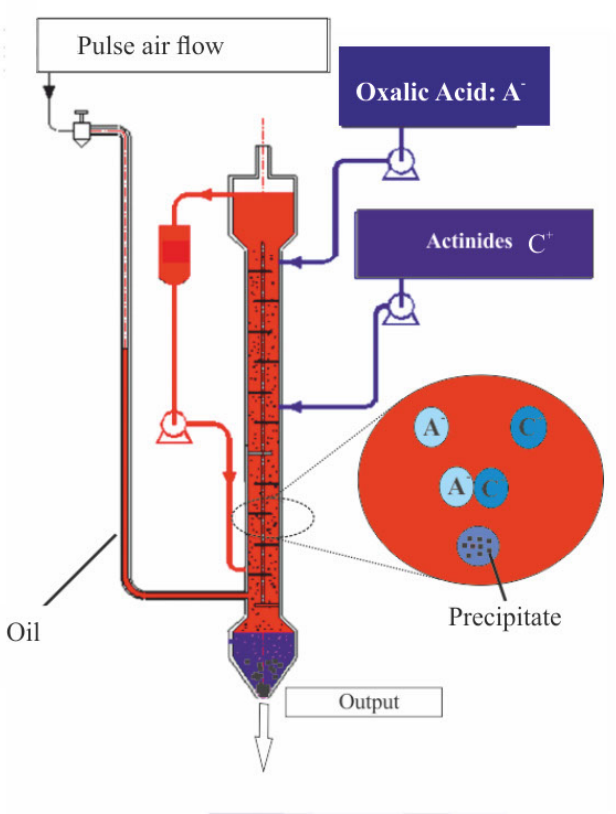

Figure 2.7: Process under development for the recovery of radioactive species from used nuclear fuel by oxalic precipitation. A water in oil emulsion is created in a column using a pulse of compressed air. The desired solid is obtained, when two drops, one containing the actinides and the second one the oxalic ions, coalesce.

2.2 General hydrodynamics of drops.

In an emulsion as presented above (this does not include microelmusion), drops are continuously breaking and coalescing. Hence, the drop distribution is a dynamical parameter. Moreover, the external forces applied to create the emulsion impact the movement of the flowing drops, potentially inducing additional flow as Hills vortex [55]. Consequently, for simplicity purpose, most of the fundamental experimental studies focus on the drop coalescence in the absence of external disturbance.

2.2.1 Drop characteristics

In the collective spirit, drops or droplets (these two terms are here used equally) are spherical liquid particles in air or in another immiscible liquid phase. However, drops

may also be deposited on a substrate and form a hemispherical domain, they are then generally called sessile drops. In the following, the state of the art on coalesce of both "spherical" and low contact angle sessile drops will be resumed.

Surface tension definition

Most of the phenomena undergone by drops are either induced or at least influenced by their surface tension, γ. In the case of liquids, the surface tension, γ is defined as the reversible work, dW, necessary to extend a surface by a value of dA (See Eq:2.7).

$$dW = \gamma dA \tag{2.7}$$

When an aqueous solution is in contact with air or an immiscible oil phase, it is energetically more favourable for most components to be at the air-liquid interface than in the liquid bulk. These components are decreasing the surface/interfacial tension of water and are called "capillary-active substances" (e.g. organic acid, ester, alcohols, etc...). Conversely, most salts, as cerium nitrate, are "capillary-inactive substances", i.e. they are depleted at the air-liquid interface (their concentrations are higher in the bulk than at the interface). In these cases, the surface tension of solutions containing only such chemical species is higher than the one of water[56].

Equilibrium and dynamic contact angles

At thermodynamic equilibrium, the equilibrium contact angle, θ_e, forming between a sessile drop and its substrate is described by the Young equation[57] (See Eq:2.8):

$$\cos(\theta_e) = \frac{\gamma_{SV} - \gamma_{SL}}{\gamma_{LV}} \tag{2.8}$$

where γ_{SV}, γ_{SL} and γ_{LV} are the solid-vapor, solid-liquid and liquid-vapor surface tensions, respectively. The equilibrium contact angle reflects the affinity between a liquid and a solid and defined the substrate wettability. However, the substrate roughness or line tension effect can impact the real contact angle measured at rest [58, 59].
Moreover, equilibrium contact angle has to be distinguished from dynamic contact angle, which refers to the contact angle formed by a surface and an a drop at an instant, t. In the case of dynamic contact angle, the considered system is not necessarily at thermodynamic equilibrium and the liquid is not necessarily at rest (e.g. spreading or pinning drop).

Capillary forces

Capillary forces are resulting from the surface tension effect on a given length. These forces are normal to the contact line in the plane of the interface. They tend to minimize the contact area between two immiscible phases. Moreover, the surface tension induces an overpressure in the drop: the so-called Laplace pressure. For a drop of radius R exhibiting a surface/interface-tension γ with the surrounding media, this over-pressure can be written as:

$$\Delta p = \frac{2\gamma}{R} \tag{2.9}$$

Marangoni flow

Although less famous, Marangoni flow is also induced by surface tension or more precisely surface tension gradient. Indeed, when the surface tension of a system is not homogeneous, the total energy of the system can be lowered by replacing a high-surface energy with a low surface energy[60]. The flow thus created is called Marangoni flow and is always directed from the low γ surface toward the high γ domain. In the literature, the existence of Marangoni flow was first highlighted in 1855 by [61] in a qualitative description of the tear of wine. Nowadays, Marangoni flow is mostly studied in the case of Bernard-Marangoni instabilities or Marangoni drying[62].

A Marangoni flow arises from a surface tension gradient, which can be induced either by a variation of the temperature (thermal Marangoni flow) or chemical species concentration (solutal Marangoni flow).

2.2.2 Coalescence of "spherical" drops immersed in viscous media

The coalescence mechanisms of high contact angle sessile drops, pendant drops or one pendant drop with a sessile drop are similar in the sense, that the coalescence occurs through the liquid/liquid interfaces. In the cases of "spherical" drops immersed in viscous media, two types of coalescence regimes are reported in the literature : the inertial regime and the viscous one [63]. The Reynolds number enables to distinguish between these two regimes, depending on the system parameters. If $Re < 1$, viscous coalescence takes place, whereas $Re > 1$ corresponds to the inertial regime.

Viscous regime, $Re < 1$

The viscous regime can be observed for liquids with high viscosity and low surface tension. For two initially spherical droplets, i.e. with negligible approaching speed (pure viscous regime), the time evolution of the neck's radius , r, was established analytically by Eggers et al. [64]:

$$r(t) = -\frac{\gamma t}{\pi \mu} \ln\left(\frac{\gamma t}{R_0 \mu}\right) \approx \frac{\gamma t}{\mu} \tag{2.10}$$

Where R_0 is the initial droplet radius. As expressed by Eq. (2.10), the neck's radius increases linearly with time.

Aarts et al. [63] have obtained similar results experimentally by recording the coalescence (on their free surface) between a pendant and a sessile drop. They managed to observe the linear dependence of the bridge's radius with time by tuning separately the viscosity and the surface tension of the fluid. In a first hand, they used silicon oils of variable viscosity (in the range $100 \leq \mu \leq 1000$ mPa.s) with constant density and surface tension (respectively $d = 0.970$ and $\gamma = 20$ mN.m^{-1}). In their experiments, the logarithmic correction for the radius was not observed. One of the difficulties of the viscous coalescence study is, that there are relatively fast phenomena taking place only for $t < \dfrac{\eta^3}{\rho\gamma^2}$, which corresponds to $r < \dfrac{\eta^2}{\rho\gamma}$. To overcome this drawback, Aarts et al. [63] used colloid-polymers mixtures to observe more precisely the viscous coalescence phenomena. Because of their low surface tension ($\gamma = 0.16$ μN.m^{-1}), their coalescence is about 10,000 times slower than for the previously considered silicon oils. From both systems, the authors concluded that the observed coalescence velocity is set by the capillary velocity u_c.

Silicone oils in the same range of viscosity were used by Ristenpart et al. [14] in the case of sessile droplets. Their study was both experimental and theoretical. The early stage of the bridge growth exhibits a $\sqrt{t}$ evolution. Moreover, the height of the spherical caps, at the contact line, highly influences the growth of the bridge. Two steps were distinguished during the coalescence process of sessile drops:

- first, a fast growth of the meniscus bridge between the droplets, perpendicularly to the line of the droplet's centers;
- then, the resulting droplet slowly rearranges from an elliptical shape to a spherical one.

The time-scale difference between sessile and free droplet coalescence is surprising. In the first case, it takes about one minute for the droplets to merge completely (without precise repeatability of the apparent velocity), while for the second case, the time-scale is of the order of one second.

Inertial regime, $Re > 1$

The following scaling law was proposed for coalescence in inertial conditions by Eggers et al. [64]:

$$r(t) \propto \left(\frac{R\gamma}{\rho}\right)^{\frac{1}{4}} t^{\frac{1}{2}} \tag{2.11}$$

In Eq. (2.11) R stands for the inverse of the drop curvature at the contact point.
One of the main assumptions of this law is that interfacial stress is mainly due to the smallest length scale, i.e. the gap width. This equation was verified experimentally for the inertial coalescence of water, methanol and a water-glycerol mixture [65]. In all the explored cases, the radius of the bridge was observed to increase proportionally to the square root of time. The initial radius of the droplet does not influence the dimensionless pre-factor of the dimensionless equation, i.e:

$$\frac{r(t)}{R} \propto \left(\frac{t}{\tau}\right)^{\frac{1}{2}} \tag{2.12}$$

Where τ, the coalescence time-scale is given by:

$$\tau = \sqrt{\frac{\rho R^3}{\gamma}} \tag{2.13}$$

The nature of the liquid has a small influence on the dimensionless parameter. A value of 1.03 ± 0.07 and 1.09 ± 0.08 was found for water and glycerol-water mixture respectively, whereas a higher value of 1.29 ± 0.05 was measured for methanol. The authors did not manage to explain this difference, but they noticed, that it is considerably lower than the theoretical value of 1.62 found by Duchemin et al. [66].

Aarts et al. [63] results regarding inertial coalescence of silicone oil with viscosities ranging from 5 to 50 mPa.s in the sessile/pendant drop configuration, are consistent with this square root evolution of the bridge radius with time. In all cases, the same liquid was used in both the sessile and pendant drops. Dimensionless parameter values between 1.11 and 1.24 where found, in agreement with the previously published results of Wu et al. [65].

2.2.3 Immediate and (Non)-Coalescence of sessile drops

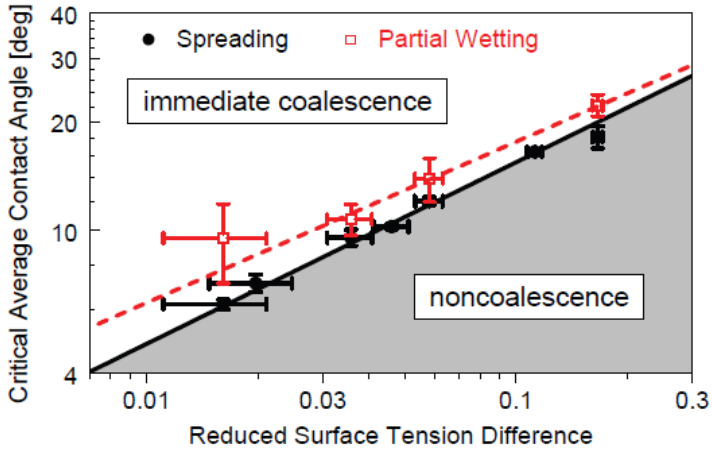

Figure 2.8: Immediate coalescence and non-coalescence domains as a function of the reduced surface tension difference and the average contact angle in case of equilibrium (partial wetting) and dynamic (spreading) contact angles. The transition between the two domains is delimited by the straight line $\bar{\theta}_{a,t} \approx (0.86 \pm 0.09)(\Delta\gamma/\gamma)^{0.45\pm0.04}$ Reprinted from [18].

As soon as two drops of identical composition get into contact, the capillary forces favour their coalescence. Hence, the total surface area of the system decreases and its total energy is lowered. However, when the two drops contain different liquids, the coalescence behaviour may be totally different[67]. Karpitschka and Riegler [16] investigated experimentally[17, 20, 19] and theoretically[18] the coalescence, in air, of low contact angle sessile drops containing completely miscible liquids. They have shown, that a difference in surface tension between both drops induces a Marangoni flow, which may delay the drop-drop coalescence and thus change the liquid-liquid mixing process. If the Marangoni flow is strong enough, the two drop volumes remain essentially separated for quite some time (up to minutes) after the drop-drop contact, connected only by a thin neck of constant height. This state is designed as "non-coalescence". The control parameters of coalescence behaviour are the surface tension difference between both liquids, $\Delta\gamma$, and the average contact angle, θ_a of the two drops at the moment of contact. These domain limits are identical for the experiment involving equilibrium or dynamic contact angles (See Fig:2.8).

In the case of non-coalescence, a thin microscopic liquid bridge connects the two drops,

through which Marangoni flow continuously removes liquid from the drop with the lower surface tension to the one with the higher surface tension. Schematically, this Marangoni flow pushes faster the liquid out of the contact zone than the capillary flows can bring liquids toward the neck for its growth. This actually stabilizes this state of temporary non-coalescence.

From these investiguations a specific Marangoni number, $\tilde{M}$, was defined (See Eq:2.14)[18]. $\tilde{M} < 2$ means immediate coalescence, $\tilde{M} > 2$ means temporary non-coalescence.

$$\tilde{M} = \frac{3|\Delta\gamma|}{2\bar{\gamma}\theta_a^2} \tag{2.14}$$

2.3 Surface tension and structured fluids

The most common way to modify a solution surface tension is to add a surface active species, *i.e.* a surfactant. Surfactants are mostly known for the increase of the solubility properties of the aqueous solution, in which they are present. They are mostly used as detergents. For instance, surfactants are used in the cosmetic industry. When the surfactant concentration is higher than the critical micelle concentration, aggregates of surfactants form spontaneously. The structure of the aggregates, *e.g.* micelles, lamellar bilayers, hexagonal structure, depend on the molecular shape[68] Although alcohols do not fulfill the requirement to be named as surfactants, because they do not form thermodynamically stable aggregates, they show properties similar to those of surfactants[69]. Hence, alcohols and diols are named co-surfactant or hydrotropes. The mixture of water/hydrotropes/oil exhibits structure, which has been only poorly studied up to recently, and presents unique properties regarding component solubility.

2.3.1 Simple surface isotherm

Generally surfactants, which are molecules composed of a hydrophilic head and hydrophobic tails, adsorb preferably at an interface. Hence, they induce a lowering of the surface (interfacial) tension. There are four different kinds of surfactants, *e. g.* anionic or cationinc head groups, zwitterioning or non ioninc surfactant. Several models of adsorption isotherms were developed to describe the equilibrium between the surfactants at an interface and the ones dissolved or aggregated in the bulk. The Gibbs model is one of the simplest for non-dissociating material. Let S be a surface and A and an adsorbing species. Equation 2.15 reflects the adsorption equilibrium.

$$I_{bulk} + S \longrightarrow IS \tag{2.15}$$

The surface excess, Γ_i^σ, is the difference between the number of active molecules n_i in a surface plane, A^σ, compared to an equal area into the bulk. The thermodynamic energy of the surface, U^σ, is given by Eq:2.16

$$U^\sigma = TS^\sigma + \gamma A + \sum \mu_i n_i^\sigma \tag{2.16}$$

where $\mu_i = \mu_i^\circ + RT \ln a_i$ is the chemical potential of the component i and μ_i° its standard chemical potential. The differentiation of Eq:2.16 leads to:

$$dU^\sigma = TdS^\sigma + S^\sigma dT + \gamma dA + Ad\gamma + \sum \mu_i dn_i^\sigma + \sum n_i^\sigma d\mu_i \tag{2.17}$$

The variation of U^σ induced by a small, isobaric, isothermal, reversible change can be expressed as:

$$dU^\sigma = TdS^\sigma + \gamma dA + \sum \mu_i dn_i^\sigma \tag{2.18}$$

A simple rearrangement of the subtraction of Eq:2.17 and Eq:2.18 leads to the Gibb's equation 2.19.

$$d\gamma = -\sum \Gamma_i^\sigma d\mu_i \tag{2.19}$$

In the case of a unique, non-dissociating, material I Eq:2.19 is equivalent to Eq:2.20.

$$\Gamma_I^\sigma = -\frac{d\gamma_I}{RTd\mu_I} \tag{2.20}$$

Figure 2.9 exhibits the typical evolution of the surface tension, as its concentration in surfactant increases, and the corresponding surfactant distribution. The surface tension first decreases linearly with the logarithm of the concentration until the CMC, after which its value is almost constant. Above the CMC the surfactants may aggregate in the bulk.

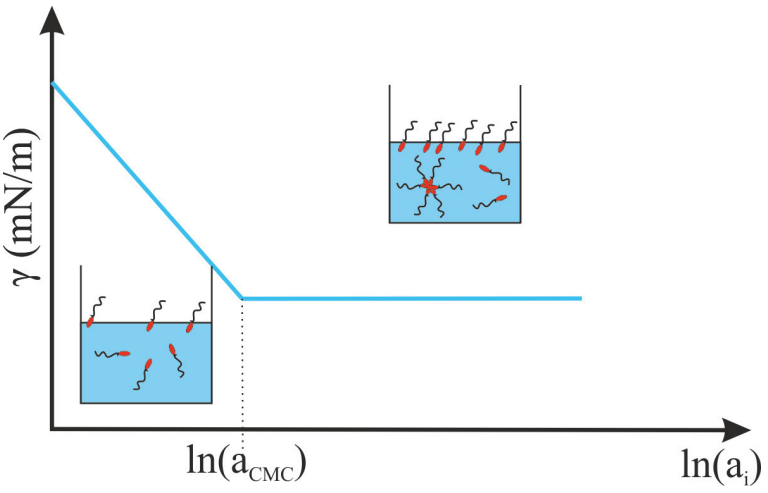

Figure 2.9: Typical evolution of the surface tension for a solution containing surfactants. Schematic of the surfactant distribution.

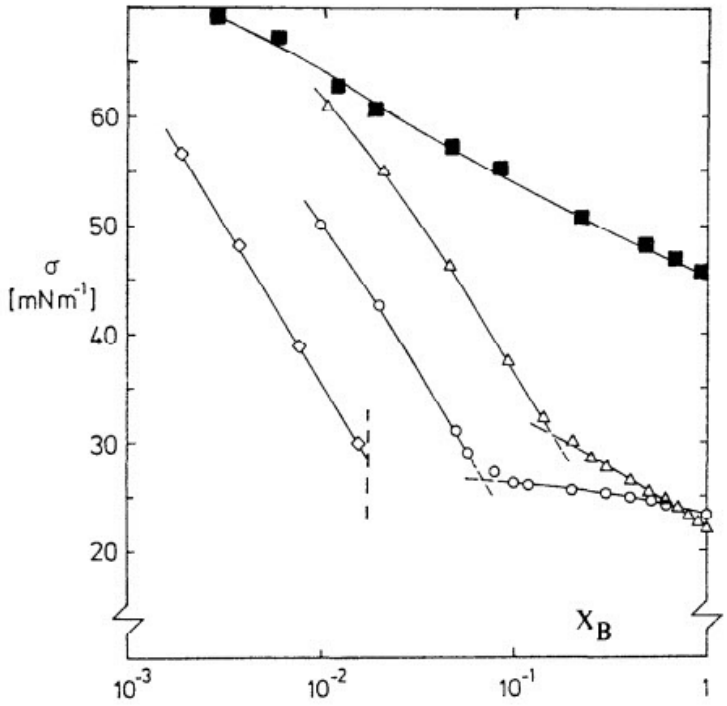

Figure 2.10: Surface tension of aqueous mixtures as a function of the component mole fraction at 25 °C, reprinted from [70]. Diamond: butanol, circle: propanol, triangle: ethanol, square: 1,4-butanediol

2.3.2 Surface tension controlled with alcohol only

Cosurfactants or hydrotropes differ from surfactants by the fact that they can not form micelles on their own either due to their restricted solubility in water or weak interactions between their hydrophobic moieties[70]. As a surfactant, a hydrotrope reduces the surface tension of the solutions, to which it is added. Moreover, cosurfactants are often used simultaneously as surfactant in order to improve the latter properties[70]. Alcohols are the most frequently used hydrotropes.

In case of butanol, its solubility in water is too low to enable the formation of aggregates (See Fig: 2.10). Although the surface tension of other alcohol mixtures investigated keeps decreasing as the mole fraction of alcohols increases, a break can clearly be identified on these curves. The break is similar to the phenomenon observed at the surfactants CMC. In the case of butandiol, which is more hydrophilic, the break is absent.

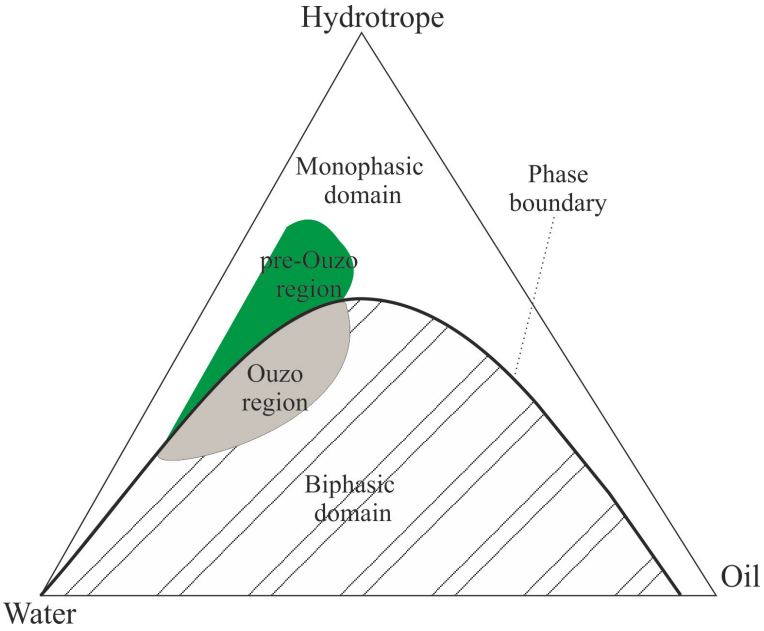

Figure 2.11: Localisation of the Ouzo and pre-Ouzo subregion in a ternary phase diagram.

2.3.3 Alcohol and immiscible fluids: structured solvent

Complex systems may be obtained by adding a third component to a water/hydrotrope mixture. When the additive is miscible with the hydrotrope but insoluble or poorly soluble in water, a bicoutinous sponge-like phase, direct or reverse microemulsion may be observed. Shortly, the phase diagram of such a ternary system is composed of two major domains, a monophasic and a biphasic domain. These two domains can be further divided in subregions in regard of the molecule distribution inside the liquid.

For example, the Ouzo region of the phase diagram refers to compositions for which microemulsions form spontaneously through a phase separation. The Ouzo region is part of the biphasic domain of the phase diagram. It received its name in reference to a Greek alcoholic beverage, Ouzo, forming a turbid microemulsion by water addition.

In the 70s, Smith et al. [71] highlighted the spontaneous formation of surfactant-free microemulsions (SFME) in the monophosic part region of the phase diagram, *i.e.* nano-size aggregates of hydrophobic and hydrotope components, with very diffuse interface, in hydrophotrope/water rich media[72, 73]. SFME exhibits unique properties, as a narrow size distribution (typically 1 µm) of the micelles and unexpected solubilization power[74]. The SFME and surfactant microemulsion differ by the distribution of the chemical species inside the system. Hence, the hydrotrope can be found everywhere

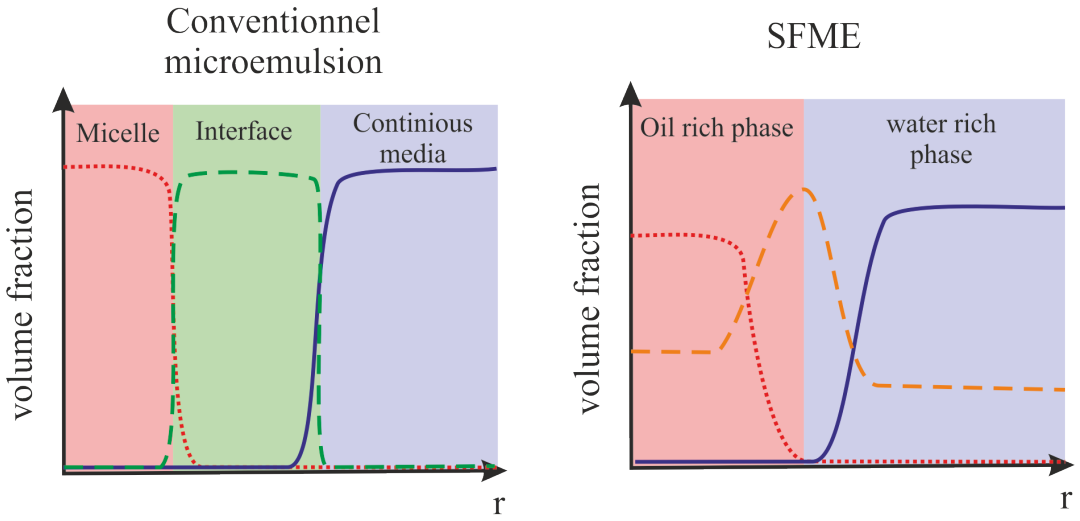

Figure 2.12: Left: Schematic curve of the molecular distribution of the water (blue, straight line) /surfactant (green, dashed line)/oil (red, dotted line) along a micelles. Right: Molecular distribution of a SFME, water (blue, straight line) /hydrotrope (orange, dashed line)/oil (red, dotted line).

in SFME, although its concentration is higher at the micelles interfaces. Conversely, in microemulsions based on surfactants, the latter are present only at the water/oil interfaces (See: Fig:2.12). More recently, research on such systems has been continued, this time under the name pre-Ouzo effect. The pre-Ouzo pseudo-phases are present in mixture composition close to the phase boundary with the Ouzo region (See: 2.11). In those systems, the formation of nanoscopic pseudo-phases, with diffuse interfaces, in the monophasic domain of the phase diagramm has been demonstrated by SAXS (small angle x-ray scanning) experiments [75]. Schöttl et al. [76] confirmed the existence of micelle-like structures in the pre-Ouzo region of the phase diagram by molecular dynamic simulation. They consist of nanometre size aggregates (typically 2 nm) swollen by the hydrotrope (See:Fig:2.13).

The pre-Ouzo effect is of interest for this study. Indeed, it has been shown, that such pseudo-phases impact the activities of the chemical components dissolved in these mixtures. For example, Tchakalova et al. [77] have observed an improvement of fragrance activities during the transition from unstructured water/ethanol/fragrance monophase to the pre-ouzo region of the phase diagram through controlled evaporation.

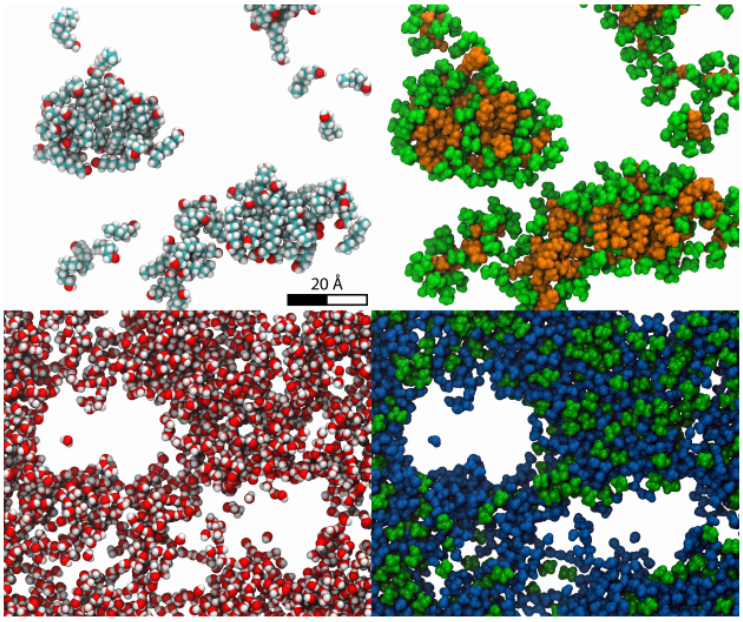

Figure 2.13: Molecular dynamic snapshot of the distribution of water, hydrotrope and oil for a composition matching the pre-Ouzo region of the phase diagram. Top left: Octanol molecules. Top right: Octanol molecules in orange and ethanol molecules strongly bound to them in green. Bottom left: water molecules. Bottom right: water molecules in blue and strongly bounded ethanol molecules in the water rich pseudo-phase in green. Snapshot reproduced from[76].

CHAPTER 3

EXPERIMENTAL SECTION

The sessile drops coalescence, the confocal experiments, most of surface tension and density measurements and some dry SEM imaging were performed at the Max Planck of Colloids and Interfaces (MPIKG). The "spherical" drop experiments and the viscosity measurements were performed at the French Comission of Nuclear Energy, in Marcoule (CEA Marcoule). The XRD, SAXS measurments, some of the dried SEM and all the wet SEM imaging were realized at Marcoule Institute of Separative Chemistry (ICSM).

3.1 Materials: Chemicals and Substrates

1,2-propanediol (purity 99.5%) and purified n-octanol (purity 98%) were purchased from Roth and VWR respectively. 1,3-propanediol (purity 99%) was purchased from Alfa Aesar. Cleaning ethanol (purity 99.8%) and acetone were purchased from Sigma Aldrich and Backed analysed respectively. Silicon wafers with artificially grown oxide layer, 300 nm thick, rms roughness $\simeq$0.4 nm[3] were purchased from LAM Research, Austria. 2 $\times$ 2 cm glass microscope slides were used as substrate for the confocal microscopy experiments. The "piranha" solutions, used for cleaning purposes, were prepared by mixing 1 volume of H_2O_2 (35%) with 2 volumes of H_2SO_4 (conc. 96%). Oxalic acid (purity 99.999%) and cerium nitrate (purity 99.99%, trace metals basis) both from Sigma Aldrich, were used as reactants.

3.2 Methods

3.2.1 Solutions and substrate preparation

All glassware were cleaned using a well established procedure. They were successively rinsed with acetone, ethanol and Milli-Q water. Dishes were then cleaned using "piranha" solution, rinsed with Milli-Q water, before being sonicated at 3,000 Hz for 30 minutes, rinsed a last time and dried overnight in an oven. Solvent mixtures were prepared less than 6 hours before finalizing the solution, by weighting the desired quantity of water, 1,2-propanediol and 1,3-propanediol into a beaker. For most solutions, the desired amount of reactant was introduced in a 5 mL freshly cleaned graduated flask, which was then filled with the solvent mixture, sonicated at 45 °C and 1.000 Hz in order to accelerate the reactant dissolution. The graduated flask was then diluted to volume with the solvent.
Regarding the experiments with structured solvent (See Sec:4.5), 25 mL of solvent mixture was prepared by weighting water, 1,2-propanediol and n-octanol into a 50 mL centrifuge tube. The mixture was separated at the desired temperature, using a cooled Heraeus Biofuge Primo R centrifuge for 90 minutes at 500 rpm. The two liquid phases were removed using micro-pipettes. Afterwards, the cerium nitrate and oxalic acid solutions were prepared following the above described steps.

3.2.2 Drop coalescence

High contact angle sessile drops coalescence in oil

A Teflon plate with a marked, approximatively 2 mm deep, T-shape is placed inclined in a glass cuvette filled with commercial Tetra Propylene Hydrogen, designed in the following as TPH. One of the drops is deposited at the intersection of the T-lines using a micropipette. The second drop is deposited at the edge of the T-feet using a second micropipette. This drop rolls along the T feet until it reaches the T-intersection. Then the two drops coalesce(See Fig: 3.1). The whole process is recorded using a high speed camera (Photron, Fastcam SA3) at a recording speed between 2,500 and 5,000 frames per seconds.

Low contact angle sessile drop coalescence in air

The coalescence of sessile drops experiments were performed in a closed chamber with controlled temperature and humidity. Two 6 µl drops, one containing oxalic acid and

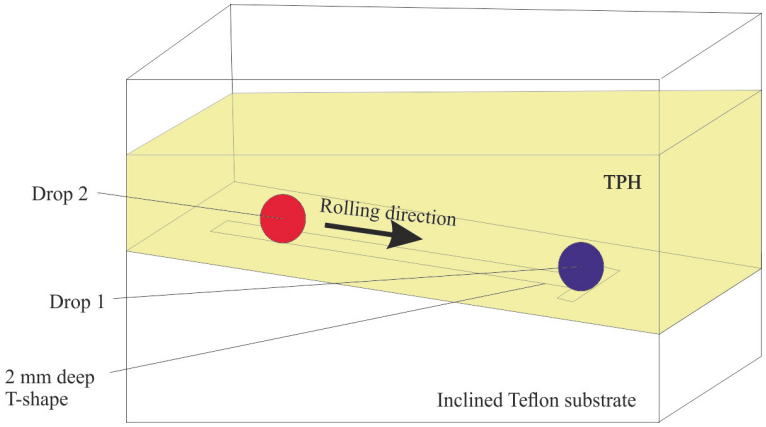

Figure 3.1: Schematic and picture of the set-up used for the coalescence of sessile drops with high contact angles.

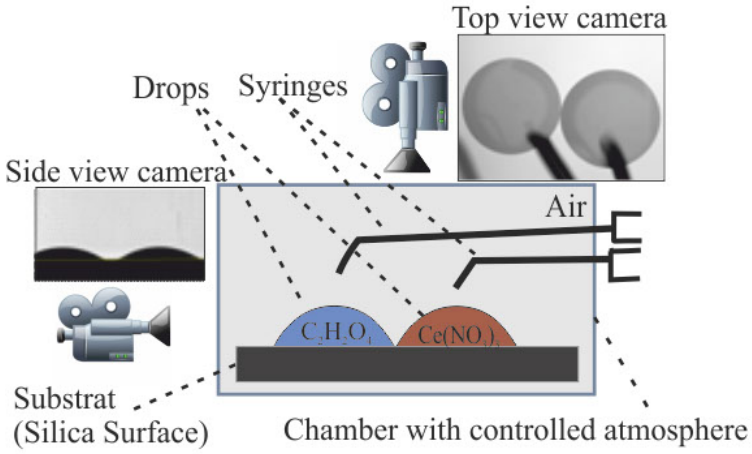

Figure 3.2: Schematic of the set-up used for the imaging of sessile drop coalescence. Two drops are deposed on a silica surface using syringes quickly removable after drop deposition. The droplet coalescence is record simultaneously from the top and the side view. Insert are images taken from each view. The coalesce occurs in a temperature and humidity controlled chamber.

one containing cerium nitrate, are deposited on a silica surface using glass syringes (see Fig. 3.2). Thus, avoiding charge effects or PDMS contamination as it has been evidenced when drops have been shaped using plastic tips[78, 79]. The two liquids wet the substrate completely. The drops spread, they get into contact by their three-phase lines and may coalesce. The whole process is recorded, at 70 frames per second, simultaneously from the side and from the top view. The side view is illuminated using a low divergence light and a telecentric lens and recorded with an object-space telecentric lens on a camera. A green light and a beam splitter are used to illuminate homogeneously the top view, recorded using a second camera and a macro lens[16]. With this set-up, only the light beam inclined by 45° with the beam splitter are transmitted to the camera. As a result, the particles, which are scattering light in the backward direction, appear as black area on the camera.

3.2.3 Solution's physico-chemical parameters

Densities were measured at 25 °C with an Anton Paar DMA 4100M densimeter. A Physica MCR 301 viscometer from Anton Paar is used in a Couette configuration to measure the viscosity of the solution at 25 °C. The viscosity is investigated for a rotation frequency ranging from 0.1 to 1000 s^{-1}. Surface tensions are measured by the pendant drop method[80] at 25 °C with a home made set-up[16]. The surface tensions of a given solvent mixtures were determined as a function of the reactant concentrations. The results appear to be a linear function of the reactants proportion in the concentration range investigated, hence allowing intermediate mixtures to be calculated from linear regression. In the case of diols/water solvent, this method was controlled by measuring the surface tension at a given concentration of reactants (i.e. oxalic acid or cerium nitrate) as a function of the 1,3-propanediol volume fraction. In that case the results are linear too, allowing again the calculation of intermediate mixtures from the linear regression.

3.2.4 Scattering and Microscopic techniques

Conventional Scanning Electron and Optical Microscopy

The obtained precipitates are dried in a two step process. First, nitrogen is introduced into the chamber for 15 minutes in order to evaporate part of the solvent. In a second step, the substrate is kept at room pressure and temperature for days (up to weeks) until total evaporation of the diols. Once the precipitates are dried, Scanning Electron

Microscopy (SEM) is performed either on a FEI QUANTA 200 ESEM FEG environmental electron microscope (ICSM) or on a LEO 1550 microscope from LEO GmbH Oberkochen (MPIKG) or on a Merlin microscope(CEA). In ICSM, experiments could be performed using the backscattered electron mode [51] that allow distinction between chemical species according to the molecular weight of the constituting atoms.
Complementary experiments are performed with an optical microscope. The sample is imaged using either an Olympus Provis AX70 (MPIKG) or a Nikon ellipse LV100 optical microscope (CEA). Optical microscopy can be held to image either dried precipitates or still wetted samples.

Confocal Microscopy Investigation

Confocal microscopy was used to investigate the dynamics of the solid growth, morphology and mobility inside the coalesced drop, at liquid state. For this purpose, a new chamber adapted to fit under a Leica DMIRBE confocal microscope was designed. The chamber is temperature (T=25 °C)and humidity (relative humidity; h=86%) controlled. For each experiment, both faces of a freshly cleaned glass microscope slide are spin-coated with 3 $\mathrm{mg\,L^{-1}}$ Rhodamine dye solution. Then, the slide is placed in the confocal chamber. The coalescence of the sessile drops is achieved as described in section 3.2.2. Two syringes are used to form two 6 μL drops above the glass substrate inside the chamber. One of the drops contains oxalic acid and the second one contains cerium nitrate. The drops are deposited some millimeters apart on the glass slide. Once the drop's coalescence is completed, the confocal microscope is adjusted to minimize the depth of focus. For each lateral location, the vertical position of the upper face of the substrate is first determined using the dye fluorescence. For this purpose, Rhodamine is excited with the 543 nm radiation of a HeNe laser. As soon as the drops have been deposited, part of the dye dissolves in the liquid drops. Since, the dyes migrate preferentially to the air/liquid interface, the vertical position can be determined. Confocal microscopy imaging was performed up to 2 hours after the drop coalescence was completed.

Structure determination

The X-Ray diffraction (XRD) measurements were performed on a Philips Xpert diffractometer equipped with a Kalpha detector. Due to the small volume of the coalescing drops and the restricted quantity of precipitates produced, the XRD experiments are performed directly on the dried substrates after the drop coalescence. For this purpose, the silicon wafer, with dried precipitates, is attached with modelling clay to an XRD

support placed upside-down. X-Ray diffraction patterns are measured for 2θ values between 5° and 90°, with a step of 0.016° between each investigated angle. Due to the unusual disposition of the support, the obtained XRD patterns are afterwards calibrated using the $2\theta = 67°$ peak of the silica mono-crystal wafer. Rietveld refinement was performed with TOPAS.

Volume/Fraction determination

Small Angle X-Ray Scattering (SAXS) experiments were performed on a home made device. The precipitates of 10 similar experiments are collected from the dried substrates using 1 mL of Milli-Q water. A 2 mm glass capillary is filled with this dispersion and is let for sedimentation during one week. For the calibration of the SAXS apparatus, Silver Behenate (SiBe) is used to calculate the sample/detector distance. The intensity is calibrated using polyethylene (PE). The X-Ray beam is directed at the level of the sedimented zone. The obtained patterns were analyzed with fit2D from ESRF (France) in order to calculate the image azimuthal average.

3.2.5 Phase diagram

Phase diagrams of water/1,2-propanediol/n-octanol mixtures were established at different temperature. For this purpose, two component mixtures (either water/diol or diol/n-octanol) at different volume fractions are stabilized in temperature in a water bath. The third component is added drop by drop until the mixture becomes cloudy. The points as determined form the phase boundary line. The solubility of n-octanol in water was determined by Karl-Fisher titration.

3.2.6 Image analysis

Side view: contact angle and height evolution

The side view was used to determine the contact angle of both drops at the contact time as well as the neck's and the drops height's evolutions with time, using a home made software, namely GolmCapture. The software allows to correlate the side and top view images thus offering a more accurate determination of the image at which the drops get into contact by their three phase line. Hence, both contact angles (for the cerium nitrate drop θ_{Ce}, and for the oxalic acid one, θ_{Ox}) can be measured by fitting the drop contour with a circle equation. For further data analysis, only the cases with similar θ_{Ce} and θ_{Ox} are considered. The baseline and its slope are adjusted using one of the images,

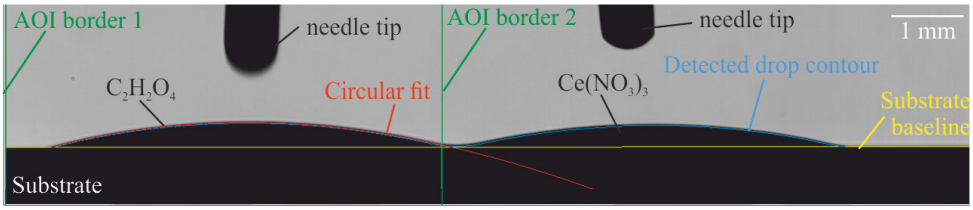

Figure 3.3: Side view of two sessile drops at the contact moment and determination of $\theta_{C_2H_2O_4}$. Yellow line: Input substrate baseline. Green lines: Input borders of the area of interest (AOI) regarding the fit. Blue curve: Drop contour detected by the software. Red curve: circle fit used for the contact angle measurement. In that case: $\theta_{C_2H_2O_4}$=12.8°

recorded prior drop deposition (See Fig:3.3). From the measured results, the average contact angle at the contact moment was calculated (See Eq:3.1).

$$\theta_a = \frac{\theta_{Ox} + \theta_{Ce}}{2} \tag{3.1}$$

Top view: surface flow speed and pattern wavelength

Speed of the surface flow

The speed of the pattern was obtained by following the position of a light-scattering fringe with time. This measurement is repeated for three different positions on the fringe, and the results average are considered to be the speed of the surface flow. t=0 s is set to the moment, when the two drops get into contact by their three phase line. However, this method leads to rather inaccurate results for the early time of the coalescence ($t \leqslant 0.5$ s), when the precipitates poorly scatter the light.

Patterns wavelength

In the case of periodic patterns, a fringe is defined as the combination of one strongly and one weakly light-scattering domain. Their wavelength evolutions are obtained by measuring the fringe widths along 5 different lines parallel to the Marangoni flow direction. Those results could be connected to the approximative appearance time of each fringe.

3.2.7 Calculation of the supersaturation ratio, s

The supersaturation ratio was calculated from equation 2.6 with the help of a CEA made SciLab code[6]. Through this code, the activities coefficient are calculated based on the

Davies modification[81] of the Debye-Hückel model (See Eq3.2). These modifications should only be applied, when the ionic strength of the system is moderate.

$$\log \gamma_i = \frac{-0.509 * z_i^2 * \sqrt{\frac{1}{2}\sum c_i z_i^2}}{1 + 0.329 * 10^8 * a_i * \sqrt{\frac{1}{2}\sum c_i z_i^2}} \tag{3.2}$$

where z_i , c_i and a_i are the charge number, the concentration in solution and the ion size of the ion i respectively. Furthermore, in the case of the oxalic precipitation of cerium nitrate and under the assumption of total dissociation of oxalic acid, the mean activity coefficient can be expressed as[82]:

$$\bar{\gamma} = (\gamma_{Ce^{3+}}^2 \times \gamma_{NO_3^-}^6 \times \gamma_{H^+}^6 \times \gamma_{C_2O_4^{2-}}^3)^{\frac{1}{17}} \tag{3.3}$$

The supersaturation ratio values calculated through this method are used in the following aim to give an overall measurement of the precipitation reaction, but are not meant to be exact. Indeed, in regard of the complexity of the oxalic precipitation, only few informations are available on the values of the related kinetic and thermodynamic constants, it is difficult to assure that the values of S presented hereby are accurate. However, the investigation of such constants is outside the scope of this thesis,

CHAPTER 4

RESULTS AND DISCUSSION

Nowadays, separation of chemical component by precipitation is a common industrial process, for example in water treatment, pharmaceutical or metallurgical industry. In the nuclear industry, oxalic precipitation is used to recover radioactive species from used nuclear fuel. This study was motivated by the development of a new process of oxalic precipitation, based on water in oil emulsion. This process could improve the production capacity and the safety concerning this step of the nuclear fuel reprocessing [6]. Oxalic precipitation is currently performed, at the industrial scale, in vortex reactors, whose size is limited due to criticality issues. The system gets rid of this issue when the precipitation occurs in a column apparatus supplied by a core of neutron absorbing material. Moreover, the water in oil emulsion configuration can be easily up-scaled. These two last points lead to the development of large columns with high production capacities.

In the vortex flow reactor, precipitation occurs by mixing two reactants, initially in completely miscible solvent. The process is highly sensitive to the mixing condition and feeding position (See Sec:2.1.4). Indeed, the control of precipitate properties is a key issue in the nuclear industry, where the precipitate morphology is important for the following steps of the recovery (suspension flowing and filtration). It is also of major interest in many non nuclear related industrial processes, for instance for the production of high valuable material as catalyst.

The aim of this study is to investigate both the effect of local flows and mixing conditions on the precipitate properties. This concerns mainly its amount, size and morphology. We studied also the impact of a precipitation reaction on the local flow conditions. For this purpose, different configurations, all based on the coalescence of

drops, were analysed. This chapter presents the results obtained. It is organized in five parts. In the first part, the effects of precipitation on the coalescence behaviour of drops immersed in a viscous medium is briefly analyzed. In the second part, the coalescence of low contact angle sessile drops, at substrate/gas interface, containing reactive species is investigated for 100% water as solvent. The third part focuses on the coalescence of sessile drops with independently controlled surface tension gradients and reactant concentrations by using water/diols mixtures as solvent. The fourth part presents how the precipitate features are linked to the experimental conditions. In the last part, preliminary experiments on the control of the precipitation, through the use of a ternary solvent, are presented and analysed.

4.1 Coalescence of "spherical" drops immersed in a viscous liquid.

The mixing resulting from the coalescence of "spherical" drops composed of identical liquids is well described in the literature, both experimentally and theoretically [83, 64, 63]. Fewer publications focus on the coalescence of drops containing different liquids [12]. To our knowledge, there are no quantitative studies concerning the impact of the flows on a chemical reaction following drop coalescence. A fundamental study of the flow induced by the coalescence of "reacting" drops is very interesting, both concerning the recent developments of microfluidics and the development of emulsion based processes.

This study first focuses on the interplay between a precipitation reaction and the flow induced by the coalescence of "spherical" drops immersed in oil. Aqueous drops on a Teflon substrate were chosen as a model system for studying the coalescence in the emulsion column. Hereby, the term "spherical" drop refers to a drop deposited on a substrate with which it forms a high equilibrium contact angle. In a first approximation, it is assumed that the coalescence of flowing drops and high-contact angle aqueous drops deposited on a hydrophobic substrate in oil are governed by the same mechanisms. In both cases the drops get in contact by their oil/water interfaces.

This section consists in a brief description of the coalescence of "spherical" drops. Two systems have been investigated. In the first part, the coalescence of drops containing reactants is investigated. In the second part, the case of inert, or non-reactive, drops has been analyzed and compared to the precipitating system.

4.1.1 Coalescence of "spherical" drops containing reactive species

The "spherical" drop model system is composed of two aqueous sessile drops on a hydrophobic substrate, namely Teflon (See Sec:3.2.2 for details). One of the drops is at rest on the substrate while the second one rolls down along a guiding track to the immobile drop (with a speed of typically $15\,\mathrm{mm\,s^{-1}}$). The drops have contact angles over 90°. They touch each other at their liquid/liquid interfaces. Once in contact, the drop coalescence is driven by capillarity. The first seconds of this process were recorded by a high speed camera (3500 fps) in a plane perpendicular to the contact plane. The maximum recording time of the camera (typically $\leq 3\,\mathrm{s}$) is limited by its internal memory as well as the field of view. In all cases, the drops were immersed in TPH (Tetra Propylene Hydrogen), an organic phase, with a viscosity of $1.3\,\mathrm{mPa\,s}$ at

20 °C.

Oxalic precipitation of cerium

Oxalic precipitation of cerium was chosen as a model system for the chemical reaction. Precipitation usually produces easily observable particles. Moreover, this reaction is a common model for the precipitation of actinides, where cerium is a substitute for plutonium. In aqueous solution, cerium nitrate and oxalic acid react and form insoluble cerium oxalate according to equation 2.5 (See Sec: 2.1.4).

Precipitation following "spherical" drop coalescence

The sequence in Figure 4.1 presents the coalescence of a rolling cerium nitrate drop with a resting oxalic acid drop in TPH. Both drop volumes are 8 µl, which corresponds to a diameter of 12 mm. First the two drops contact each other. After few milliseconds, they form a connecting liquid bridge. The first image, on which the bridge can be clearly distinguishable, was set as time zero.

The coalescence proceeds in three consecutive steps. First, a liquid bridge between the two drops is formed and is rapidly growing, typically in 5 ms. A thin membrane of precipitate can be distinguished right away inside the liquid bridge. The precipitate membrane remains at the contact area. It forms a barrier, which separates vertically the daughter drop. In a second step, this drop begins to oscillate. This capillary wave lasts around 10 ms. During this process, the precipitate remains in the drop center. In a last slower step, the drop rotates until the precipitate membrane gets horizontally placed. The time scale of this rearrangement is typically half a second. As a result, the final drop is divided into two hemispheres separated by the precipitate membrane, with the upper hemisphere containing oxalic acid and the lower one cerium nitrate.

This is similar to Lombardi et al. [84], who observed a horizontal rearrangement of liquids during the coalescence of sessile drops with different densities. They used salt and glycerol to vary the density independently from the viscosity and fluorescent dye to distinguish the two initial liquids. As in the third step presented here, the rearrangement occurs after the neck growth is completed. The authors ascribe this flow to gravity. The rearrangement leads to the lighter liquid being localized on top of the heavier one. The densities of the solutions used in the reactive case are summarized in table 4.1. The less dense oxalic acid half drop is located in the upper part of the drop, as expected from gravity driven rearrangement. Moreover, if gravity is indeed the origin of the observed

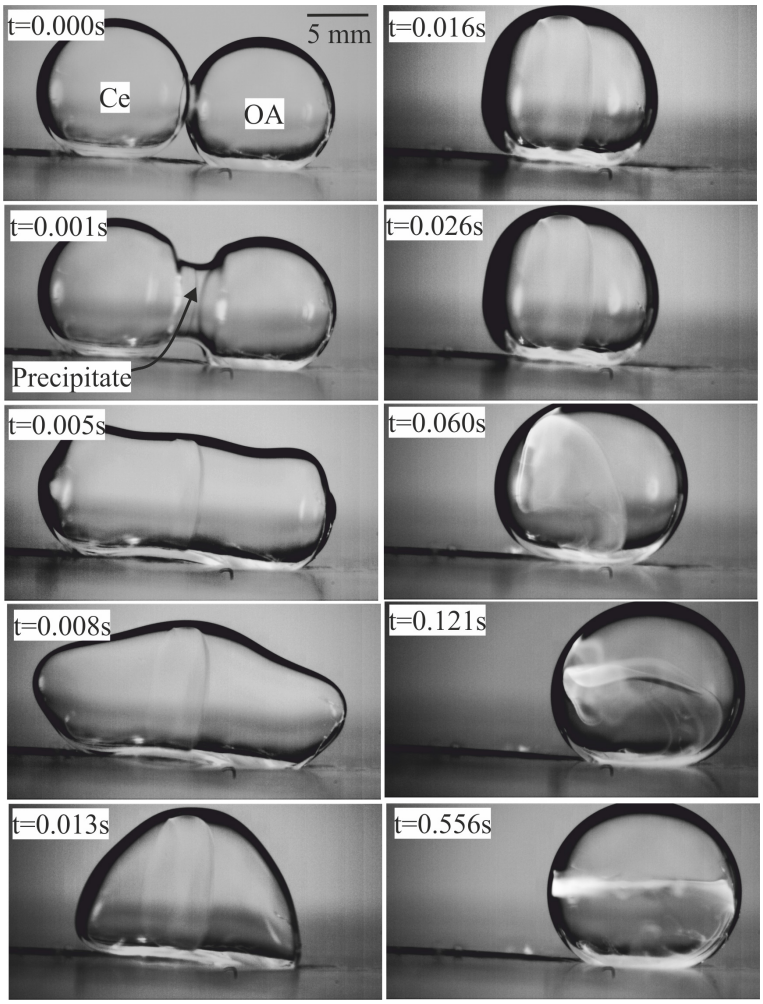

Figure 4.1: Coalescence of "spherical" cerium nitrate and oxalic acid drops in TPH. The immobile drop (right one) contained the oxalic acid (0.7M) and the moving one (left one) cerium nitrate (0.17M)

rearrangement, the final position of the liquids should be independent from the initial drops configuration, *i. e.* which drop is at rest or mobile.

This was been investigated. In Figure 4.2 a drop containing oxalic acid rolls on the substrate until it touches a drop of cerium nitrate which is fixed. The coalescence process follows the same three steps as previously described. A precipitate barrier is clearly distinguishable after 3 ms. After the final drop rearrangement, now again, the oxalic acid is located in the higher part of the daughter drop, as in the previous configuration and in agreement with a gravity driven flow.

In both configurations, the precipitate seems to form a barrier between the two volumes

	TPH	Oxalic acid	Cerium nitrate
concentration (M)	-	0.70	0.17
density	0.75	1.03	1.05
Interfacial tension (mN.m-1)	-	31.8	34.3

Table 4.1: Solution density and interfacial tension in TPH.

of the daughter drop, which prevents mixing and hinders the precipitation reaction.

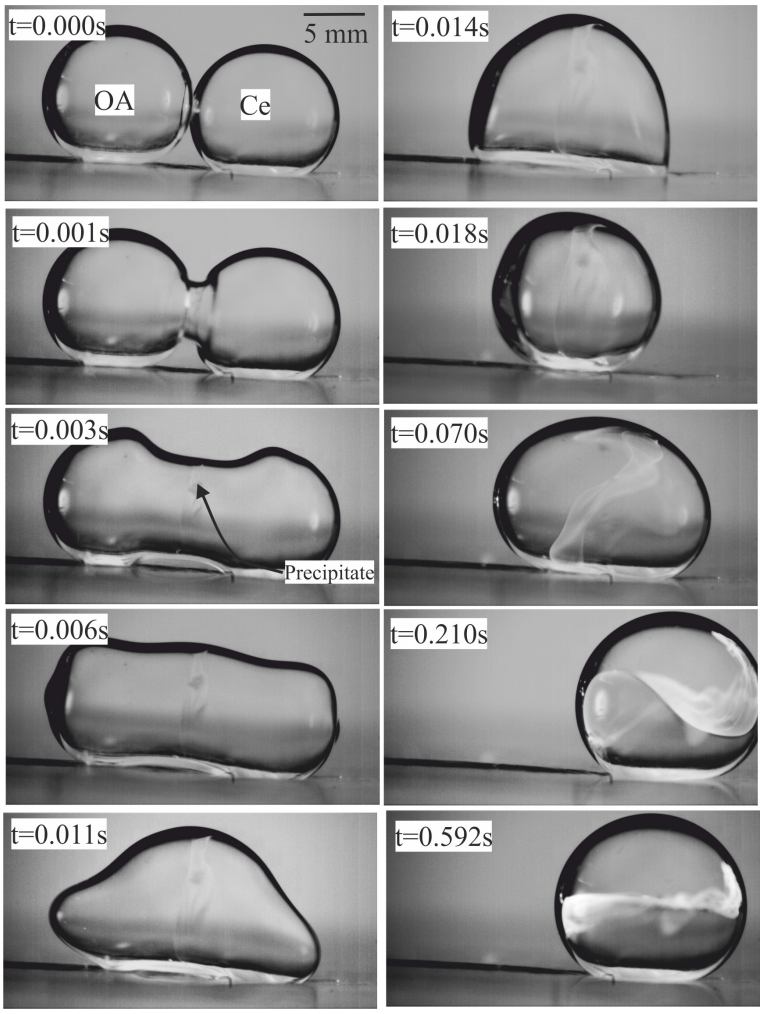

Figure 4.2: Coalescence of 8 µl high contact angle drops in TPH. A drop containing oxalic acid (0.7M) is moving toward a fixed drop of cerium nitrate (0.17M).

To conclude, during the coalescence of two "spherical" drops, one containing oxalic acid and the second one cerium nitrate, the precipitation occurs in the contact region between the two drops. A precipitate membrane appears, which restricts the amount

of mixing between both liquids and thus hinders the precipitation reaction. In a last step, on the time scale investigated, the liquid rearrangement inside the daughter drops is driven by gravity. The membrane is conserved during this step preventing mixing, at least at a short time scale. In this configuration, although there is a surface tension difference between the liquid of both drops, no Marangoni flow has been observed. This configuration is not adequate to investigate the link between flow and precipitation reaction.

4.1.2 Coalescence of high contact angle drops with non-reactive liquids

Coalescence of drops without reactants has been investigated in order to determine, if the mixing obtained during the coalescence of reactive "spherical" drops is hindered by the precipitate barrier. Both drops contain oxalic acid (0.7M). Methylene blue (MB) is added to one of the drops in order to trace the resulting mixing (Fig:4.3).

In that case, the two drops again get in contact via their oil/water interfaces. The coalescence mechanism appears similar to the reactive case. The bridge growth, promoted by the capillary forces, is complete in 5 ms. The resulting elongated shape then rearranges in a spherical drop within a few millisecond. During the whole process, no substantial mixing is observed between the liquids of the two drops. The MB remains to the left side of the daughter drop at the end of the first step. The separation between the BM-free and BM-rich domains is initially vertical. Then, as in the precipitating case, the drop rearranges further until the separation between the two drop volumes is horizontal. However, this process is slower than with reactive drops ($\simeq$1 s). The rearrangement is suppository driven by gravity also in the non-reactive case.

4.1.3 Conclusion on coalescence of water drops in oil

To conclude, during the coalescence of "spherical" drops in oil, three processes can be identified. First, a liquid bridge is formed and is growing between the two drops. Then, capillarity tends to minimize the surface energy. As a results, the daughter drop becomes spherical. In a last step, the liquids rearrange inside the drops due to gravity. In the final state, the daughter drop is divided by a horizontal layer, with the heavier liquid located on the bottom. In case of precipitation following drop coalescence, the product remains confined in the plane divided the two drop volumes. The coalescence

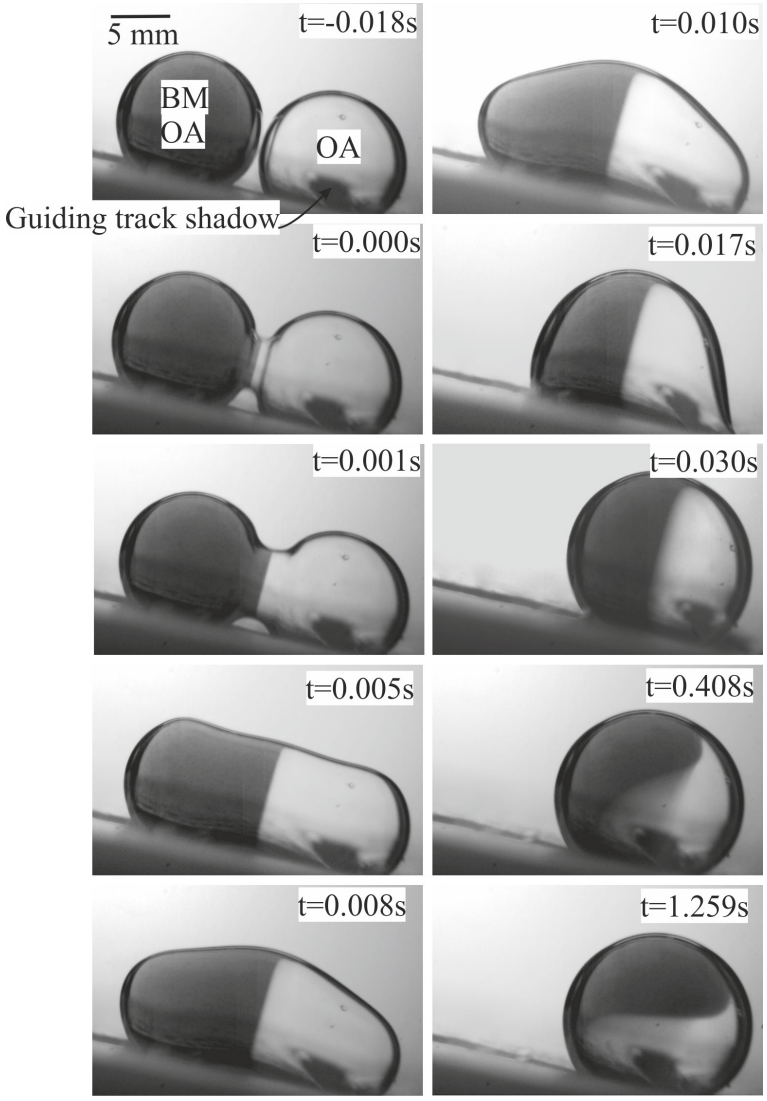

Figure 4.3: Coalescence of high contact angle sessile drops in oil media. Both drops contain oxalic acid (0.7 M), methylene blue (MB) has been added to the mobile drop (on the left).

behaviours are the same for reactive and non-reactive systems.

The coalescence of high contact angle sessile drops in oil does not lead to a substantial mixing between both liquids on a short time scale. This makes the system inadequate to investigate the links between flow and precipitation reaction. There are several ways to increase mixing between both drops. For instance, the coalescence of drops with very different volumes would lead to a capillary flow, increasing the mixing between both liquids [83]. Alternatively a strong surface tension gradient could lead to a Marangoni flow. In air, it has been shown that Marangoni flow may even be strong enough to delay temporarily the coalescence of low contact angle sessile drops [16]. The latter phenomena was chosen to investigate the link between a precipitation reaction and flows.

4.2 Sessile drop coalescence and precipitation with pure water as solvent

So far, the coalescence of "spherical" drops followed by precipitation has been introduced. However, the low mixing generated in this configuration restricts the chemical reaction. This makes such a configuration inadequate for our study of the link between flow and precipitation. Regarding the coalescence of low contact angle sessile drops in air, Karpitschka and Riegler [16] demonstrated, that high surface tension difference produces an additional flow. This Marangoni flow, always directed from the low surface tension domain to the high surface tension one, is quite strong. Under certain conditions, it may even dominate the droplet coalescence behaviour and cause temporary "noncoalescence" (See Sec:2.2.3). This was shown for drops with non-reactive (or inert) liquids. Marangoni flow may be a good process to improve the mixing during the coalescence of drops containing reactive species.
The focus will be on the interplay between precipitation and Marangoni flow. A model system composed of two aqueous sessile drops in air, deposited on a smooth silica surface, with contact angle below 20°, is used. One drop is composed of an aqueous solution containing oxalic acid, in the other one cerium nitrate is dissolved (for further details about the coalescence set-up, refer to Sec:3.2.2). In the following, the coalescence and precipitation behaviour of sessile drops will be investigated as a function of the initial concentration of the reactants, *i.e.* supersaturation ratio, S, and surface tension difference, $\Delta\gamma$ between both drop liquids.

4.2.1 Mixture characteristics

Supersaturation ratio

Supersaturation is the driving force for precipitation The level of supersaturation in the precipitating solution governs the rates of individual components, such as nucleation, growth, and Ostwald ripening [85].
The supersaturation ratio is calculated using equation 2.6 through a SciLab home-made code. The calculation of activity coefficients was based on the Davies model (See Sec:3.2.7). The initial concentrations of the drops were chosen as reactant concentrations. The results are shown in Figure 4.4.
In general, the values calculated for the supersaturation ratio depend on the model used. Moreover, the supersaturation is not representative of the local concentrations. Here,

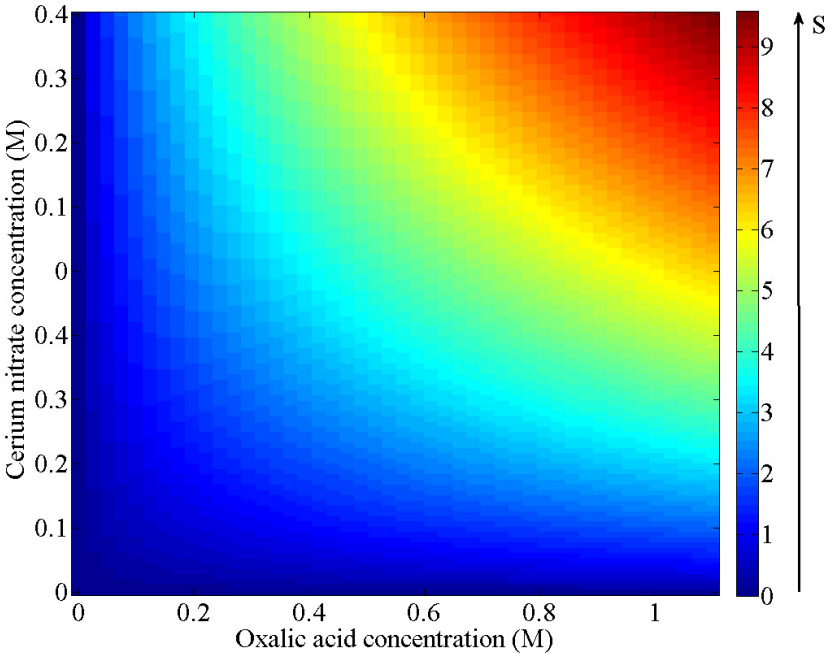

Figure 4.4: Global supersaturation ratio, S, as a function of the initial oxalic acid and initial cerium nitrate concentrations.

we use S as a general measure for the precipitation conditions.

Surface tension

The surface tension of the initial mixture is displayed in figure4.5. The solid lines are the experimental values measured at 25 °C by the pendant drop method. The experimental data from Hyvärinen et al. [86] (dashed line) are shown for comparison. Cerium nitrate depletes at the air/water interface. Consequently, the surface tension of its solution increases with increasing concentration. Oxalic acid is a "capillary-active substance". The surface tension of an oxalic acid solution decreases with increasing concentration. It is energetically more favourable for the molecule to be at the air-liquid interface. Although the tendency is the same between our experimental values and the Hyvärinen data set, the surface tensions measured here are systemically higher. This gap is probably induced by calibrating the data with different values for the surface tension of water at 25 °C.

In the following, we will consider the surface tension difference of the oxalic acid and cerium nitrate solutions, $\Delta\gamma = \gamma_{Ce_2(NO_3)_3} - \gamma_{C_2H_2O_4}$. The Marangoni flow is generated

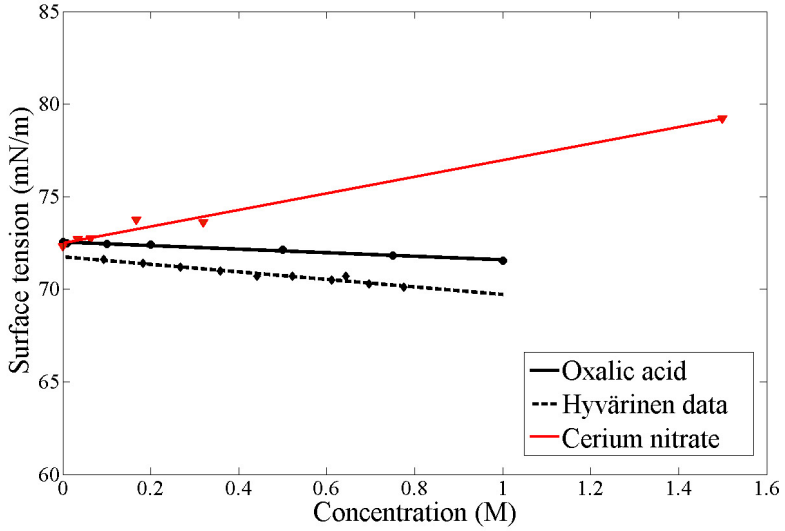

Figure 4.5: Surface tension of aqueous solution as a function of the reactant concentration at 25 °C. Solid line: experimental data from this study. Dashed line: Experimental data from Hyvärinen et al. [86]

by the surface tension difference between the two liquids. Hence, the control parameter is $\Delta\gamma$, and thus the slope in Figure 4.5 only matters. This flow is always directed from lower surface tension area to higher surface tension area (See Sec:2.2.3). Marangoni flow is expected to go from the oxalic acid drop to the cerium nitrate drop.

In this section, we will only consider the cases, for which immediate coalescence is observed. This behaviour is characterized by a fast growth of the neck between the two droplets as soon as they contact. Typically, this process takes less than a second. The surface tension gradient considered, $\Delta\gamma$, ranges between 0 and 4 mN/m for typical average contact angles between 5° and 20°. For more details on coalescence and non-coalescence regimes see section: 4.3.2

The coalescence experiments were performed under high humidity to reduce the solvent evaporation. Water condenses on the chamber walls and windows, if the air environment is saturated in water (*i. e.* 100% relative humidity). Hence, the experiments were realized at 93% relative humidity at 25 °C.

4.2.2 Precipitation patterns

The coalescence behaviours were investigated for cerium nitrate concentration below 0.8M and oxalic acid concentration below 1.1M (See Fig:4.6). A solubility limit of 1.2M in water at 20 °C was determined experimentally for the oxalic acid. When one of the reactants concentration was lower than 0.05M, no or very few precipitates could be observed. These cases were not investigated further.

For concentrations of both reactants above 0.05M, solid particles can be observed in the region of the initial cerium nitrate drops. Three precipitation regimes were found as a function of the reactant concentrations. For $[Ce(NO_3)_3] \leq 0.3[C_2H_2O_4]$, (case I), particles, which strongly scatter light are formed. For $[Ce(NO_3)_3] \geq 0.3[C_2H_2O_4]$, (case II), a large weakly scattering-light area surrounded by a strongly scattering light boundary is produced. At the transition range between both cases, indications of a periodic precipitation pattern were found (case III). The width of concentration, over which periodic precipitation occurs, is very narrow. Experimental results show, that the contact angle between both drops at the moment of contact does not influence the precipitation behaviour.

It can be seen in Figure 4.6 that the transition in the precipitation regime is governed neither by the system stoichiometric nor by the surface tension difference. Indeed, different reactant concentrations may give rise to an identical surface tension difference but different precipitation regimes. For example, the combination $[Ce(NO_3)_3]$=0.16 M/$[C_2H_2O_4]$=0.24 M leads to a weakly light-scattering pattern, whereas the combination $[Ce(NO_3)_3]$=0.10 M/$[C_2H_2O_4]$=0.55 M results in strongly light-scattering particles. In both cases, $\Delta\gamma = 0.9\,\mathrm{mN\,m^{-1}}$. In a similar way, the comparison between Figures 4.4 and 4.6 enables to conclude, that the supersaturation ratio is not the control parameter between the precipitation regimes. Instead, the domains are separated by a line, which indicates, that the ratio of both reactants is the control parameter.

4.2.3 Precipitation pattern evolution

The flows generated by the coalescence of sessile drops influence the precipitation patterns. The pattern evolution along the coalescence process was recorded from the top view for the two major precipitation regimes (See Fig:4.7 and 4.8). Here we do not discuss the boundary case, which will be presented in details in the following chapter. The first frame, where the drops come into contact, was used to define time zero.

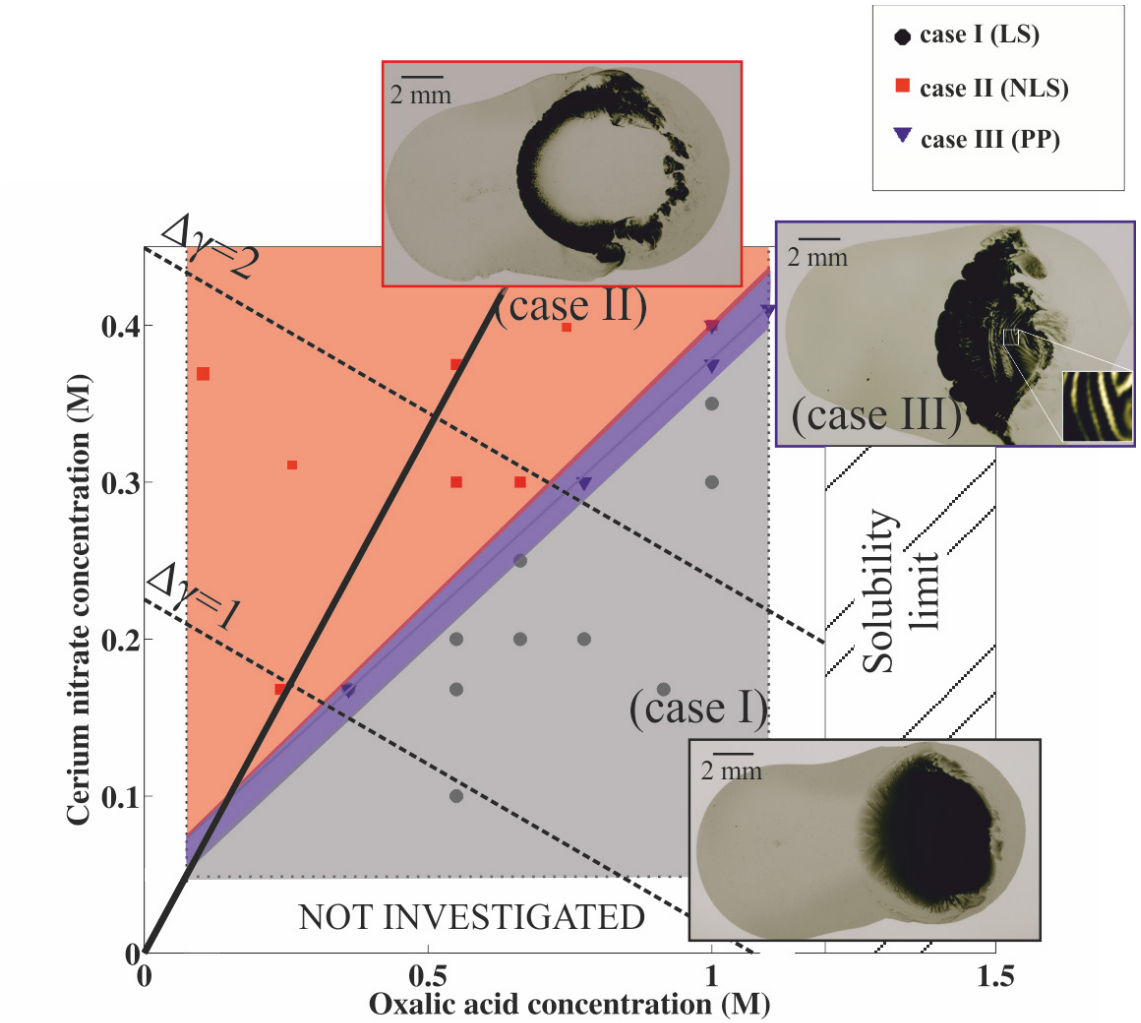

Figure 4.6: Phase diagram of the precipitation regimes obtained in pure water solvent. At high concentration in oxalic acid (case I), a homogeneous domain, which strongly scatters light, precipitates. At high concentration in cerium nitrate (case II), a large weakly light-scattering domain surrounded by a strongly light-scattering boundary is formed. There is evidence of a periodic pattern in the transition range (case III). Solid line: stoichiometric line. Dotted line: iso-surface tension difference line.

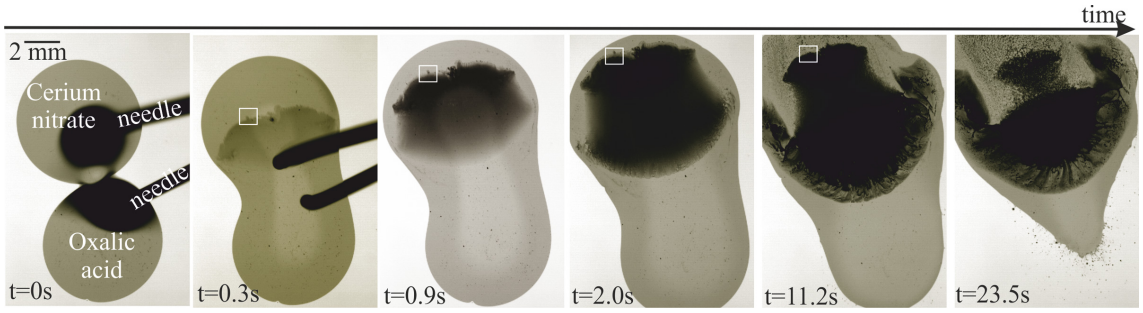

Figure 4.7: Evolution of the light-scattering pattern, case I, as a function of time. White squares surrounding a front line detail. At t=0 s, the dark spots on the drops are curvature effects. Conditions: $\Delta\gamma$=1.1 mN m^{-1} and drop composition ($[C_2H_2O_4] = 0.36M$ and $[Ce(NO_3)_3] = 0.17M$)

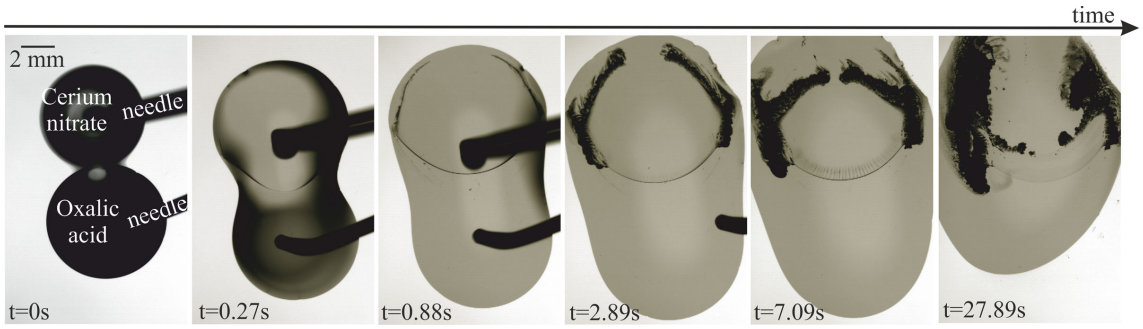

Figure 4.8: Evolution of the precipitation pattern, in case II (high amount of cerium nitrate), as a function of time. At t=0 s, the drops appear dark due to their high curvature. Conditions: $\Delta\gamma$=4.9 mN m^{-1} and drop composition ($[C_2H_2O_4] = 0.24M$ and $[Ce(NO_3)_3] = 0.84M$)

In both cases, a macroscopic liquid film is formed between the two drops as soon as they get into contact at their three-phase line. The fast growth of the neck evidences the rapid drop coalescence. Hereby, we define coalescence according to the evolution of the drop contour into a single drop.

In the oxalic acid rich domain (case I), a strongly light-scattering precipitation pattern is formed over the cerium nitrate drop in less than half a second. Precipitates are pushed away from the neck region of the drops over the cerium nitrate drops. The solid moves from the oxalic acid solution (low γ) to the cerium nitrate solution (high γ). This is coherent with the direction of the Marangoni flow. The front line contour is stable along time. In other words, the particle precipitates in the contact region of the drop before be-

ing pushed by the Marangoni flow over the high surface tension drop. Simultaneously, new precipitates are created in the neck. It takes around a second for the precipitates to completely cover the initial cerium nitrate drop. Then the Marangoni flow vanishes. Afterwards the precipitates begin to collapse through the center of the daughter drops. This process is much slower (typically tens of seconds).

In the case of high cerium nitrate concentration (case II), a black narrow line is observable in the neck region between the two drops typically 0.1 s after the drop contact. In a second step (t=0.9 s), another narrow line is formed at the opposite side of the cerium nitrate drop, while the center of the drop is only weakly scattering the light. The line becomes thicker, up to 0.5 mm. In a last step, the precipitate is pushed toward the center of the daughter drop, in a process similar to the shrinkage observed in case I.
In case II, the formation of an isolated narrow line of precipitates far from the contact area is quite astonishing regarding the high initial supersaturation, at which these experiments are performed. This leads to the suggestion, that numerous weakly light-scattering precipitates are present over the cerium nitrate drop center.

4.2.4 Surface flow speed

Front line velocity inside a sample

Hereby, the front line designs the line of the first precipitates formed at the neck, that are localised at the edge of the Marangoni flow, in the case of a strongly light-scattering pattern. The displacement of particular details present along this front line can be followed with time. The pattern velocity, in case I, will be associated to the front line velocity, v_{fl}, determined by following the front line distinctive details.
To check the homogeneity of the precipitate velocity along the front line, the speeds of four distinct positions have been measured as a function of time inside a sample. The typical speed evolution resulting from this analysis is displayed in Figure 4.9. The insert represents the final state of the sample, on which the details investigated are reported. As usual, time origin was set at the moment of contact between the two drops. The dashed lines are a guide to the eyes.
The speed of the front line is homogeneous inside a sample. Its decreases rapidly from initially around 15 mm s^{-1} to few $mm.s^{-1}$ after half a second. Two possible reasons are considered for the decrease of the front line speed with time. First, this could be caused by a progressive decrease of $\Delta\gamma$ with time, due to solvent inter-diffusion and consumption of reactive species, leading to a weakening of the Marangoni flow. Secondly, the

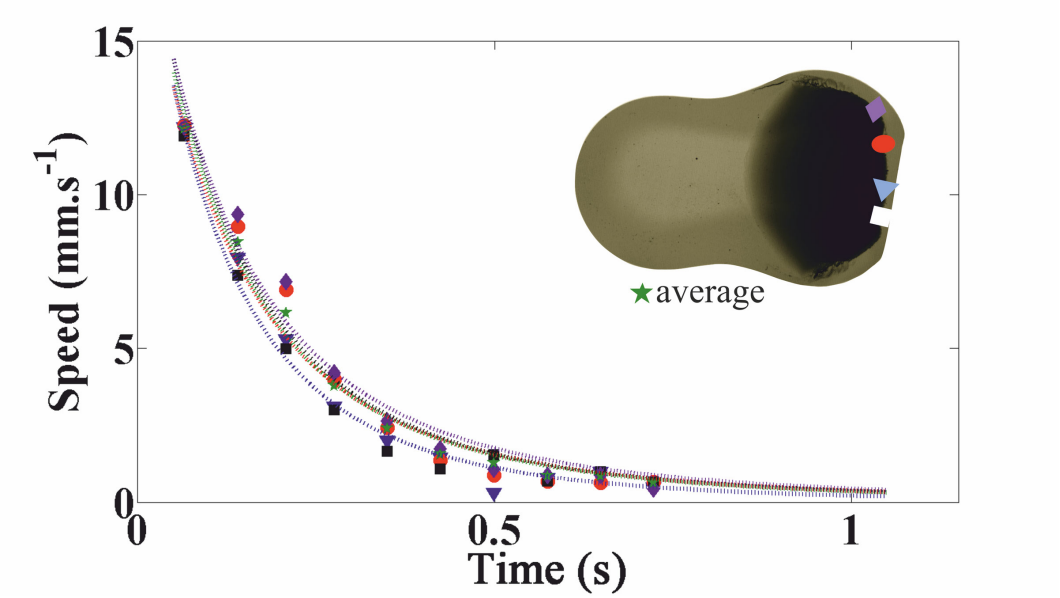

Figure 4.9: Speed of different front line positions inside a sample. Insert: final shape of the investigated precipitate and distribution of the distinct positions followed (symbols), Conditions: $\Delta\gamma$=0.9 mN m^{-1} and drop composition ($[C_2H_2O_4] = 0.8M$ and $[Ce(NO_3)_3] = 0.08M$).

presence of solid particles, resulting from the precipitation, probably induce shear stress which would lead to the same effect.

Flow speed as a function of θ_a and $\Delta\gamma$

Karpitschka and Riegler [18] have shown that $\Delta\gamma$ and θ_a are the control parameters for the coalescence behaviour of sessile drops composed of inert liquids in air. In the following, the effect of those parameters on the Marangoni flow speed during the rapid coalescence of drops containing reactants will be investigated.

Variation of θ_a

Figure 4.10 shows the precipitate front line speed as a function of time for three different values of the average contact angle at a given concentration of reactants and surface tension difference. The same tendency is observed as previously, the speed decreases rapidly in half a second from tens to few $mm.s^{-1}$. The speeds are identical in the three cases. In other words, the surface flow speed is independent of the average contact angle.

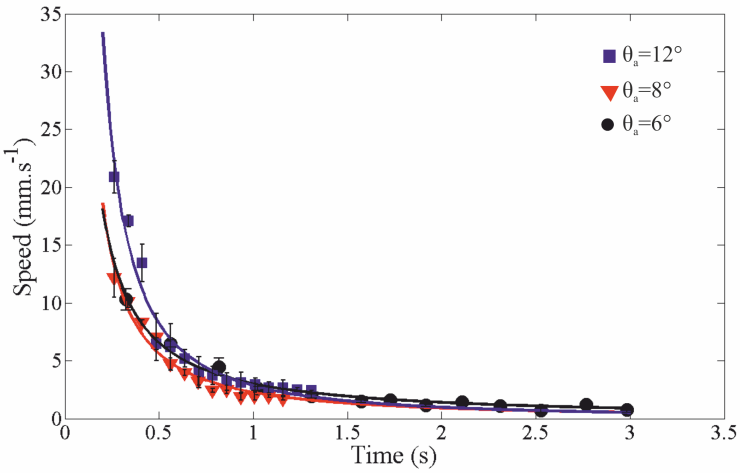

Figure 4.10: Speed of the precipitate front for different θ_a. In the three cases $\Delta\gamma = 1.8\,\mathrm{mN\,m^{-1}}$ and $[C_2H_2O_4] = 1.1M$ and $[Ce(NO_3)_3] = 0.17M$.

Variation of $\Delta\gamma$

The influence of $\Delta\gamma$ on the front line precipitates has been investigated (See Fig:4.11). Surprisingly, this speed does not depend on $\Delta\gamma$. As previously, the initial front line speed, tens of millimeters per second, rapidly decreases. A second after the coalescence, the precipitates move with a speed below $2.5\,\mathrm{mm\,s^{-1}}$.

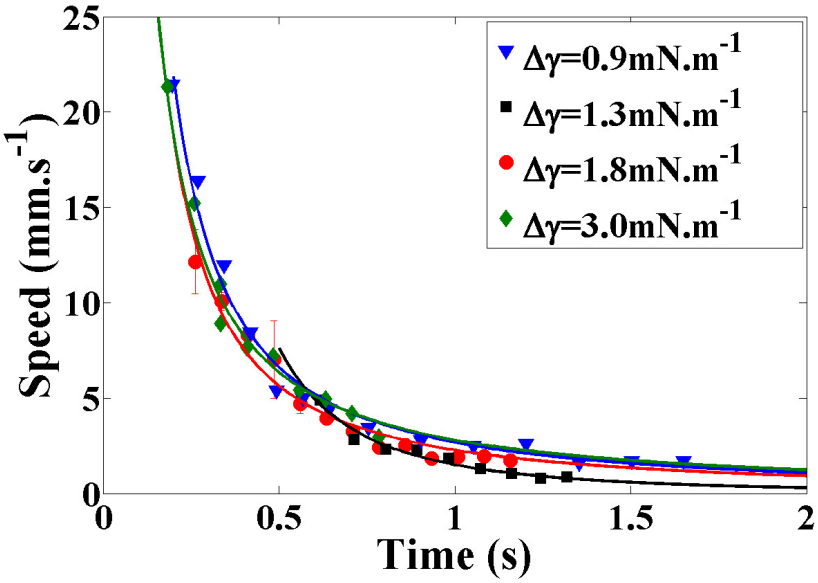

Figure 4.11: Speed of the front line as a function of time for $\Delta\gamma$ varying between $0.9 - 3.0\,\mathrm{mN\,m^{-1}}$

The surface flow speed at high cerium nitrate concentration (case II) could not be measured due to the absence of sufficiently light-scattering particles.

4.2.5 Conclusion on precipitate pattern in pure water solvent

To conclude, three precipitation patterns were observed during the rapid coalescence of low contact angle sessile drops in air. These precipitation regimes are controlled by the ratio of the reactant concentrations. At high ratio in oxalic acid (case I), a strongly light-scattering precipitation pattern is covering the cerium nitrate drop after some seconds. At high ratio in cerium nitrate (case II), a central domain scattering weakly the light is surrounded by a boundary of strongly light-scattering precipitates. The transition between these two regimes occurs for $[Ce(NO_3)_3] \sim 0.3[C_2H_2O_4]$. Indications of periodic precipitation were found in the transition zones (case III).

In the three cases, the Marangoni flow plays a major role in the spacial distribution of the precipitates. This flow decreases rapidly from tens to few $mm.s^{-1}$. The particle speed is independent of $\Delta\gamma$ and θ_a, in the case of strongly light-scattering precipitation.

However, this system presents a major drawback. The surface tension difference between the liquid drops , $\Delta\gamma$, and the supersaturation ratio, S, are linked by the concentration in reactants. Thus, changing the supersaturation ratio leads to a modification in $\Delta\gamma$.

4.3 Variation of surface tension and viscosity

So far, the precipitation reaction has been linked to the Marangoni flow through the reactant concentrations. Indeed, the surface tension difference, $\Delta\gamma$, which is at the origin of the Maranoni flow, depends on the surface tension of each solution, *i.e.* the reactant concentrations. On the other hand, the reaction supersaturation ratio, S, is linked to the reactant concentrations or their activities. In this part, a solution to decorrelate the surface tension from the concentration in reactive species is proposed, applied and analyzed.

4.3.1 Effect of non reactive species

Water/diols mixtures

Adding a third specie as a surface active agent, is the most common way to change the surface tension of a solution [80]. In the case of precipitation in sessile drops, it is a promising way to vary the surface tension difference between the two liquids without modifying the concentration of reactants. However, the system should also reach the criteria listed below:

- The added species should be inert, *i.e.* non-reactive, regarding the reactants and the product of the precipitation.
- The surface tension change should not induce a significant variation of solution densities and viscosities.
- The distribution of the reactants inside the drop (interface vs bulk) should not be significantly modified by the additive.

1,2-propanediol and 1,3-propanediol are isomers with relatively close physico-chemical properties (see Table 4.2), but significantly different surface tension. They are completely miscible with water and react neither with oxalic acid, nor cerium nitrate, nor cerium oxalate. By mixing 50% water, x% 1,3propanediol and $(50-x)$% 1,2-propanediol as solvent, it is possible to vary the surface tension difference, $\Delta\gamma$ of the liquids between 0 mN/N and above 10 mN/m (see Figure 4.12) without modifying the reactant concentrations. This way, the solvent solutions of both drops have basically identical densities and similar viscosities.
Another advantage of this system lies in the higher viscosity of the solutions compared to the case with 100% water solvent. This induces a slower spreading of the drops,

	1,2-propanediol	1,3-propanediol
density (-)	1.06	1.06
viscosity ($mPa.s$)	58	53
surface tension ($mN.m^1$)	40	46

Table 4.2: Physico-chemical parameters of 1,2-propanediol and 1,3-propanediol

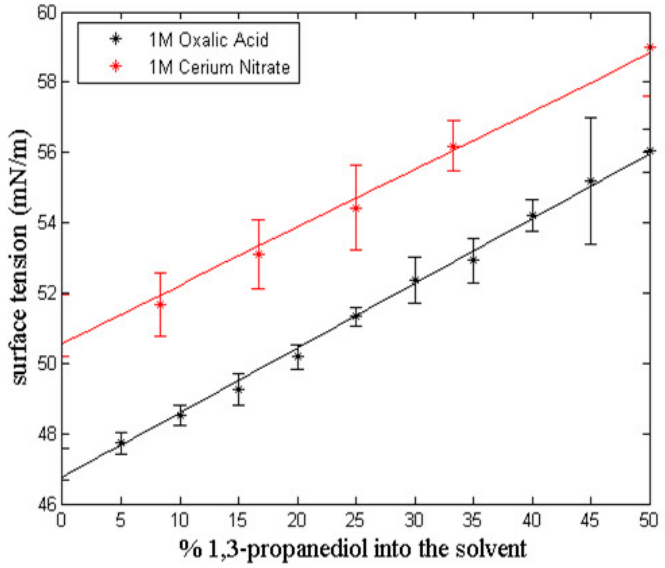

Figure 4.12: Surface tension of 1.1M oxalic acid solution (black) and cerium nitrate solution at 25 °C as a function of the volume fraction of 1,3-propanediol for 50% water/ 50%diols mixture as solvent. The solvent composition has to be read as 50% water/ x% 1,3-propanediols/ $(50-x)$% 1,2-propanediol.

before the coalescence, which facilitates the removal of the needles before the drops get into contact.

In the following, due to the unknown influence of the propanediols on the super saturation ratio, the precipitation reaction will be quantified by the oxalic acid excess, OE (see Eq. 4.1).

$$\mathrm{OE} = \left[\mathrm{C_2H_2O_4}\right] - 3/2\left[\mathrm{Ce(NO_3)_3}\right] \tag{4.1}$$

We keep the initial concentration of the oxalic acid solution at 1.1M. The oxalic acid excess is tuned only by changing the initial cerium nitrate concentration (see Eq:4.1). In our case, reducing the cerium nitrate concentration leads to an increase of OE. As

a comparison with the results from the previous section, the oxalic acid excess and the estimated corresponding supersaturation ratio, S, in pure water (See Sec:4.2.1), are displayed in Figure 4.13

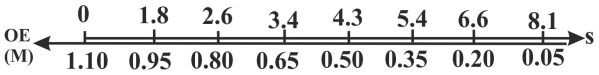

Figure 4.13: Comparison between supersaturation ratio and oxalic acid excess, in water as solvent, for a concentration in the oxalic acid drop of 1.1M

Equilibrium relative humidity

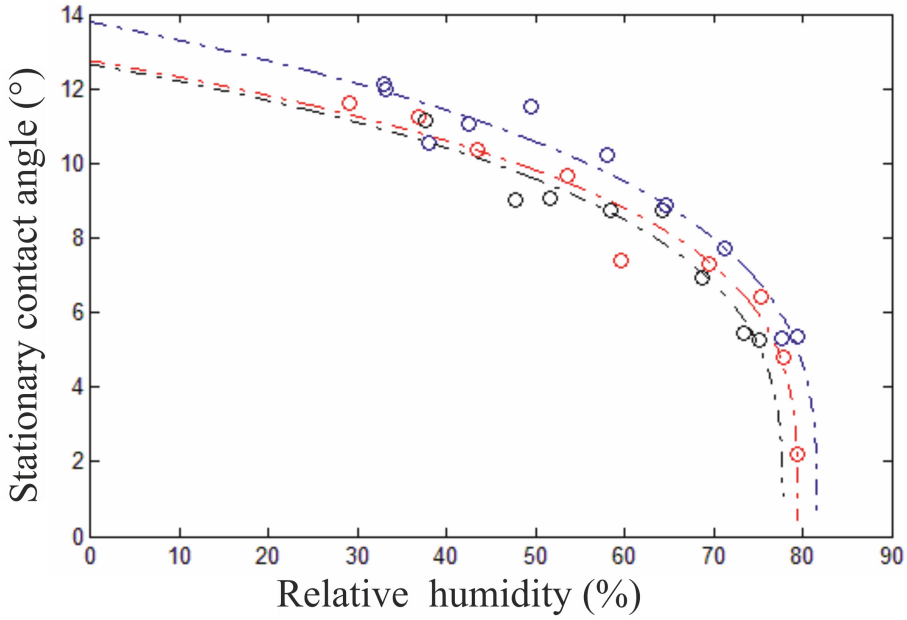

Figure 4.14: Stationary contact angle as a function of the relative humidity for several oxalic acid (1.1 M) mixtures. Mixture composition: red-50% water/50% 1,3-propanediol, black-50% water/5% 1,2-propanediol 45% 1,3-propanediol, blue-50% water/10% 1,2-propanediol 5% 1,3-propanediol. The x-axis intercept corresponds to the equilibrium relative humidity for the investigated solutions.

Propanediols have low saturation vapor pressure at atmospheric pressure. The equilibrium relative humidity of the mixtures, h_{eq} was measured in order to avoid evaporation

and reduce condensation of the drops in the coalescence chamber. This was performed by measuring the stationary contact angle $\theta(h)$ of the solution for different relative humidities. The curve of the equilibrium contact angle as a function of the humidity was fitted using equation 4.2[87].

$$\theta(h) = A * (h - h_{eq})^Z \tag{4.2}$$

where A is a constant depending on the solution and the substrate and Z is equal to 0.3. The equilibrium relative humidity of the investigated solution, h_{eq}, is the abscissa intercept from this fit (See Fig. 4.14). In our case, the two coalescing drops do not have the same composition and, hence, they may have different equilibrium relative humidities. The relative humidity in the chamber, for all experiments, was set slightly above the highest measured h_{eq} value, *i.e.* 83%.

4.3.2 Coalescence behaviour

For sessile drops containing inert miscible liquids, two coalescence behaviours have been identified, namely non-coalescence and immediate coalescence[16]. When the system involves reactive species, new mechanisms appear, induced by the precipitates. In the reactive case, four coalescence behaviours have been identified depending on the surface tension difference between the liquids, the average contact angle between the two drops and the initial oxalic acid excess.

The four behaviours have been analyzed from the top view, regarding the drops and precipitate shapes and displacement, and from the side view, for the neck evolution between the drops. In the following these four precipitation behaviours are named non-coalescence, partial coalescence with Marangoni flow, complete coalescence with Marangoni flow and barrier precipitation. In this section, we will first describe each of the coalescence behaviours before the conditions in which they appear will be discussed and outlined. The surface tension of the cerium nitrate drop (on the right side for each picture) is higher than the oxalic acid one (on the left side).

(Non)-coalescence

As for inert liquids, the coalescence of sessile drops in air containing reactants may be delayed by a Marangoni flow. Figure 4.15 presents top-view pictures of non-coalescencing drops containing reactants. The middle column shows the drop contours detected by the side view camera at the corresponding time. The curves of the neck and droplet height

evolution are displayed on the right. As usual, $t = 0s$ corresponds to the time at which the two drops get into contact by their three phase lines.

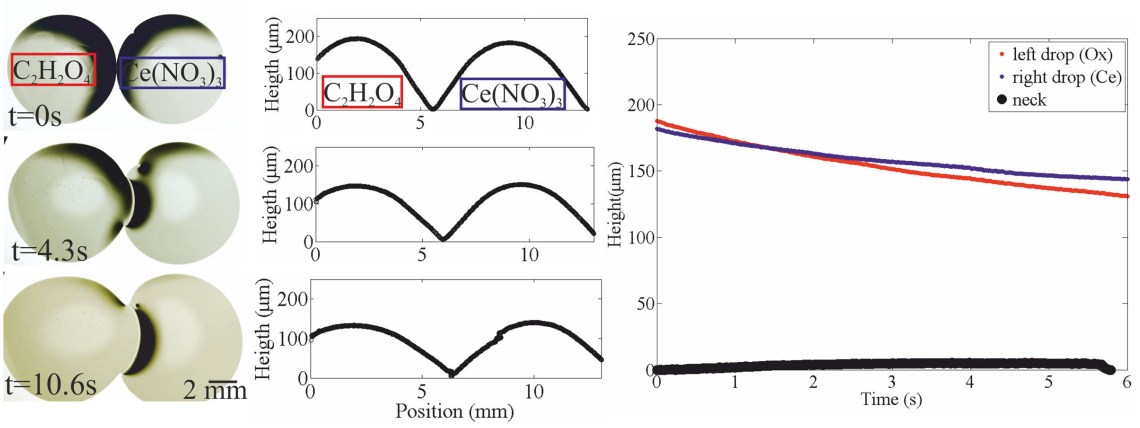

Figure 4.15: Non coalescence of drops containing dissolved reactive species ($\Delta\gamma$=4.1 mN m^{-1}, θ_a=6° and OE=0.6M). Left column: Top views of the non-coalescence behaviour at different time. Middle column: Side views reconstruction at different times. Right column: Corresponding neck and drop heightss evolution in time.

As for inert drops, non-coalescence is obtained at high surface tension difference, $\Delta\gamma$ (See: 2.2.3). During the non-coalescence, the neck height, $n_h(t)$, remains negligible compared to the drop heights, $d_h(t)$, for several seconds and up to minutes after the contact time ($n_h << d_h$). Both drop heights, $d_h(t)$, are decreasing with time, at a similar speed, due to the drop spreading. Simultaneously, the low surface tension drop, *i. e.* the oxalic acid drop, chases the second one along the substrate. The Marangoni flow outweighs the capillary forces. This is at the origin of the non-coalescence behaviour. Moreover, although reactive species are dissolved inside the non-coalescing drops, no precipitate is observed in the neck region or over the high surface tension drop, even 10 s after the drop contact.

The absence of precipitate is surprising. Indeed, it has been shown that the non-coalescence behaviour is associated to a continuous exchange of liquids between both drops through a microscopic neck. The solubility of cerium oxalate in aqueous solution is very low, which implies that some cerium oxalate should precipitate as soon as the reactants come into contact. Consequently, cerium oxalate precipitates are probably produced during the non-coalescence. However, the small quantity or size of the product supposedly makes it non detectable by the used OM. In addition, it can be imagined that the strong Marangoni flow pushes the precipitate away from the contact zone and

distribute them over the drop volume. This would lead to very low concentration in precipitates, which are hard to detect.

Partial coalescence with Marangoni flow

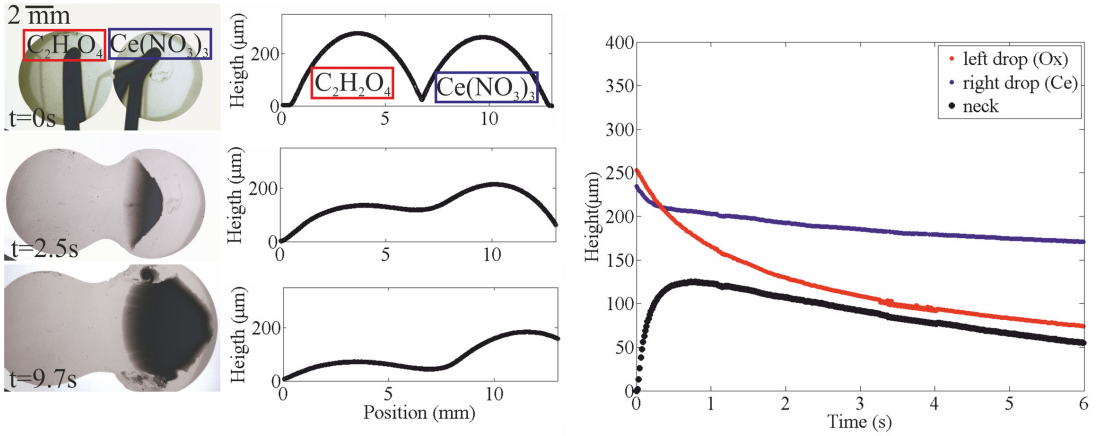

Figure 4.16: Partial coalescence with Marangoni flow ($\Delta\gamma$=1.3 mN m^{-1}, θ_a=12° and OE=0.6M). Left column: Top-views of the non-coalescence behaviour at different times. Middle column: corresponding contour reconstruction from the side-view camera. Right column:Corresponding neck and drop heights as a function of time.

In case of partial coalescence with Marangoni flow, precipitates are observable above the high surface tension drop, a few seconds after the drop/drop contact (See Fig:4.16). This precipitate pattern is pushed away from the neck region toward the opposite edge of the cerium nitrate drop. As a result, the oldest precipitates are always located at the front of the precipitate raft. In that sense, the precipitate growth process can be compared to the growth of hair. After ten seconds, the high surface tension drop is completely covered by precipitate.

The neck height, $n_h(t)$, increases rapidly to about 100 µm, as soon as the drops get into contact. Simultaneously, both drop heights decrease because of spreading. They decrease at different rates because one of the drop fill the other one by the Marangoni flow. However, the neck persists for several seconds after drop/drop contact ("partial" coalescence), probably due to the Marangoni flow. thus revealing a partial compensation of the capillary forces by the Marangoni flow. The Marangoni flow vanishes once it has emptied the low surface tension drop or the high surface tension drop is covered by the precipitate.

s

Complete coalescence with Marangoni flow

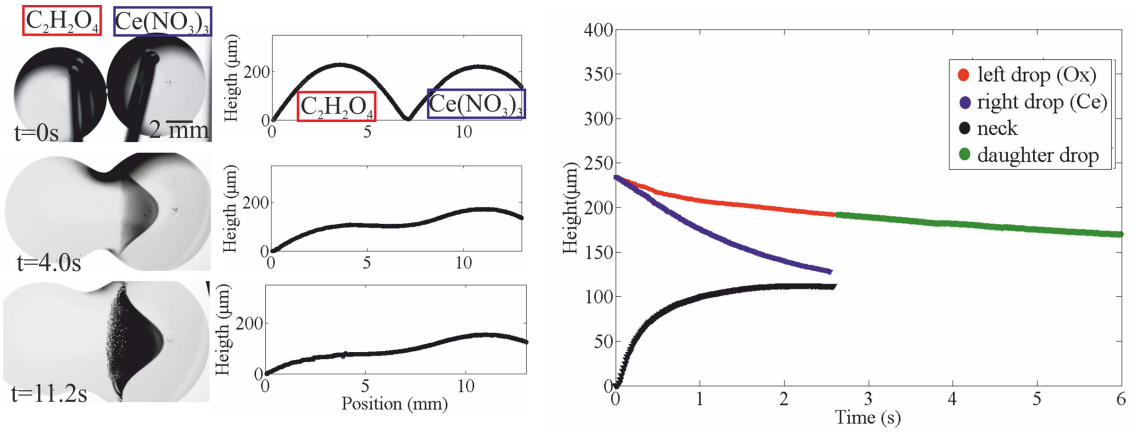

Figure 4.17: Complete coalescence with Marangoni flow ($\Delta\gamma$=0.8 mN m^{-1}, θ_a=7° and OE=0.8M). Left column: Top-views of the complete coalescence behaviour at different times. Middle column: corresponding contour reconstruction from the side-view camera. Right column: Corresponding neck and drop height evolutions in time.

As previously, in the case of complete coalescence with Maranoni flow, precipitates are formed in the contact region and pushed above the high surface tension drop. Moreover, the neck between the two drops growths rapidly. Eventually, a single daughter drop remains ("complete" coalescence) As in the case of partial coalescence, the drop height(s) decrease(s) continuously because of spreading. .
From the top view, the main difference between the partial and complete coalescence cases with Marangoni flow is the coverage of the precipitate. In case of partial coalescence, the high surface tension drop is completely covered by particles whereas for complete coalescence the high surface tension drop is only partially covered by the solid.

Coalescence and barrier precipitate

The last behaviour is the coalescence limited by neck precipitation. As in the previous case, the neck between the two drops is rapidly filled up, in this case typically in less than a second. A precipitate barrier is produced in the neck region between the two drops. Although there is a $\Delta\gamma$, there is basically no Marangoni flow, presumably because of the precipitate barrier. In the first seconds, the precipitation is restricted to the contact area between the two drops. The thickness of the precipitate zone slowly increases with time. But, in contrast to the other cases, precipitates once formed are rather immobile.

Similar to the "spherical" drop case (See Sec:4.1), the precipitate acts as a barrier which restricts the liquid mixing and thereby hinders the progress of the precipitation reaction.

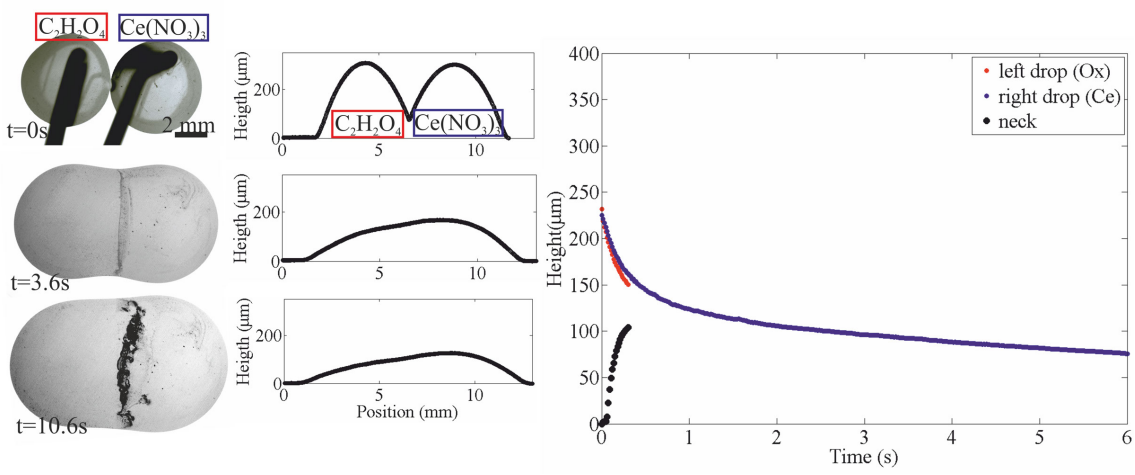

Figure 4.18: Coalescence with mixing limited by neck precipitation ($\Delta\gamma$=0.9 mN m^{-1}, θ_a=12° and OE=0.8M). Left column: Top-views of the barrier coalescence behaviour at different times. Middle column: corresponding contours reconstruction from the side-view camera. Right column:Corresponding neck and drop height evolutions in time.

To conclude, four coalescence behaviours were identified and analyzed for the coalescence of sessile drops containing reactive species, namely non-coalescence, partial coalescence with Marangon flow, complete coalescence with Marangoni flow and barrier precipitation. This has to be compared with the two cases occurring for the coalescence of inert liquids. The additional coalescence behaviours are due to the precipitate influences on the flow conditions. It can be assumed that the transition between coalescence and non-coalescence is very similar in case of reacting and non-reacting liquids. This means that the transition can be linked to the specific Marangoni number, $\tilde{M}$, (See Sec:2.2.3)

4.3.3 Precipitation patterns induced by Marangoni flow.

In the following, we will focus only on the cases where a Marangoni flow was evidenced, namely the partial or complete coalescence with Marangoni flow. Indeed these cases exhibit the strongest mixing of the reactive liquids and are therefore relevant in the focus of this study. The precipitation behaviours of either partial or complete coalescence are quite similar and will not be distinguished here. The precipitation pattern will be first investigated as a function of the initial OE.

Phase diagram in the case of Marangoni flow

Three precipitation patterns are observed depending on the initial oxalic acid excess (see Fig. 4.19) in the case of partial and complete coalescence with a Marangoni flow. At high oxalic acid excess (OE $\geq$ 0.6M), a large homogeneous and strongly scattering area emerges over the cerium nitrate drop. Its shape and scattering properties resemble the precipitate patterns obtained in 100% water solvent at large oxalic acid concentration.

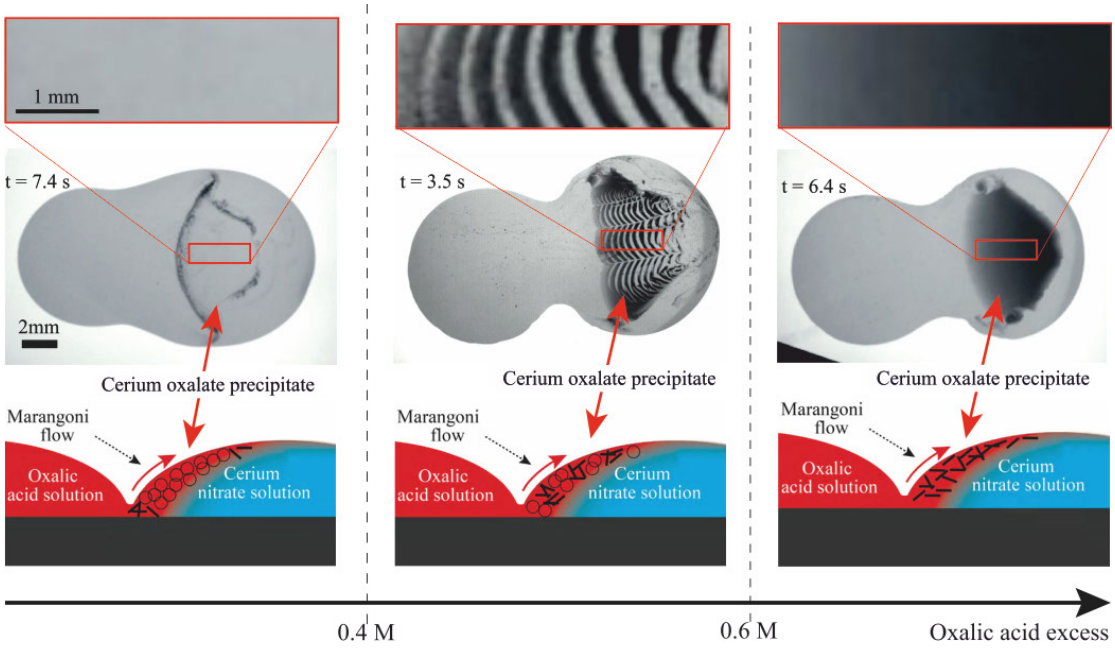

Figure 4.19: Three precipitation patterns observed as a function of the oxalic excess for high volume fraction in 1,2-propanediols. Left column: a large transparent domain covers the cerium nitrate drop (OE=0.35M, $\Delta\gamma$=2.4 mN/m). Middle column: periodic precipitation pattern (OE=0.43M, $\Delta\gamma$=2.6 mN/m). Right column: A large strongly light-scattering pattern covers the high surface tension drop (OE=0.65M, $\Delta\gamma$=1.3 mN/m). Reprinted from [88].

At low oxalic acid excess (OE $\leq$ 0.4M), a weakly scattering domain surrounded by a boundary of precipitate that scatters light strongly is produced. Low OE means a high absolute concentration of cerium nitrate. This corresponds to a high superpaturation ratio, S, which should result in a higher amount of precipitates compared to the high OE case. In Figure 4.19, it seems that there is less precipitate. As will be shown later, the central area, which scatters only weakly the light, contains particles. The pattern looks similar to the one obtained in water solvent at high cerium nitrate ratio.

For oxalic acid excess between 0.4M and 0.6M, the precipitate forms a regular pattern of alternating strongly and weakly light-scattering domains. These stripes are formed of, at least, two kinds of particles exhibiting different light scattering properties. In the primary pattern the stripes are oriented normal to the flow direction. There is also a second pattern parallel to the flow direction and cutting the stripes into segments. The characteristic length of the second pattern is larger than the primary one.

In the literature, oscillatory behaviours can arise in convection-reaction-diffusion systems. The primary stripes formed here supposedly result from a combination between the transport of reactant and the precipitation reaction (See Sec:4.3.5). Their characteristic wavelengths vary between 100 and 400 µm.

To resume, at large and low oxalic excess, the precipitate patterns are similar to the ones obtained in pure water solvent. At OE$\geq$ 0.6M, homogeneous strongly light scattering precipitates are formed above the cerium nitrate drop. At OE$\leq$ 0.4M, a large weakly light scattering domain surrounded by a boundary of strongly light scattering aggregates is observed. In 50% water/ 50% diols, well defined periodic patterns are observed at the transition between this two regimes. The latter are composed of alternated weakly light scattering and strongly light scattering fringes.

Formation of the precipitate patterns

The formation of the precipitate patterns is highlighted in figure 4.20 for the three precipitation regimes. At high OE, weakly scattering light precipitate are formed on the high surface tension drop close to the drop neck. This precipitation occurs within the first second after the two drops contact. While the solid is pushed toward the other edge of the high surface tension drop, its scattering intensity increases. It takes typically less than 10 s for the pattern to completely cover the cerium nitrate drop whereas the same process takes around 2 s in 100% water solvent. In the case performed in pure water, it was shown, that the precipitate may change after the coalescence process. When 50% water/50% diols mixtures are used as solvent, the patterns obtained do not shrink and remain stable over the observation time (See Sec:4.4.2).

At intermediate OE, the front fringes appear within the first second after the drop/drop contact. The fringes emerge from the initial neck region between the two drops, which will be named the reaction zone in the following. Weakly and strongly light scattering fringes appear alternately before being pushed over the high surface tension drop until the cerium nitrate drop is completely covered by the periodic pattern.

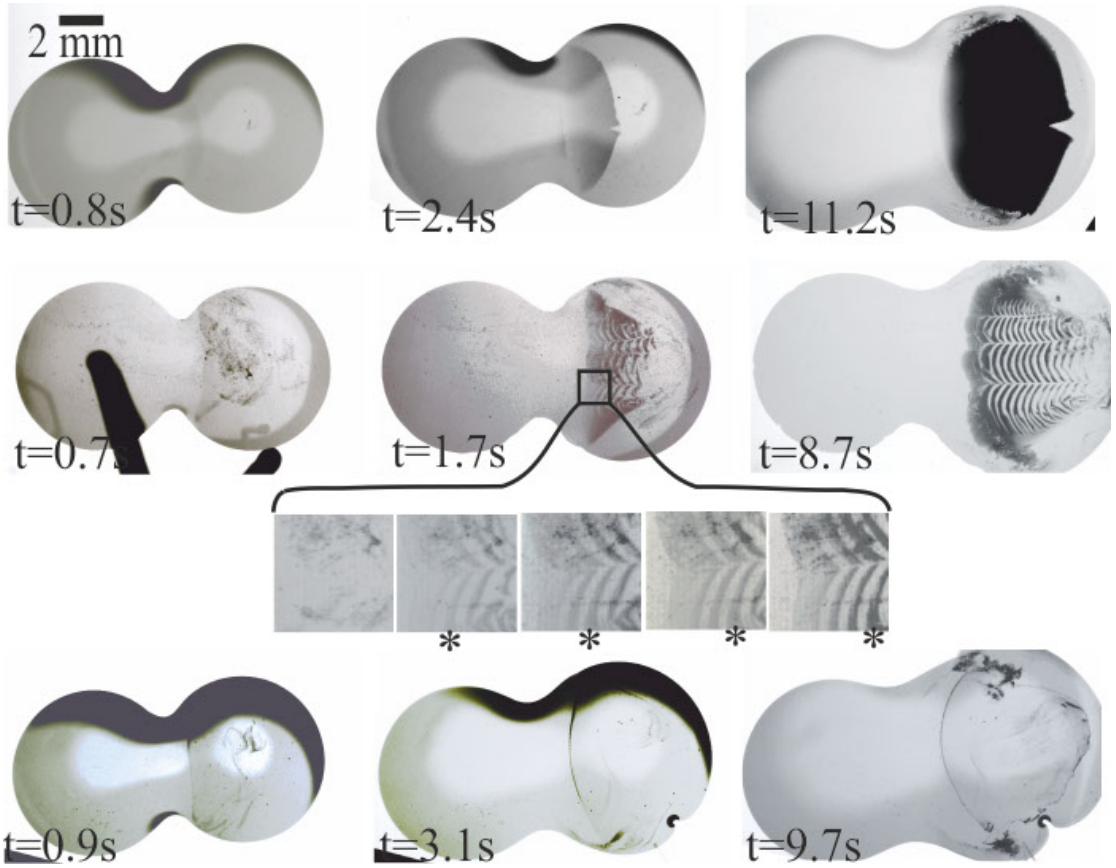

Figure 4.20: Short time evolution of the three precipitation regimes after the drop contact (t=0 s). Upper row: light scattering pattern formation (OE=0.95 M, $\Delta\gamma$=1.3 mN m^{-1}), the precipitate is formed continuously in the neck region before being pushed by the Marangoni flow. Middle row: fringe precipitation (OE=0.45 M, $\Delta\gamma$=2.1 mN m^{-1}). In the insert, the stars refer always to the same fringe and its displacement along time. There is 0.1s between each insert image. Lower row: formation of a large weakly light scattering domain (OE=0.40 M, $\Delta\gamma$=2.0 mN m^{-1}).

At low OE, a thin light scattering line can be observed in the neck region between the two drops within the first second after the drop/drop contact. This line seems to be stable during the whole process. Presumably, it may precipitate and attach to the substrate. A second line formed some seconds after coalescence is pushed toward the high surface tension drop, possibly at the front of the Marangoni flow.

The formation of the precipitate pattern is slower in 50%water-50% diols solvent (slightly less than 10 s) than in 100% water (typically 2 s). This is most likely due to the different solvent viscosities. It is worth mentioning, in the case of immediate coalescence of inert liquids composed of water and diol mixtures, when a Marangoni flow arises, it vanishes

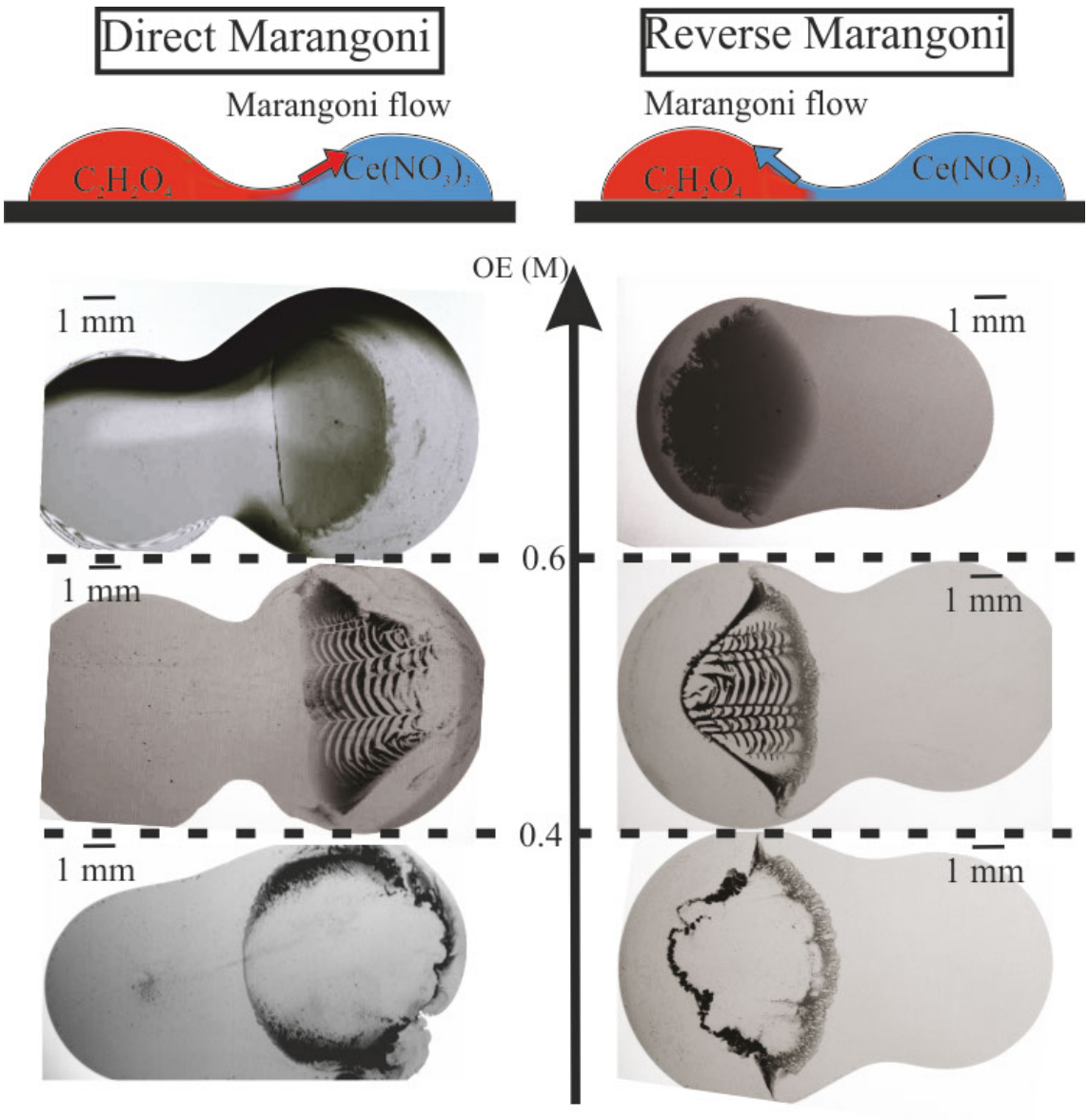

Figure 4.21: The precipitation patterns as a function of the oxalic excess, OE, for both directions of the Marangoni flow.

within a second after the drop contact. In the case of precipitating systems, with similar solvent, the Marangoni flow carries on up to 10 s after the drop/drop contact. It seems, that somehow the precipitate slows down the Marangoni flow and the liquid mixing.

Reverse configuration

Up to now, the Marangoni flow was always directed from the oxalic acid drop to the cerium nitrate drop, as is the case in water solvent. However, in 50% water/ 50% diols systems, $\Delta\gamma$ is fixed by the volume fraction of 1,3-propanediol in each drop. By adjusting this amount, the direction of the Marangoni flow can be reversed. In other words, couples of solutions for which the cerium nitrate solution surface tension is lower than the oxalic acid one can be prepared. During the coalescence of drops from such solutions, the Marangoni flow is directed from the cerium nitrate drop to the one containing oxalic acid. In the following, this configuration will be named "reverse Marangoni flow" in opposition to the "direct Marangoni flow" investigated so far. The experiments show that coalescence behaviours (neck precipitation, partial coalescence with Marangoni, complete coalescence with Marangoni, non-coalescence) are not influenced by the direction of the Marangoni flow.

The impact of the Marangoni flow direction on the precipitation regimes is presented in Figure 4.21. The figure shows the top view of coalescing sessile drops for different OE and for both Marangoni flow directions (direct vs reverse). As for direct Marangoni flow, strongly scattering precipitate patterns are formed for OE$\geq$0.6M, a periodic pattern develops for OE between 0.6M and 0.4M, and a transparent domain surrounded by a boundary of strongly light scattering precipitate emerges at OE$\leq$0.4M. Hence, at high and low oxalic excess identical patterns are observed regardless of the Marangoni flow directions. At intermediate OE, periodic precipitation is also obtained in case of the reverse Marangoni flow. The fringe details are slightly different from the ones obtained for direct Marangoni flow. Indeed, the periodic patterns observed in one direction look like a photographic negative of the other one. In the direct configuration, the secondary patterns are delimited by transparent domains. Conversely, for reverse Marangoni flow, strongly light scattering lines parallel to the flow direction are dividing the pattern. The pattern observed in the reverse case is surrounded by strongly light scattering precipitate. In the same way, the entire pattern area is possibly surrounded by a boundary of weakly scattering precipitate.

Effect of the propanediols

Up to now, 1,2-propanediol and 1,3-propanediol were considered to have identical effects on the coalescence and precipitation behaviours due to their similar physical properties (*e.g.* density, viscosity). However, the difference in the chemical structure be-

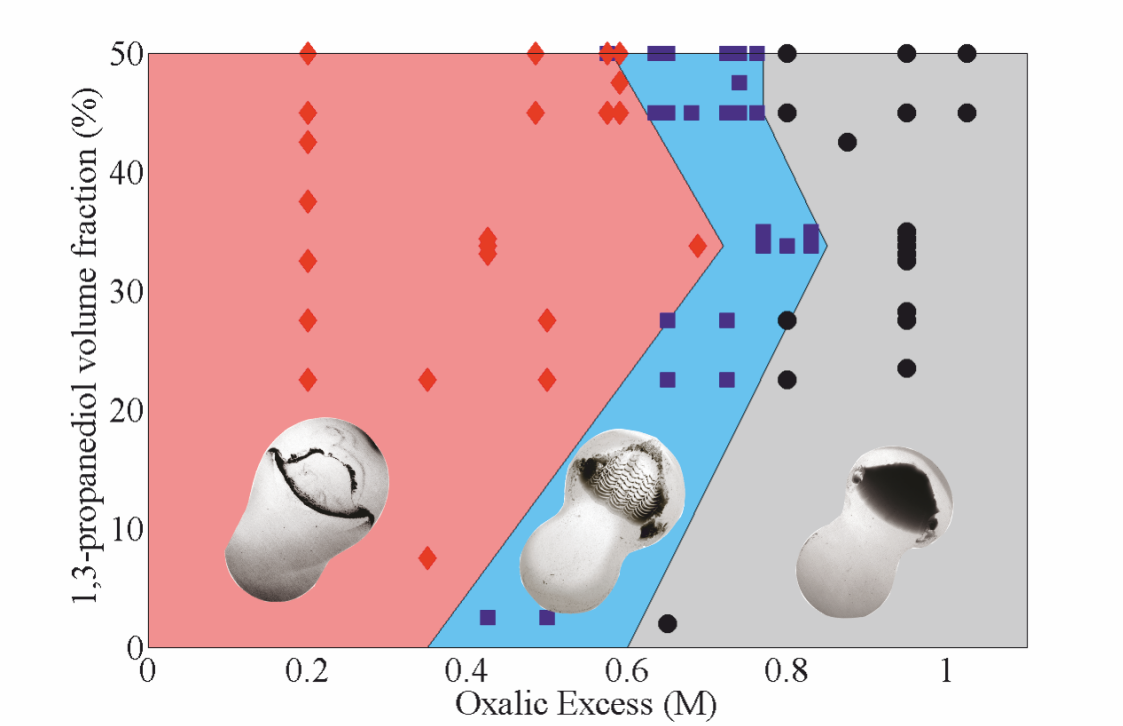

Figure 4.22: Phase diagram according to the average volume fraction of 1,3-propanediols considering 50% water / 50 % diol mixtures and the OE. ♦: weakly light scattering regime, ■: periodic precipitation, •: large strongly light scattering domain. The background colours are an interpolation of the precipitation regimes.

tween both isomers may have an impact on the reaction and the precipitate features. The quantitative hydrodynamic drop-drop behaviour is indeed independent from the solvent used. In order to investigate the influence of each propanediol on the precipitation reaction, the phase diagram of the observed precipitation behaviour was measured as a function of the volume fraction in 1,3-propanediol and the oxalic acid excess (See Fig4.22). In fact, all the three precipitation behaviours are observed for all 1,3-propanediol volume fractions. However the volume fraction of 1,3-propanediol influences the threshold oxalic acid excess value, *i.e.* the value at which the transition between the behaviours occurs. This shift in the phase diagram may be explained by a difference in the intrinsic chemical effect of the propanediols on the precipitation reaction. This hypothesis is supported by recent CEA internal studies on the effects of various additives, among them 1,2-propanediol and 1,3-propanediol, on the precipitation of neodymium oxalate. Experiments show, that the Marangoni flow direction (direct/reverse) does not have an impact on this phase diagram.

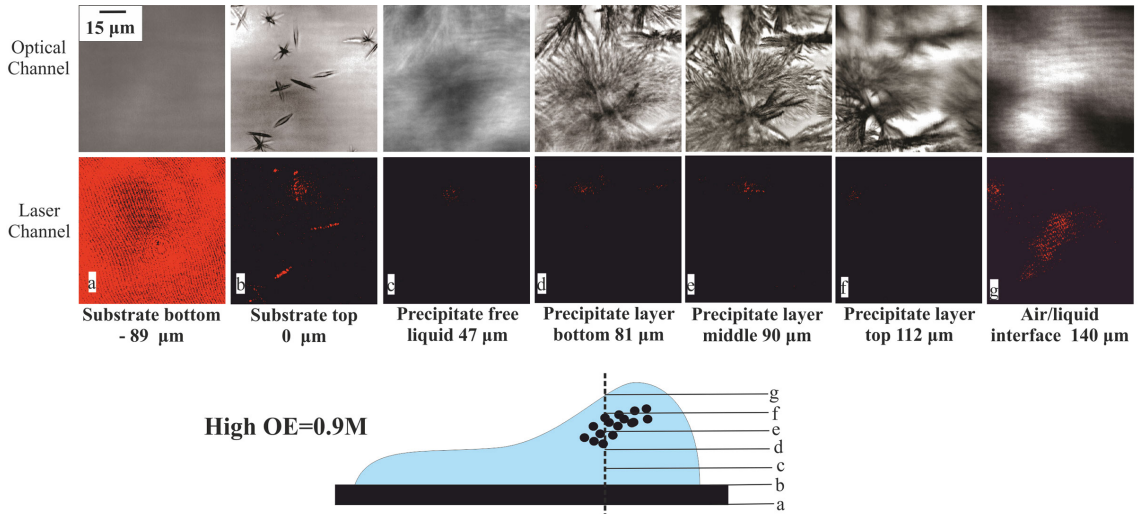

Figure 4.23: Vertical distribution in the daughter drop at high OE determined by confocal microscopy. The air/liquid interface and the substrate faces are determined by fluorescence.

Vertical distribution of the precipitates

Up to now, the lateral distribution of the precipitate was analysed from the top view by optical microscopy (OM). Information on the vertical distribution of the precipitate could not be achieved by this technique. Therefore, confocal microscopy was used to localize the precipitate particles inside the drop along the vertical direction. For this purpose, the drops are deposited on a glass substrate (See Sec:3.2.4). Experiments show, that the precipitation regimes are identical on silica and glass surfaces. For details about precipitate morphologies, refer to section 4.4.2, here, we focus on the vertical distribution of the precipitate particles. Confocal imaging was performed in the area of the samples with high particle density. The vertical position of the precipitate was determined with the higher magnification of the microscope resulting in a probe area of $158 \times 158\,\mu m$, which is small compared to the area covered by the coalesced drops.

The vertical position of both the substrate/liquid and liquid/air interface have been identified through the fluorescence of rhodamine, which is enriched on both interfaces. Rhodamine has been spin-coated on the substrate before the drop deposition (for more details see Sec:3.2.4). The vertical precipitate position was determined by "conventional" optical microscopy. The drop heights that were measured with this technique (between 80-200 µm) are consistent with the data derived from the side view of the optical microscope after the drop coalescence (10 s after contact). Note that the heights measured

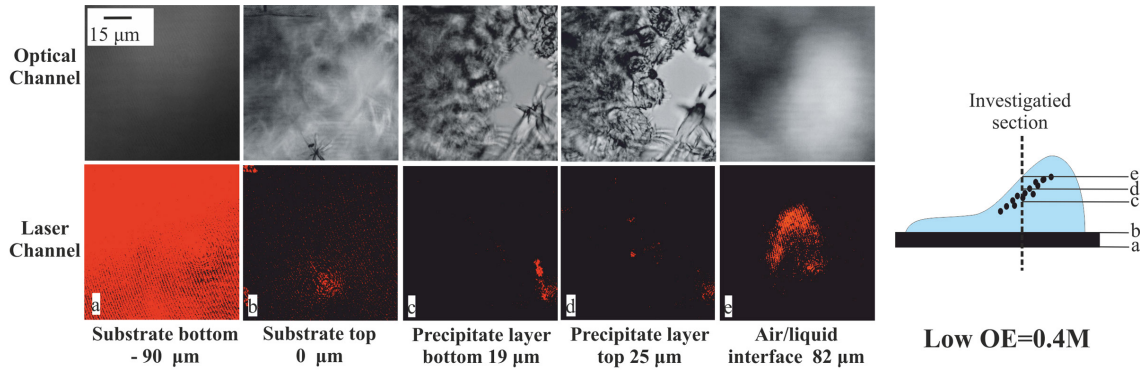

Figure 4.24: Vertical distribution in the daughter drop at low OE determined by confocal microscopy. The air/liquid interface and the substrate faces are determined by fluorescence.

with confocal microscopy are local and dependent on the (x, y) coordinates at which the images are recorded, whereas only the maximum height is considered for the samples investigated by optical microscopy.

Regardless of the OE and the drop height, most of the precipitate are localized between 30-80 µm below the air-liquid interface. At high oxalic acid excess (See Fig:4.24), the precipitate layer thickness is typically 30 µm, whereas at low oxalic excess only a thin layer of typically 5 µm is observed (See Fig:4.23). Moreover, in both cases, a precipitate free zone exists between the top of the substrate and the lower limit of the precipitate layer. Besides, few small precipitate particles are settled on the glass substrate.
The precision on the vertical position is limited by the variation of the drop contour. Long time confocal experiments show that the precipitate does not sediment during the first 30 minutes after the drop/drop contact (See Sec:4.4.2).

4.3.4 Hydrodynamic and relevant parameters

As discussed previously, the flow induced by the drop coalescence influences the transport and mixing of the liquids and thus the local composition of the reactants. As a consequence, it is a control parameter of the precipitate features and distribution. On the other side, precipitate may affect the flow characteristics, *i.e.* speed and direction, and thus the liquid mixing. In the following, the flow speed during the coalescence of sessile drops containing cerium nitrate and oxalic acid will be investigated as a function of θ_a, OE, $\Delta\gamma$ and η. As in the case of water solvent, the precipitate speeds were measured by following the motion of individual spots.

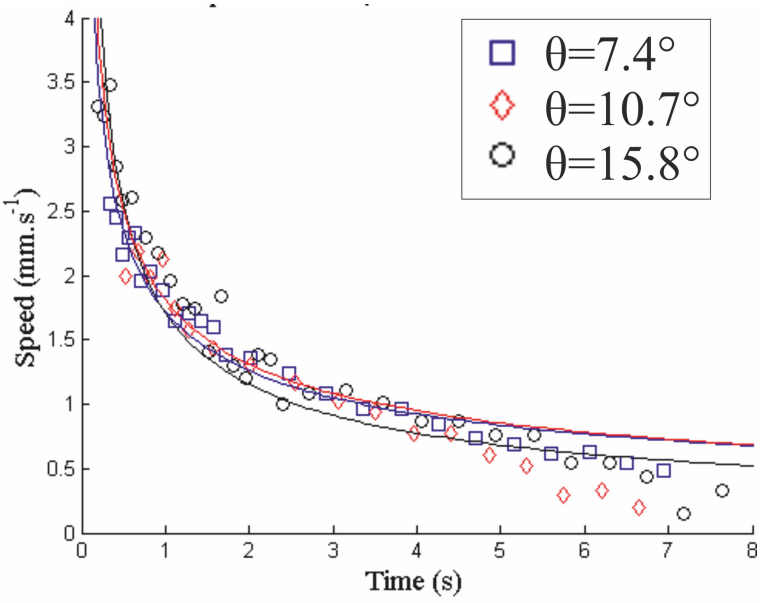

Figure 4.25: Surface flow speed for periodic pattern formation in the case of an initial $\Delta\gamma = -0.78\,\mathrm{mN\,m^{-1}}$ for various contact angles. The speed is determined by following the first fringe. The solid lines are guides for the eyes. The contact angle does not affect the surface flow speed.

Effect of the contact angle

The evolution of the surface flow speeds for $\Delta\gamma = -0.78\,\mathrm{mN\,m^{-1}}$ and OE =0.5 mol at various average contact angles are displayed in Figure 4.25. As in the case of 100% water solvent, the data points are fitted by a solid line which is a guide for the eyes. All the cases shown in Figure4.25 depict cases of periodic pattern formation for the complete coalescence with Marangoni flow. The contact angles do not play a role on the surface flow speed (See Fig 4.25). This has already been shown for 100% water as solvent (See Fig:4.10).

Speed of the surface flow for different precipitation regimes

In suspension flows, it is well known that, due to shear stress, solid particles tend to slow down the fluid velocity. The effect of the two kinds of cerium oxalate particles on surface flow has been investigated with a constant $\Delta\gamma =$ of $1.4\,\mathrm{mN\,m^{-1}}$ for different OE leading to three different precipitation regimes in the case of partial coalescence with Marigoni flow (See Fig: 4.26). For the cases of strongly light-scattering pattern and periodic pattern regimes, the speeds were determined by following the displacement of

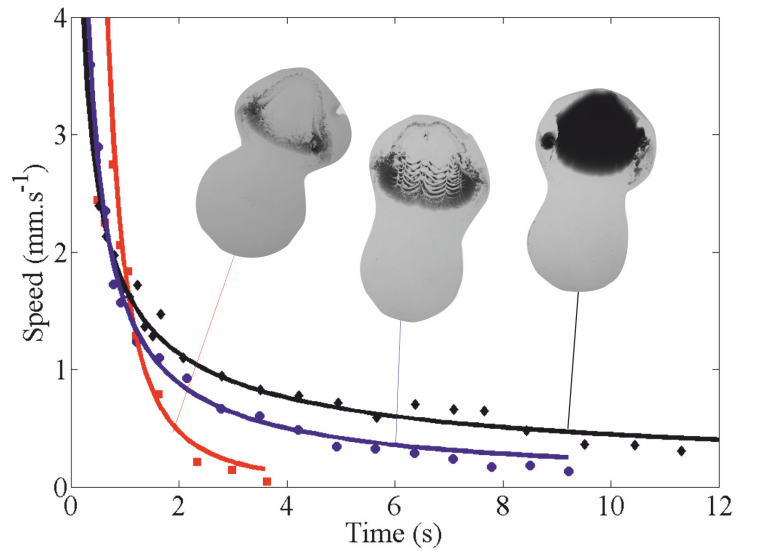

Figure 4.26: Speed of the pattern front line as a function of time for the three precipitation regimes. Black line: strongly light scattering regime, blue line: fringes, red line: weakly light scattering regime.

the front line. At low OE (*i.e.* weakly light-scattering pattern), this technique could not be applied. Instead, in that case, the speed was analyzed by following dust particles present in the initial drops.

The speed of the three precipitation regimes decreases over time, however with different rates. In the case of low OE, which means weakly light-scattering pattern, the surface flow velocity exhibits the fastest decrease. The speed decrease is intermediate in the case of periodic precipitation. At high OE, *i.e.* for strongly light-scattering pattern, the decrease is slower.
It would be expected that, at low OE (*i.e.* high s), a higher number of precipitate is formed which would slow down the flow due to viscous drag. This is in agreement with the finding. As a second assumption, one could argue that the precipitate prevents the mixing between both liquids, thus prolongs $\Delta\gamma$ and the Marangoni flow. However, this scenario does not fit with the experimental results. The validity of both hypotheses should be confirmed from the measurement of the surface flow evolution during the immediate coalescence of inert liquids. Such an investigation could be performed by adding methylene blue to the low surface tension drop.

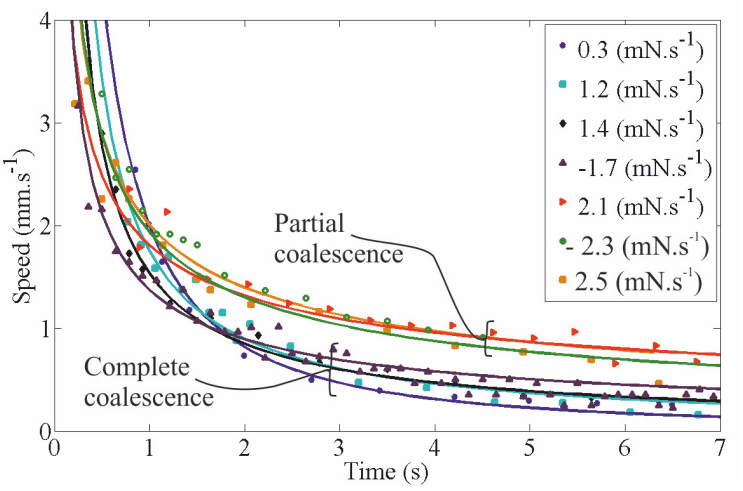

Figure 4.27: Precipitate speed as a function of time for different $\Delta\gamma$ in the case of periodic precipitation.

Correlation between the surface flow speed and the coalescence behaviours

The surface flow speeds of periodic patterns at different $\Delta\gamma$ are displayed in Figure 4.27. Once again, it is observed that the speed decreases with time. Regarding the sensitivity to $\Delta\gamma$ two trends emerge. At low $\Delta\gamma$ (here below $1.7\,\mathrm{mN\,m^{-1}}$), a higher decreasing rate is observed. For the second group ($\Delta\gamma \geq 1.7\,\mathrm{mN\,m^{-1}}$), the speed decreases with a slower rate. It is remarkable that for the low $\Delta\gamma$ case, we observe complete coalescence with Marangoni flow, whereas for high $\Delta\gamma$, all cases correspond to a partial coalescence with Marangoni flow. Hence, we can conclude that the quantitatively different speed behaviour is linked to the two different coalescence behaviours.

It seems that the neck persistence leads to a lengthening of the capillary forces and an increase of the precipitate speed.

Viscosity effects

The effect of the solvent viscosity was investigated by increasing the volume fraction of diols to 75%. This way, the solvent viscosity increases from previously 5 mPa s to 16 mPa s. Again, in this case, three precipitate patterns (*i.e.* strongly light-scattering pattern, fringes and weakly light-scattering domain) are observed (See Fig:4.28). However, the OE boundary between the precipitation regimes is different. For example, a periodic pattern appears in viscous solvent only for an OE of 0.22 M compared to typically OE=0.5 M for 50% water/50% diols mixtures. Again, the results are indepen-

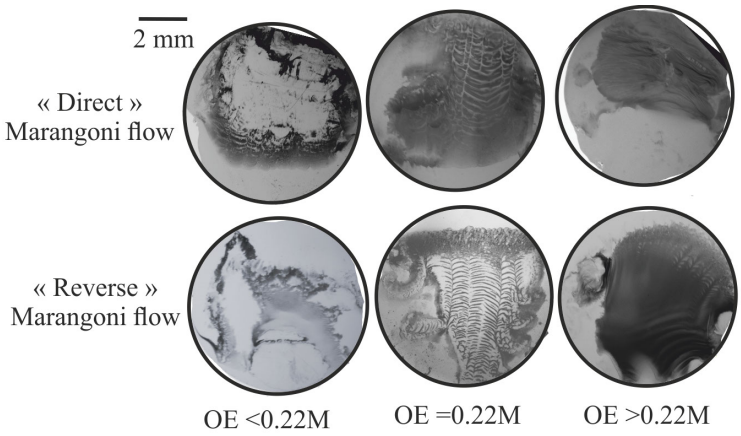

Figure 4.28: Patterns of the precipitation regime for highly viscous solvents (η=16 mPa s). Fringes occurs at OE=0.22M.

dently from the Marangoni flow direction.

The speeds of the periodic precipitate patterns are exhibited in Figure 4.29 for different solvent viscosities (25% water/75% diols, 50% water/50% diols, 100% water). In all cases, the pattern velocity decreases with increasing viscosities. However, a very big difference between the surface flow velocity right after the drop/drop contact can be observed. Indeed, at low viscosity, the surface flow is initially an order of magnitude higher than the one of the viscous solution. Moreover, the Marangoni flow vanishes earlier at low viscosity (typically 2 s for η=1 mPa s compared to 20 s for η=16 mPa s).

To resume, the solvent viscosity enables to tune the surface flow velocity. However, by changing the solvent viscosity, the Marangoni flow, the diffusion rate of the reactive species and the growth kinetic of the precipitate are modified. These modifications have a significant impact on the periodic pattern characteristics.

4.3.5 Detail properties of the periodic patterns

The formation of periodic patterns at intermediate oxalic excess is intriguing (See 4.3.3). The observed fringes are produced in the reaction zone, close to the drop/drop contact area. After a fringe is formed, its shape remains basically the same. The fringe is pushed away by the Marangoni flow above the higher surface tension drop. Then a new fringe can be produced in the reaction region. In that sense, the periodic pattern formation in sessile drops containing reactants is similar to drifting patterns[89]. Well defined periodic patterns have been produced in water/diols mixtures at the same OE

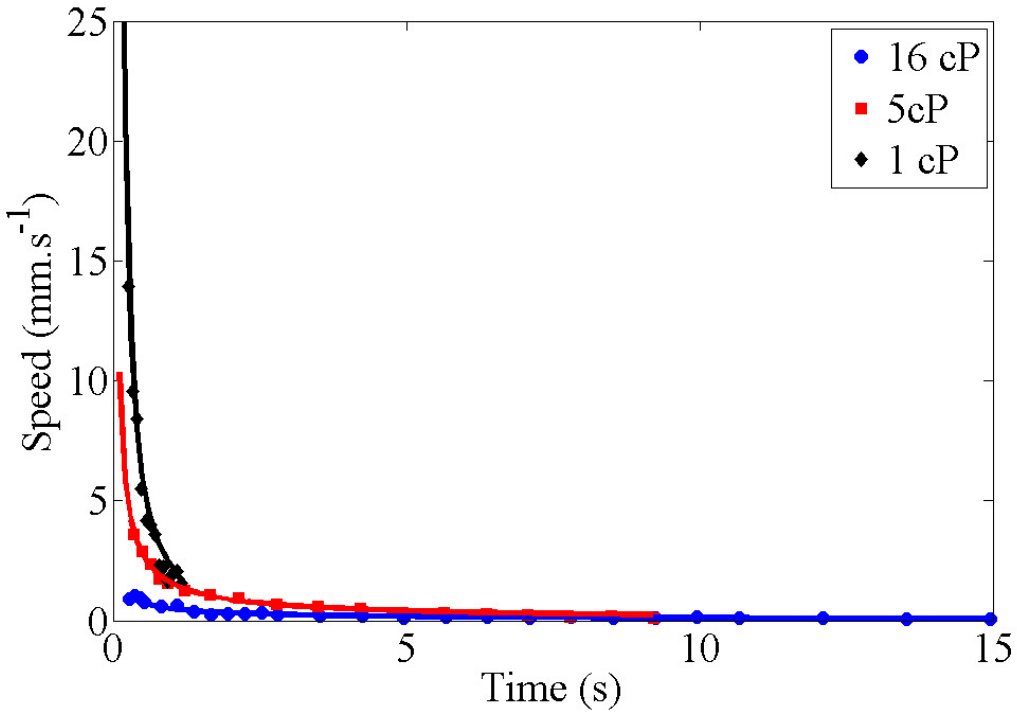

Figure 4.29: Speed of the precipitation pattern for different viscosities. Water solvent: η =1 mPa s^{-1}, 50% water/50% diols: η =5 mPa s^{-1}, 25% water/75% diols: η =16 mPa s^{-1}

independently from the Marangoni flow direction. However, the OE range at which the stripes arise depends on the solution viscosities. Moreover, fringes are observed for η = between 1 mPa s and 16 mPa s. The end of this section will focus on the description, characterization and explanation of periodic pattern formation during the coalescence of reacting sessile drops.

Speed and wavelength

For the following, the wavelength, λ, is defined as the length of one weakly light-scattering and one strongly light-scattering fringe. The evolution of λ along an individual experiment has been investigated for different coalescence behaviours and Marangoni flow directions (See Fig:4.30). The analysis shows that λ decreases with the surface flow speed in case of "direct" Marangoni flow, whereas it increases with time in the case of "reverse" Marangoni flow . Moreover, λ varies between 100 and 400 µm. Independent from the Marangoni flow direction, the faster the surface flow the

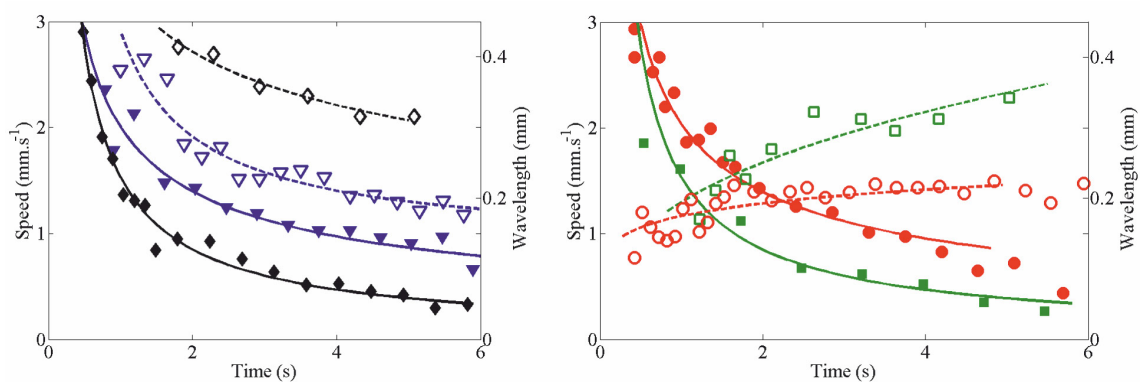

Figure 4.30: Speed (close symbol) and wavelength (open symbol) evolutions, in case of "direct" (left graphic) and "reverse" (right graphic) Marangoni flow for partial and complete coalescence.

smaller the fringes. λ typically tends to 350 µm in case of complete coalescence and 200 µm in the partial coalescence case.

Thus the wavelength of the periodic pattern is intrinsically linked to the surface flow speed and its evolution depends on the flow direction.

Viscosity effect

Typical periodic patterns in both Marangoni flow directions at different viscosities are exhibited in figure 4.31. Here the viscosity affects simultaneously the surface flow speed, and the diffusion rate of the reactive species. Moreover, the reaction rate is probably impacted through the activity coefficients, due to the changes in the solvent composition.

Periodic pattern and confocal microscopy

At intermediate OE, periodic pattern can also be seen through confocal microscopy (See Fig:4.32). The pattern wavelengths observed by confocal microscopy, typically 275 µm, are consistent with the ones determined by optical microscopy.

With confocal microscopy the strongly and weakly light scattering domains can be identified. The confocal microscope runs in transmission mode, the weakly light-scattering fringes appear clear, because the light can pass through. On the contrary the strongly light-scattering fringes, which can not be traversed by light, come into view as dark. Hence, the light-scattering properties could be associated to the particle morphologies

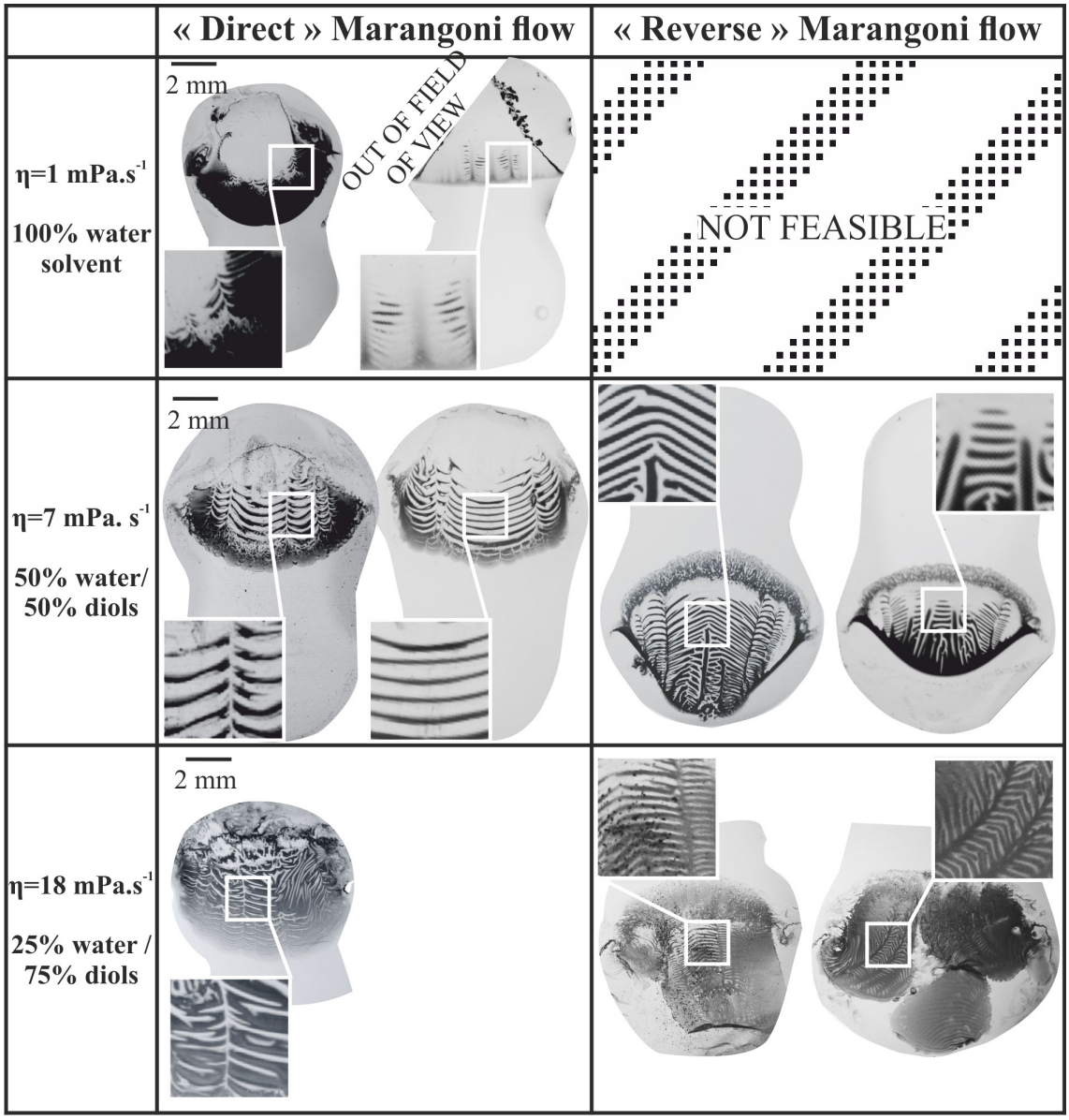

Figure 4.31: Typical periodic patterns for different solvent viscosities and Marangoni flow directions.

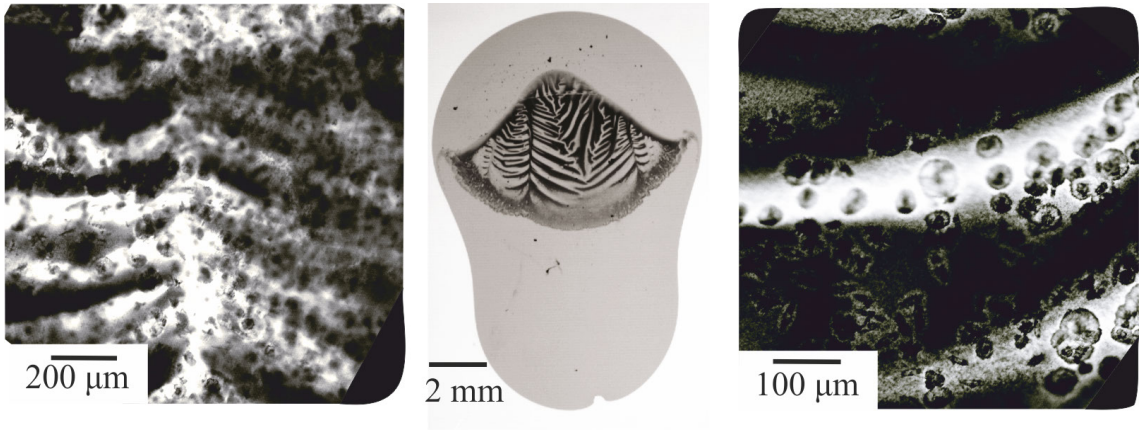

Figure 4.32: Periodic patterns imaged on a confocal microscope at different scales (left and right rows) compared with a similar pattern obtained by optical microscopy at smaller magnification (middle row).

(See Sec:4.4.2). These two domains appear approximately at the same vertical position but exhibit different thickness (similar to the results detailed in Sec:4.3.3).

Origin of the periodic pattern

Experimentally two precipitate types, exhibiting different light scattering properties, are formed depending on the OE. When the OE is low, weakly light-scattering precipitate is formed while at high OE, the precipitated particles scatter strongly the light. Thus, the "local" OE is the control parameter leading to the different precipitates. With OE_{th} the oxalic excess threshold value delimiting the two regimes, in this range close to the threshold, we find oscillation. The fringes most probably appear when the local oxalic excess in the reaction zone oscillates below and above OE_{th}. The OE oscillations are due to a combination of the reactant consumption by the chemical reaction and their transport toward the reaction zone by the convective Marangoni flow and, or the diffusion process.

On the contrary, in the case of reverse flow a light scattering domain precipitates as soon as the two drops get in contact. In conclusion, prior to the fringe formation, it is always the relative concentration of the component dissolved in the high surface tension drop, which decreases in the reaction zone. Thus, the limiting transport phenomenon is the diffusion of the reactant dissolved in the high surface tension drop. Conversely, the Marangoni flow acts as an infinite reservoir of the other reactant. In other words, the periodic pattern would be produced by a feedback mechanism between the precipitation

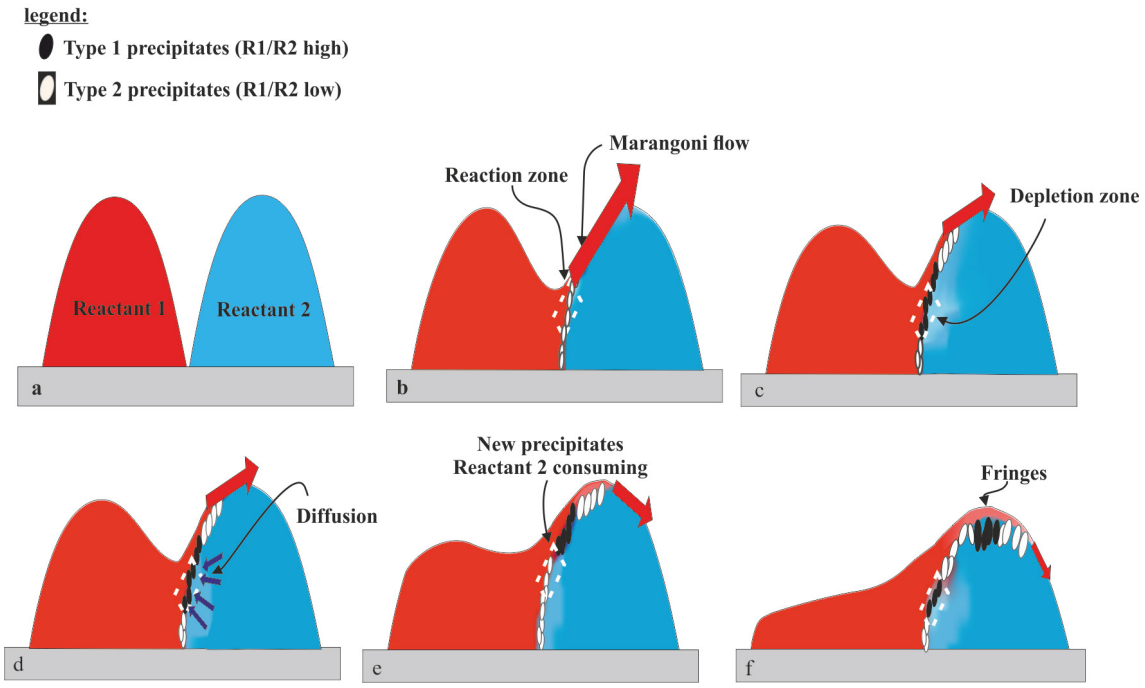

Figure 4.33: Schematic proposition of the mechanisms at the origin of the periodic precipitation. The reaction induces a depletion zone in reactant 2 close to the reaction zone. The gradient in concentration of reactant 2 leads to a diffusion flow and an oscillation of the local concentration.

reaction and the diffusion of the reactant dissolved in the high surface tension drop. While the surface flow speed is independent from the Marangoni flow direction, λ increases over time in the "direct" case whereas it decreases in the "reverse" case. In other words, along time, the frequency at which the OE crossed the threshold value increases in case of "reverse" flow and decreases in case of "direct" flow. We can not explain those two tendencies yet. It seems that they are related to both the diffusion coefficient of each species and the speed of the Marangoni flow.

More generally, a schematic description of the feedback mechanism is proposed in figure 4.33. Initially, after the two drops got into contact, a small amount of reactant 1 is introduced in a reservoir of reactant 2. First, precipitate formed at high $\frac{R1}{R2}$ (reactant 1 over reactant 2 ratio), called here type 2, are formed in the neck region between the two drops, *i. e.* the reaction zone. They are continuously produced and pushed away by the Marangoni flow, hence forming the primary domain. The length of the later depends on the difference between the initial OE and the threshold value. Indeed, the higher the difference between these two, the longer the primary domain. At that time, reactant 2 is consumed by precipitation whereas new reactant 1 is continuously fed to the reac-

tion zone by the Marangoni flow, generating a depletion zone in reactant 2 close to the reaction zone. The $\frac{R1}{R2}$ decreases until it reaches the threshold value. Then, type 1 precipitates are produced in the reaction zone before being pushed away by the Marangoni flow. Simultaneously, the gradient created by the depletion gives rise to a diffusion flow of reactant 2 from the drop center toward the reaction zone until $\frac{R1}{R2}$ oversteps the threshold value.

To resume, our precipitation process is a convection-diffusion-reaction system i. e., a system described typically by a non-linear equation. Non-linear systems are known to show oscillatory or oscillation-free behaviour depending on the system parameters. For instance, in 1950, Turing [50] was the first who gave a complete theoretical description of pattern formation for chemical systems.

4.3.6 Conclusion on hydrodynamic

To conclude, four behaviours have been identified after the contact of sessile drops in air containing reactive species, namely non-coalescence, partial and complete coalescence with Marangoni flow and neck restricted coalescence. The achieved behaviour is dependent on the initial surface tension difference, $\Delta\gamma$, on the average contact angle, θ_a, and on the oxalic excess, OE. This study focuses on the partial and complete coalescence with Marangoni flow, because a strong mixing is obtained in this case. Depending on OE, three precipitation regimes may occur in this case. At high OE, a strongly light-scattering precipitate pattern is formed over the high surface tension drop. At low OE, a weakly light-scattering precipitate pattern is pushed over the high surface tension drop and surrounded by a boundary of scattering light precipitates. Surprisingly, at intermediate OE, periodic patterns, which are composed of weakly and strongly light-scattering fringes, arise. In all the three cases, most of the precipitates are produced close to the neck between the two initial drops, and the precipitate is pushed over the high surface tension drop by the Marangoni flow. The three regimes have been observed independently from the Marangoni flow direction and for solvent viscosities ranging from 1 mPa s to 15 mPa s.

Formation of periodic pattern during the coalescence of sessile drops is an intriguing process. It is probably caused by a combination of transport and reaction conditions. The cerium oxalate precipitates in either strongly or weakly light-scattering material according to the local cerium over oxalate ratio, adjusted here as the oxalic acid excess. In other words, over a threshold value of oxalic excess, cerium oxalate, which strongly

scatters the light, precipitates, whereas below this value, weakly light-scattering cerium oxalate solid particles are produced. During periodic pattern precipitation, the local oxalic excess in the reactive zone oscillates periodically around this threshold value. The oscillations are presumably due to the feedback mechanism between the transport of reactant to the reaction zone , by the Marangoni flow for the low surface tension liquids, and by diffusion from the drop bulk for the high surface tension liquids, and the precipitation.

4.4 Precipitate features: size, morphology, structure.

So far, this report has been focusing on the mutual impact of a precipitation reaction and the general hydrodynamics of coalescing sessile drops. More precisely, both the effects of the precipitation on the transport of reactants by the capillary and the Marangoni flows, and the impact of the subsequent reactants feed mechanisms on the general precipitation patterns were investigated. Two different features were observed during the study (strongly and weakly light-scattering).
It is known that the hydrodynamic conditions and the resulting mass transport may impact the microscopic features of the chemical product. Indeed, mass transport was shown to be a control parameter for the formation of either calcite or vaterite, two polymorphs of calcium carbonate, in the presence of an electrolyte[90].
In the same way, it is well established that solvent or chemical species addition can play a major role on the precipitate morphologies. In particular, polyols were observed to impact the morphology of copper oxalate precipitates. Copper oxalate particles display a cushion-like geometry once precipitated in purely aqueous solution[91], while these particles exhibit a lens morphology when the precipitation is performed in the presence of glycerol[92]. The precipitate sizes and shapes may impact the solid physical properties, as for metallic particles [3, 4], or the shaping possibilities. In the nuclear fuel reprocessing industry, the shape and size of the solid particles obtained during the oxalate precipitation is an issue for the following steps of the reprocessing, *e.g.* their filtration and calcination.
In this part, the characteristics, as size, morphology, structure and growth kinetic, of the precipitates formed during the coalescence of sessile drops will be described as a function of the chemical environment prevailing during the experiments.

4.4.1 100 % water solvent

The sizes, morphologies and structures of the particles obtained during the coalescence of low contact angle sessile drops in 100% water solvent is discussed below.

Precipitate morphology in pure water solvent

SEM images of dried precipitates obtained in water, for different supersaturation ratios, *S*, are shown on figure 4.34. These SEM images were taken in the denser area of the precipitation patterns and are representative of the most common morphologies inside these dried samples. The corresponding precipitation patterns at the drop scale and their

time evolutions are also presented. The supersaturation ratios are calculated using the model described previously (See Sec: 3.2.7).

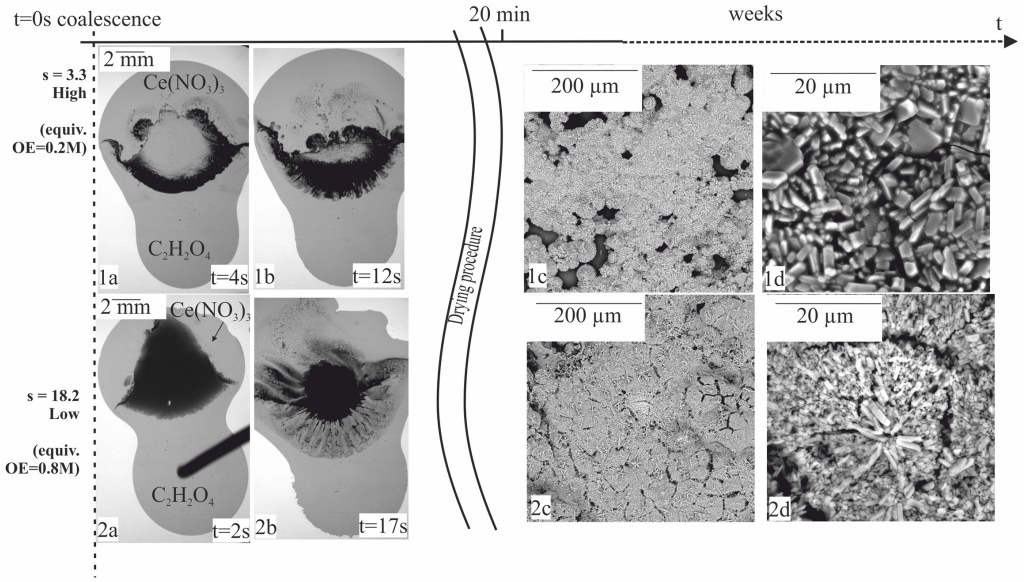

Figure 4.34: Optical microscopy and SEM images of coalescing cerium nitrate (at different concentration) and oxalic acid (1.1 M) sessile drops in air in the case of 100% water solvent. The supersaturation ratios are s=18.2 (top row) and s=3.3 (lower row). The optical images present the evolution of the precipitation patterns up to tens of seconds after the drop coalescence. The SEM images, at different magnifications, come from the denser part of the dried precipitation patterns. The SEM images were recorded weeks after the sample preparation.

As already discussed (See Sec:4.2.3), the precipitation patterns obtained during the coalescence of sessile drops with purely aqueous solvent are not stable after the Marangoni flow vanishes. Instead, the apparent solid domain is observed to collapse in tens of seconds (Fig: 4.34 1a and b and 2a and b). The drying procedure is much longer (tens of minutes) than the shrinkage. For this reason, the link between the precipitate positions when the Marangoni flow switches off and the precipitate distribution on the SEM images is not obvious. In other words, the SEM images may not be representative of the precipitate features before the drop collapses.

At low magnification, the samples can hardly be differentiated in the SEM images (Fig: 4.34 1c and 2c). In both cases, the particles are aggregated. However, small variations can be observed. At high supersaturation ratio, the edges between the solid-

rich and the solid-free areas exhibits high curvatures. There are no cracks inside this sample. The lower supersaturation ratio sample is highly compact and contains deep cracks.

At higher magnification (Fig: 4.34 1d and 2d), both samples mainly exhibit needle like precipitates. However, the particles can be differentiated by their sizes. The precipitates of the high supersaturation ratio sample are thicker than the low supersaturation ratio ones and look like slabs of typical length 4 µm, for an average width and thickness of 1.5 µm. A small amount of these particles displays a square like morphology. The precipitates are randomly distributed inside this sample.
At lower supersaturation ratio, the precipitates size distribution is larger. Slightly smaller precipitates with length varying typically from 0.8 µm to 5 µm, and width and thickness around 0.5 µm are formed. The precipitates appear organized according to their sizes. Longer particles are observed on the top of the precipitation pattern in a nearly circular arrangement, with their smaller faces oriented toward the centre (See Fig: 4.34-2d). The smaller precipitates located under and beside the circle are all oriented in the same direction.

Due to the precipitation pattern shrinkage, it is not possible to relate the precipitate morphologies with their localization inside the drop, when the Marangoni flow vanished. Consequently, SEM images do not enable to know, whether the weakly light scattering areas, at high supersaturation ratio, are precipitate free zones.

Structure determination: X-Ray Diffraction

XRD measurements were performed to investigate the structure of the precipitates in the different regimes. Due to a lack of product, each experiment was realized directly on the substrate used for the drop coalescence, after drying of the solvent and without any washing step (See Sec: 3.2.4). The coalescence substrate was fixed on an upside down XRD powder support with modelling clay. To avoid experimental issues with this unusual set-up, the samples were not rotating during the measurement. Consequently, the XRD patterns peaks intensities are not meaningful and only their positions will be analysed. Hence, preferential orientation of the sample could not be average in our configuration, as for conventional powder diffractograms.

Figure 4.35 upper sub-plot, displays the XRD patterns of the dried precipitates for

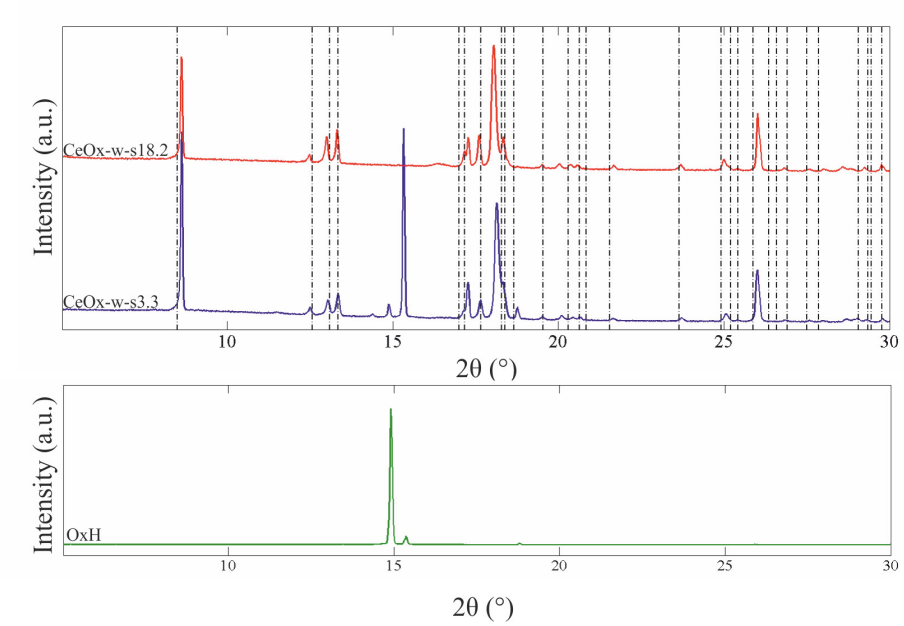

Figure 4.35: Upper subplot: XRD pattern of the precipitates obtained during the coalescence of sessile drops in air for different supersaturation ratios. The higher curve is obtained for a transparent precipitate pattern (s=18.8). The lower curve corresponds to the XRD patterns obtained at low supersaturation ratio (s=3.3). Lower subplot: XRD pattern of a dried 1.1M oxalic acid drop on a silica surface.

a transparent pattern (upper raw, s=18.2M) and a strongly light scattering precipitate pattern (lower raw, s=3.3). The black dash lines indicate the theoretical positions of the diffraction peaks for the cerium oxalate decahydrated structure resolved by Ollendorf[93]. The lower sub-plot corresponds to the XRD pattern of a dried 1.1M oxalic acid drop on a silica surface, under the same experimental conditions (upside down XRD support, no rotation)

Both XRD patterns are similar although, at low supersaturation ratio, the XRD pattern exhibits additional diffraction peaks at $2\theta = 14.9°$, $15.3°$ and $18.8°$. The latter can be attributed to crystallized oxalic acid, as shown by the XRD pattern of this component (See Fig: 4.35, lower sub-plot). Other peaks are revealed at the same 2θ values in both regimes. This indicates that the structure of the precipitates are the same. Moreover, the peak positions are close to the ones of the cerium oxalate decahydrated, for which the structure was resolved by Ollendorf[94]. However, some shifts between the 2θ values remained. For instance, the first diffraction peak at $2\theta = 8.59°$ according to Ollendorf is observed at $2\theta = 8.62°$ for both samples. From these XRD patterns, it can be concluded

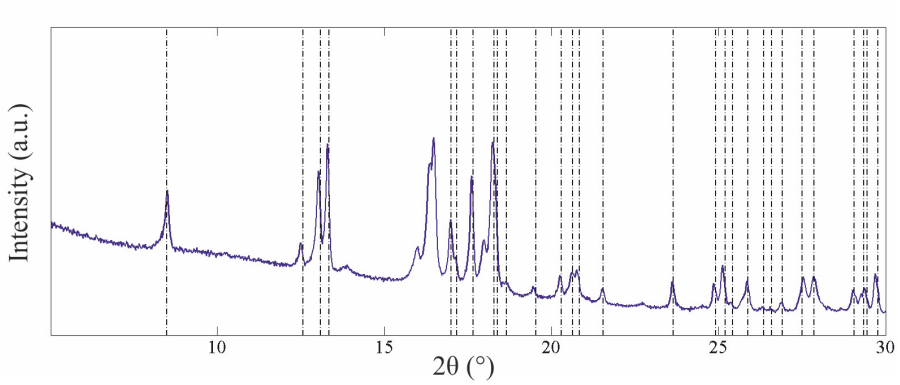

Figure 4.36: Powder XRD pattern of commercial Cerium oxalate.

that in both regimes the precipitates are cerium oxalate exhibiting the same crystalline structure.

The shifts may have different possible explanations. First of all, a systematic error could be introduced by a misalignment of the diffractometer. To rule out this hypothesis, the XRD pattern of commercial powder cerium oxalate was measured (See Fig: 4.36). The diffraction peaks appear at the exact position of the structure resolved by Ollendorf. Other peaks are observed on the commercial XRD pattern due to the coexistence of cerium oxalate with different hydration levels.
A second explanation is that the shifts arise from the unusual set-up configuration of the sample holder. The use of Si monocrystal peak for the calibration of the diffractogram could be a poor choice in the case of thick samples. Indeed, if the dried drop is thick, its vertical position is different from the one of the substrate. This height difference would induce a systematic error on the measured diffraction pattern. However, if it was the case, all peaks would be shifted by the same quantity, which is not what we observe here.

To conclude, in pure water solvent, the two coalescence regimes lead to the precipitation of needle like precipitates. The particles obtained have both the same structure. This structure is similar to the one resolved by Ollendorf for cerium oxalate decahydrated. At high supersaturation ratio, i.e. in the weakly light scattering regime, the dried precipitates are bigger than the ones obtained at low supersaturation ratio, i.e for the strongly light scattering regime. However, due to the substantial shrinkage of the precipitation patterns after coalescence, the precipitates features (size, morphologies...)

can hardly be related to the scattering properties of the particles.

4.4.2 Solvent composed of 50% water/ 50% diols mixtures

Propanediols are added to the drop mixture in order to fix the drop surface tension difference independently from the reactants concentration (See Sec: 4.3.1). However, the diols may have an impact on the precipitation reaction. First, the higher viscosity of diol mixtures may modify the flow properties and, therefore, the transport of reactants, which influences the precipitation reaction. Moreover, the interactions between the cerium oxalate precipitates and the diols have not been investigated yet. Diols, by absorbing on the different precipitate faces could modify the growth mechanisms. In this section, the size, morphology and structure of precipitates obtained during coalescence of low contact angle sessile drops in half water, half diols solvent will be characterized. The effects of the diols on the precipitates will be analyzed. Hereby, the oxalic excess will be preferred to quantify the reaction instead of the supersaturation ratio, since diols impact on the oxalate solubility and on the species mobility and thus activities. As discussed previously, the oxalic excess is inversely proportional to the supersaturation ratio.

Pattern long-term evolution

Figure 4.37 displays the evolution of the precipitation patterns over an extended time scale (up to 10 minutes) for the three precipitation patterns achieved in 50% water/ 50% diols solvents.

In the three cases, the overall aspect of the precipitation patterns are stable over time. At high OE , the initially compact strongly scattering pattern slowly becomes more and more diffuse (See Fig:4.37 bottom row). After 10 minutes, the pattern appears as an assembly of strongly scattering dots and weakly scattering dots within the micrometer range. Conversely, at low OE (See Fig:4.37 top row), dark spots appear after minutes over the initially weakly light scattering domain. However, the initially strongly light scattering and weakly light scattering domains remain distinguishable over time by their optical properties. At intermediate OE (See Fig:4.37 middle rows), the oldest and predominantly transparent fringes can hardly be distinguished after some minutes at the magnification used. Simultaneously, the youngest stripes are still visible after minutes. The latter are made mainly of strongly light scattering areas.

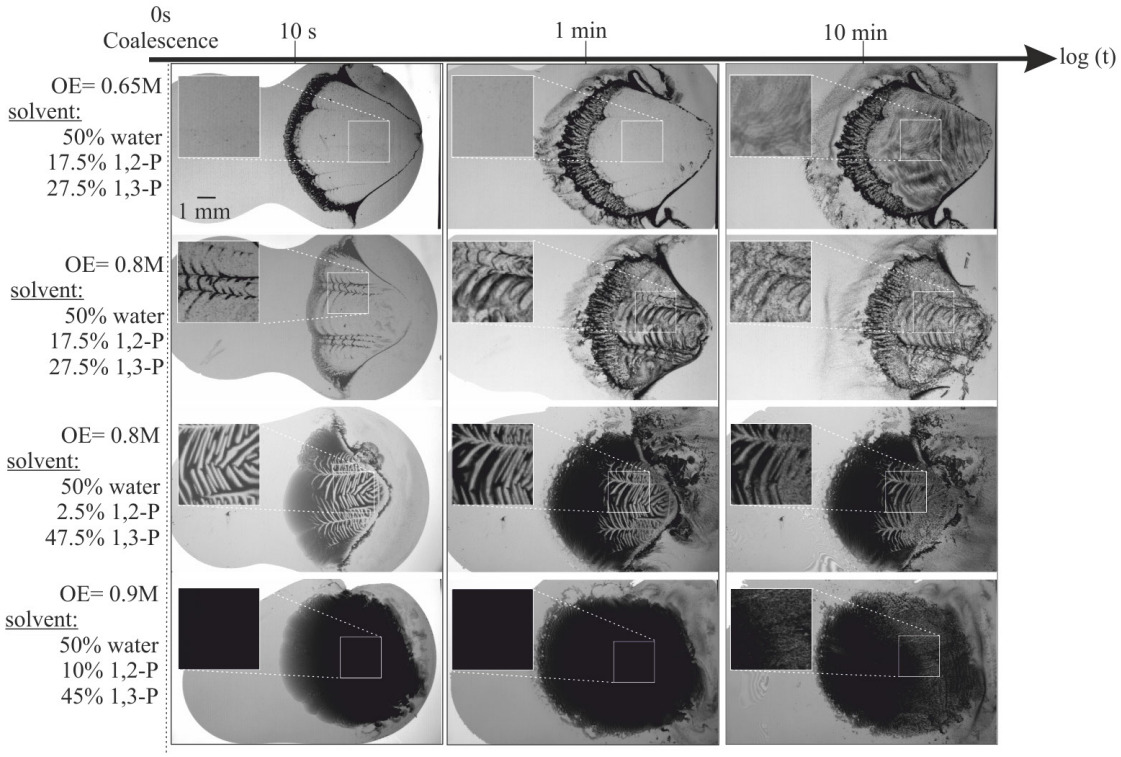

Figure 4.37: Evolution of the three precipitation patterns over a long time scale.

The evolutions of the precipitate light scattering properties are probably related to the growth of the precipitate (See Sec:4.4.2)

Since, the patterns do not evolve much over time, (at least compared to the pattern obtained in 100% water), it is possible to dry and characterize the precipitates. The dried particle features were then correlated to the initial optical precipitates properties.

Dried precipitate morphologies

As for 100% water solvent samples, SEM analysis was performed directly on the dried substrate in order to investigate the morphology of the precipitates. The sample was divided into 10 zones which characterize the complete sample. SEM images were taken with a FEI QUANTA 200 ESEM FEG electron microscope (ICSM), and assembled using a software based on a correlation function. A sample mapping is thus achieved.

Figure 4.38 illustrates an optical microscopy image of a high oxalic excess precipitation pattern from the drop set-up (a), the SEM mapping of the same sample after drying (b)

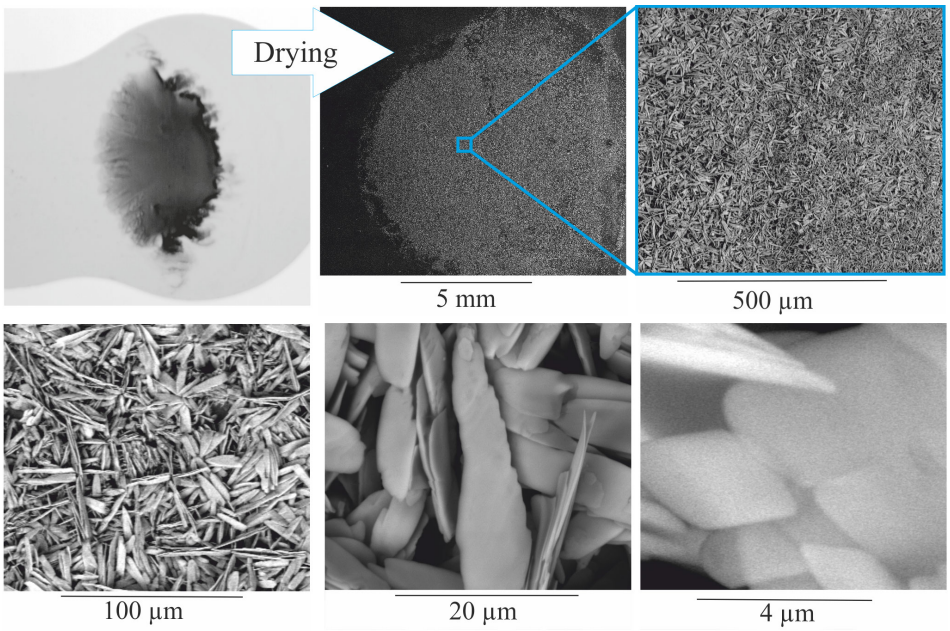

Figure 4.38: Morphologies of the cerium oxalate precipitates at high oxalic excess. a) Precipitation pattern recorded with the droplet set-up. b) Mapping of the sample using SEM. c, d, e and f) SEM images of the sample with increasing magnification.

and SEM images of the dried precipitates at different magnifications (c-f). The sample is homogenous, as can be observed on the SEM mapping and the low magnification SEM image. The precipitates have a needle-like morphology. Needles is the usual morphology observed for cerium oxalate precipitates [95]. However, these needles differ significantly from the solid particles obtained in pure water solvent by their sizes. Their typical length is 25 µm, for a width of 5 µm (compared to a length of 4 µm in pure water). The thickness of these precipitates, around 0.7 µm, is comparable to the precipitates thickness observed in purely aqueous solvent. The particles appear overall randomly distributed in the sample. However, locally several needles are arranged in a circular shape, contacting each other by the needle tips. This effect is particularly pronounced on figure 4.38 d, recalling the semi-organisation of low supersaturation samples in purely aqueous solvent. On the higher magnification SEM image (Fig:4.38 f), it can be observed that these needles have microscopic roughness, surprisingly their faces are not smooth.

At low OE, particles with completely different morphologies are obtained (See Fig: 4.39) In this figure, the drawn squares and circles indicate the approximative position at which the SEM images were realized.

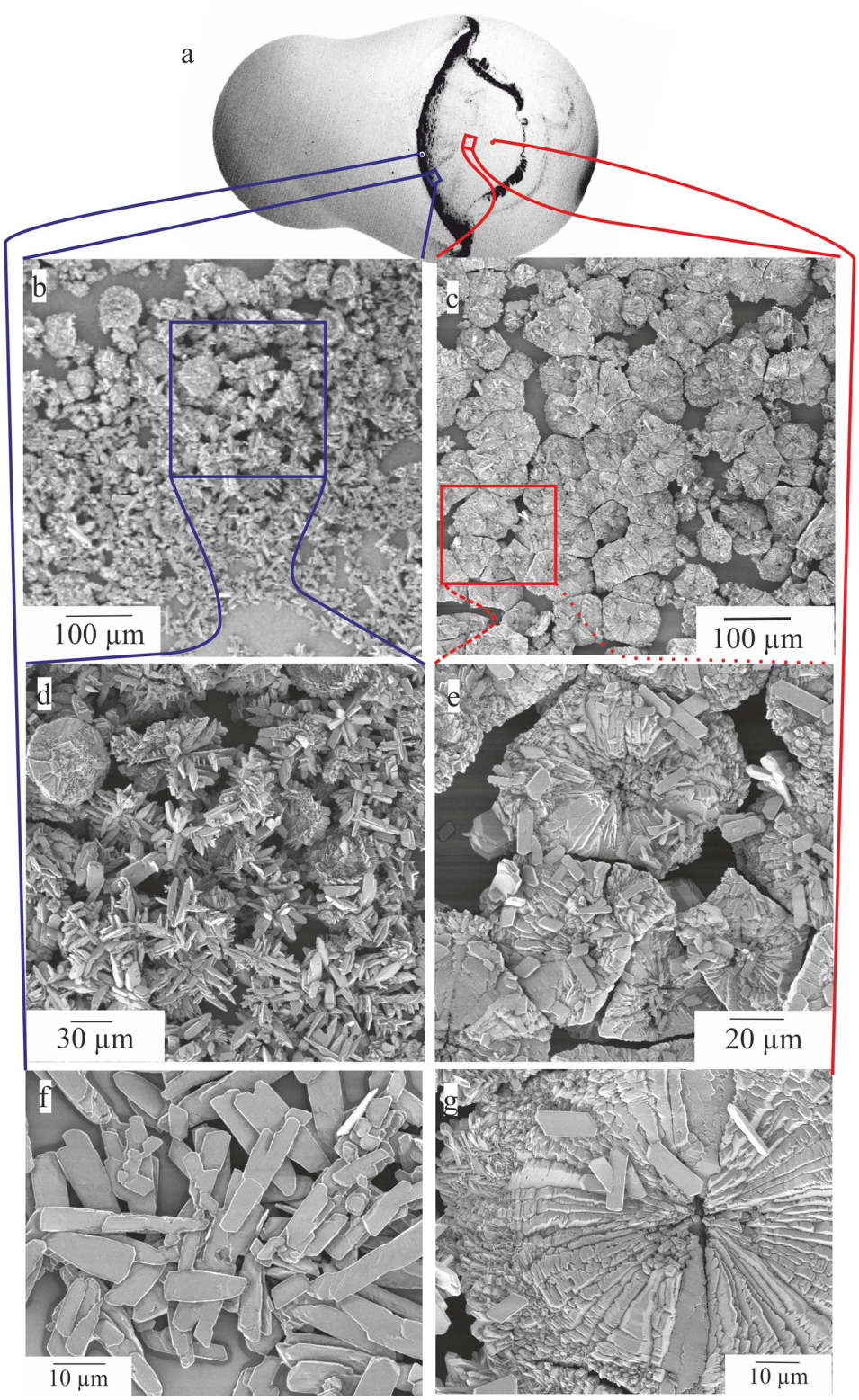

Figure 4.39: a) Optical microscopy of a high oxalic excess precipitation pattern and approximate location of the SEM images. b-g) SEM images of the corresponding precipitates. b, d) Mixture of microflower and needle in the transition area between strongly and weakly light scattering domains. c, e,g) Microflower like precipitates at different magnifications. f) Needle precipitates from the strongly light scattering boundary.

The low oxalic excess sample is not homogeneous (See Fig:4.39). On the external edge of the pattern, a line of needle-like precipitates is observed. Their size is in the same range as the one exhibited by the high oxalic excess samples (e.g. length 15 µm, width 5 µm). The location of the needles matches approximately the position of the strongly light scattering boundary observed by optical microscopy. Moving toward the sample center, the morphology of the particles changes. First, a mixture of needles and organized needle aggregates comes across. Then, "microflower"-like particles are displayed in the pattern center, which corresponds to the weakly light scattering area observed by optical microscopy. The microflowers look like a perfectly well organized arrangement of needles with a typical dimension of 65 µm. Thanks to the higher magnification image (See Fig:4.39-g) three features can be distinguished: (i) an empty core in the middle, (ii) long needles perfectly organized, (iii) a compact shell composed of a high density of smaller particles. This arrangement likely results from a multi-step process. In that regards, the shell could be formed during the drying step of the precipitates due to unmixed remaining reactants. In the transition zone between strongly and weakly light scattering domains, mixtures of needles and less organized microflowers can be observed (See fig:4.39).

Unlike needles, microflowers are not the usual morphology of cerium oxalate. However, unusual morphologies of oxalate compounds have been observed, when the precipitation is achieved in the presence of additive species. For instance, Liu et al. [96] synthesized nanoflower-likes cerium oxalate particles in presence of polyvinylpyrrolidone. In our case, the propanediols probably play the role of modifying agent. Furthermore, numerous examples of enhanced organisation by additives are related in the literature for similar precipitation systems[97, 98, 96]. Two explanations are highlighted for this gain in organisation. First, the additives may absorb preferentially on some faces, due to favourable interactions, thus, slowing down the growth rate of such faces in favour of others. Second, the higher viscosity induced by the addition of such components hinders the diffusion process. Thus, the elementary units have more time to organize themself, hence promoting positions that minimize the interfacial energy.

The SEM images of the dried periodic patterns exhibit fringes (See Fig:4.40), which are an alternation of microflower-like precipitates and needle-like precipitates. The boundary line between the two domains is sharp. The length of a fringe, a microflower domain plus a needle domain, is around 400 µm, which is comparable to the periodic pattern wavelength previously deduced from optical microscopy.

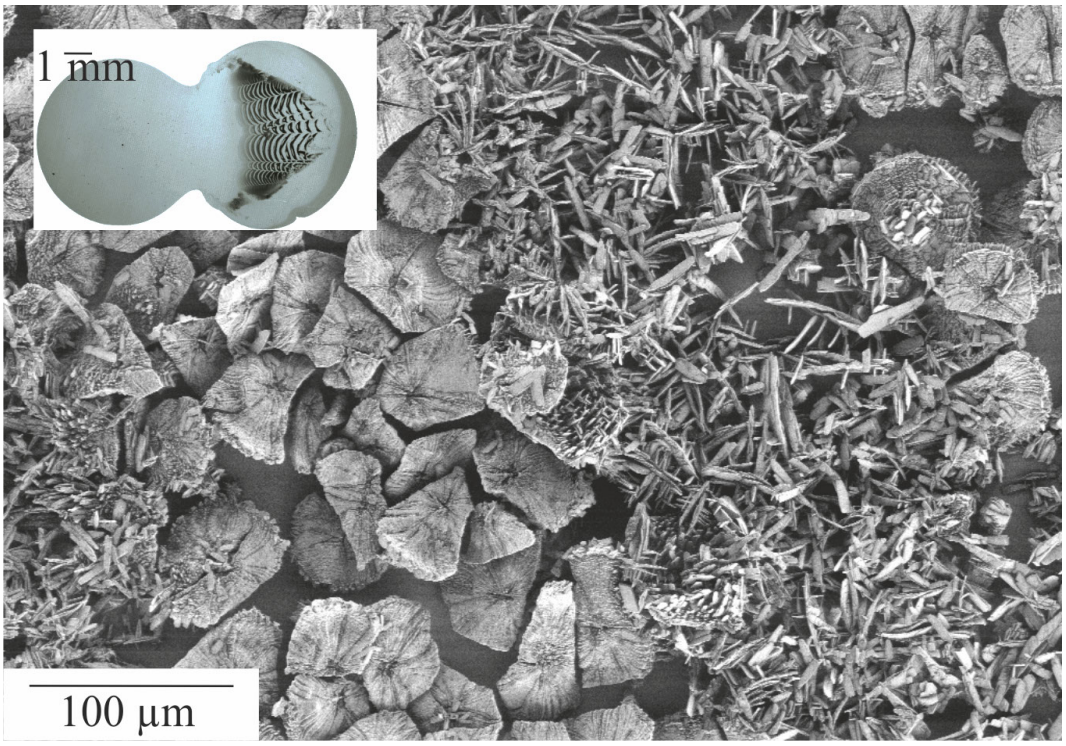

Figure 4.40: SEM image of cerium oxalate morphology alternation in the case of periodic precipitation (from right to left needles/microflowers/needles/microflowers). Insert: OM image of the corresponding sample before drying.

This result indicates, that the periodic pattern is an alternation of two kinds of particles with different scattering properties. These particles are either (or evolve into) needles and or microflowers during growth or drying. By comparison with the particles obtained at low and high oxalic excess, it is highly probable that the microflower particles are issued from weakly light scattering domains, whereas the needles are issued from the strongly light scattering ones. Note that SEM measurements show, that the precipitate morphology is independent from the Marangoni flow direction in the three regimes.

While the needles appear always with the same shape, it is not true for microflowers. Some of them are spherical, others hemi-spherical and others have more or less thick polygon shapes. These particles indeed evolve differently regarding the aggregation and growth conditions (See Sec:4.4.2 for further details).

To conclude, in the three precipitation patterns observed in half diols/ half water media, weakly light scattering domains correspond to microflowers (or microflower precursors) whereas strongly light scattering domains are typical of needles (or needles precursors).

If needles is the usual morphology for oxalate, it is not the case of microflowers. By comparison with other studies, it can be deduced that microflowers are obtained only in the presence of additive species, in this case propanediols. The nucleation/growth mechanisms which lead to the formation of microflowers are still not fully understood nowadays. Moreover, the mandatory drying step preceding the SEM measurements could modify the morphology of the solid particles. To rule out this uncertainty, the solid particles where imaged *in situ* using confocal microscopy.

Growth kinetics and mechanisms

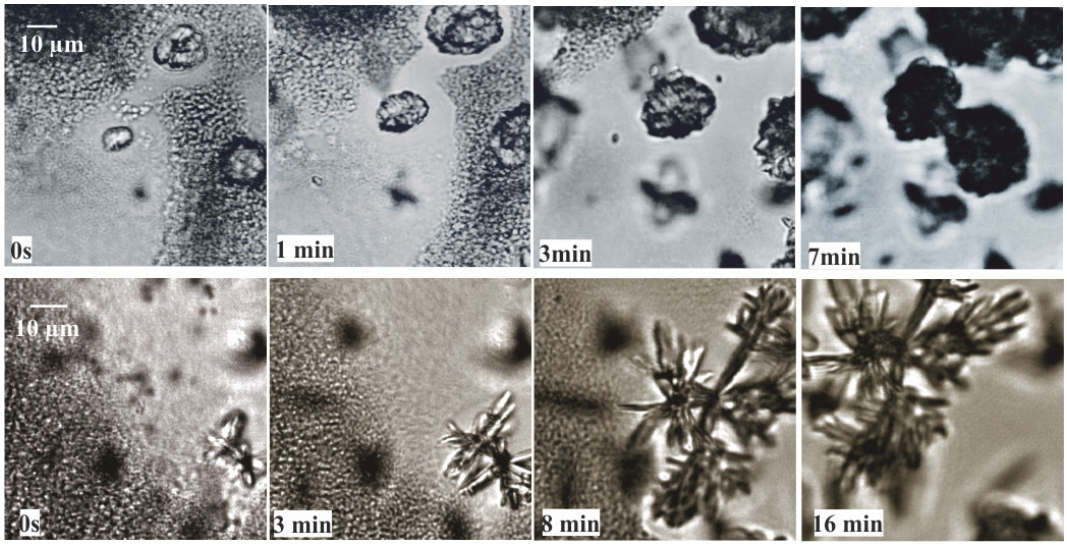

Figure 4.41: Confocal microscopy images of the precipitate evolution in drops. The oxalic excess are 0.6M and 0.8M for the upper and lower row respectively.

Confocal microscopy enables to image the precipitates inside the drops, thus providing informations both on their morphology before the drying step and on their growth kinetics and mechanisms. Confocal microscopy images on figure 4.41 show the typical precipitate evolution with time. The OE of the sample imaged on the lower line images is 0.8M for a volume fraction of 25% in 1,3-propanediol, in this condition strongly light scattering precipitation patterns are expected, whereas, in the upper line image conditions (OE=0.6M in 25% 1,3-propanediol), a weakly light scattering precipitation pattern is expected. For these measurements, the time origin corresponds to the first image recorded. A delay of approximately 1 to 3 minutes is usually obtained between the beginning of the drop coalescence and the imaging, due to the microscope parameter adjustment.

At low oxalic excess, spherical micrometer size precipitates are observed after some minutes. Although the confocal microscope does not enable to access the topography details of such precipitates, the latter appear similar to microflowers. Their diameter, typically around 20 µm, is slightly smaller than the one of microflowers observed by SEM. This size difference is likely induced by an additional growth during the drying procedure. At high oxalic excess, needle-like precipitates are observed inside the drop. Once the growth is completed, their typical length is 23 µm. Regardless of the OE level, submicrometer size particles are produced during the first seconds after coalescence. Most of them slowly disappear, while the bigger particles are growing. Moreover a depletion zone can be observed around the growing particles. The disappearance of the smaller particles in favour of the bigger ones and the depletion zone are indications for Ostwald ripening.

Precipitation pattern formation takes tens of seconds whereas tens of minutes are necessary for the precipitate growth. As a result, the strongly and weakly light scattering precipitation patterns reveal a difference in the optical properties of the submicrometers particles. Their optical properties can arise from their size, shape, structure or density. Furthermore, it seems that the aggregation behaviour of these submicrometer particles differs (See below). As shown on figure 4.37, the optical difference persists a long time. In other words, microflowers and needles have different optical properties too. The needles are randomly oriented, as a consequence, they behave as randomly disperse mirrors, which scatter the light in all directions. For this reason, the precipitation pattern composed of needles appears white to human eyes and black through the drop set-up. The microflowers orientation inside the drop do not scatter the light.

Deduced from the confocal and the SEM measurement, cartons (Figs: 4.42, 4.43 and 4.44), present the proposed mechanisms and aggregation/growth conditions which would lead to the different precipitate shapes.

At high oxalic excess, submicrometer particles of cerium oxalate precipitate as soon as the two liquids get into contact. These light scattering particles do not have tendency to aggregate. Moreover, the growth rate of one of the faces is significantly higher than the others. Hence, the precipitates grow as needles. The smaller particles redissolved to enable the growth of the bigger ones according to the Ostwald ripening process. The precipitates probably grow through ion attachment as described in the classical nucleation and growth theory.

In the same way, at low oxalic excess (See figs: 4.43 and 4.44), submicrometer par-

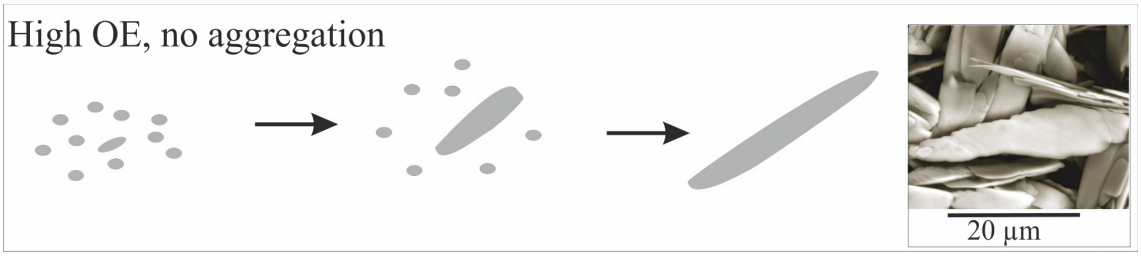

Figure 4.42: Proposed mechanisms for the needle growth at high oxalic excess. First submicrometer particles are formed, which slowly redissolve in favour of the bigger particles.

ticles precipitate first. These particles have tendency to aggregates. Thus they lead to either pre-microflowers or microflowers, depending on the aggregation and growth conditions. At extremely low oxalic excess, the precipitate growth is limited by the reactant supply, pre-microflowers are obtained as shown on figure 4.43. When the local oxalic excess is slightly higher, both aggregation and growth are more important (See Fig:4.44). Assuming that the observed precipitate were produced inside the Marangoni flow, the qualitative relation between oxalic excess and precipitates morphology is deduced from the precipitates location inside the dried sample. More precisely, in the case of direct Marangoni flow, the global tendency of the oxalic excess in the neck region is to decrease with time. In that respect, the first particles issued from the neck, in the dried sample, are the ones produced in the higher oxalic excess conditions.
In all cases, growth is achieved by Ostwald ripening.

Precipitates structure

Backscattering electron microscopy (See Fig:4.45) enables to distinguish species with different molecular weight. In that mode, low molecular weight components appear darker as the high ones. Hence regarding our sample, the solid, which appears darker is assumed to be oxalic acid crystallized during the drying step. Moreover, heigh molecular weight atoms are present in the needle solid particles and since cerium is the heavier atom in the system, the needles must be cerium oxalate precipitates.
Figure 4.46 displays the XRD patterns of the precipitates obtained in the different precipitation regimes. The measurements were performed in the same conditions as previously (See Sec:4.4.1).
The XRD patterns are similar to the ones obtained in pure water. At high and intermediate oxalic excess, peaks at $2\theta = 14.9°$, $15.3°$ and $18.8°$ are indicative of the presence

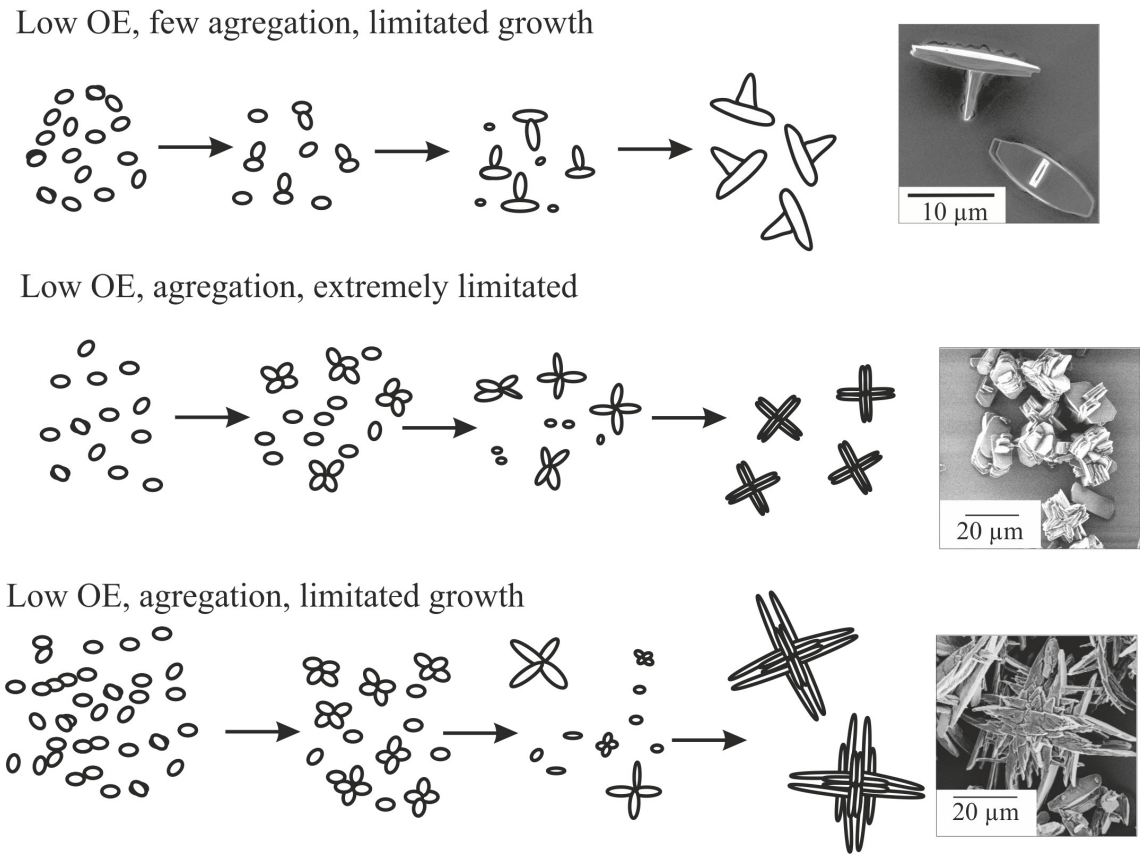

Figure 4.43: Proposed growth mechanism for the microflowers particles at low oxalic excess and with a growth limited by the supply in reactants. These mechanisms are compared to the precipitate morphologies imaged by SEM.

of crystallized oxalic acid inside these samples. The other peak positions are identical for the three patterns and correspond to the one obtained for precipitates in pure water solvent. Rietveld refinement was performed on these XRD patterns in order to determine the lattice parameters of these precipitates. The results are given on table 4.3 and compared with the theoretical parameter for the structure resolved by Ollendorf. The difference between the two XRD patterns can be evaluated on figure 4.47

Rietveld refinement highlights a monoclinic P21/c structure, as the one resolved by Ollendorf with minor modifications in the lattice parameters (maximum 0.2 Å).

The similarity with the XRD patterns of particles produced in pure water indicates that the solvent does not influence the structures of the precipitates. The needle and microflower particles are both cerium oxalate precipitates with, at a first approximation, identical structures. However, regarding the low oxalic excess sample, in which SEM always revealed booth needles and microflowers, a local diffraction measurement could

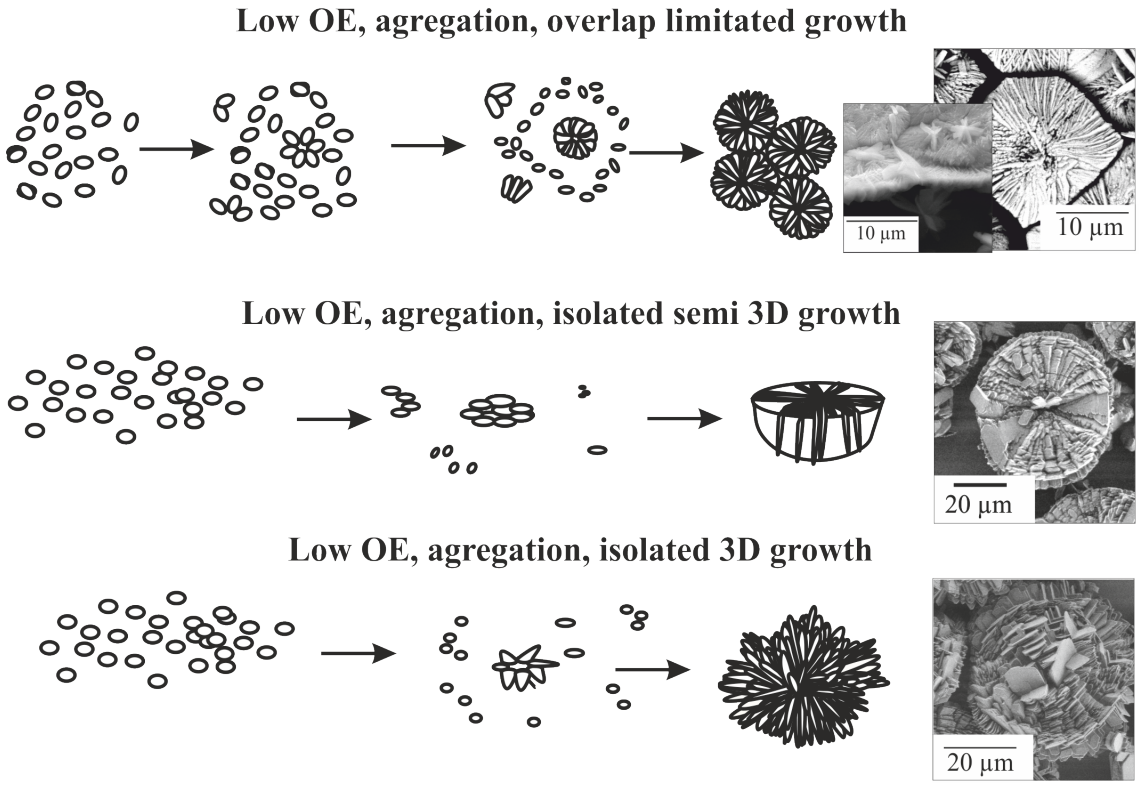

Figure 4.44: Proposed growth mechanisms for the microflower particles at low oxalic excess and with a growth kinetics limited by the reactant supply.

	Ollendorf structure	Rietveld refinement
a (Å)	11.34	11.26
b (Å)	9.63	9.84
c (Å)	10.39	10.38
β (°)	114.50	114.23

Table 4.3: Lattice parameters determined by Rietveld refinement and theoretical value of the cerium oxalate decahydrated structure as resolved by Ollendorf

be performed in order to check further the XRD pattern of pure microflowers. Moreover, because XRD measurements are achieved on the dry precipitates, the patterns do not enable to conclude on the structure of the strongly and weakly light scattering submicrometer particles before the growth.

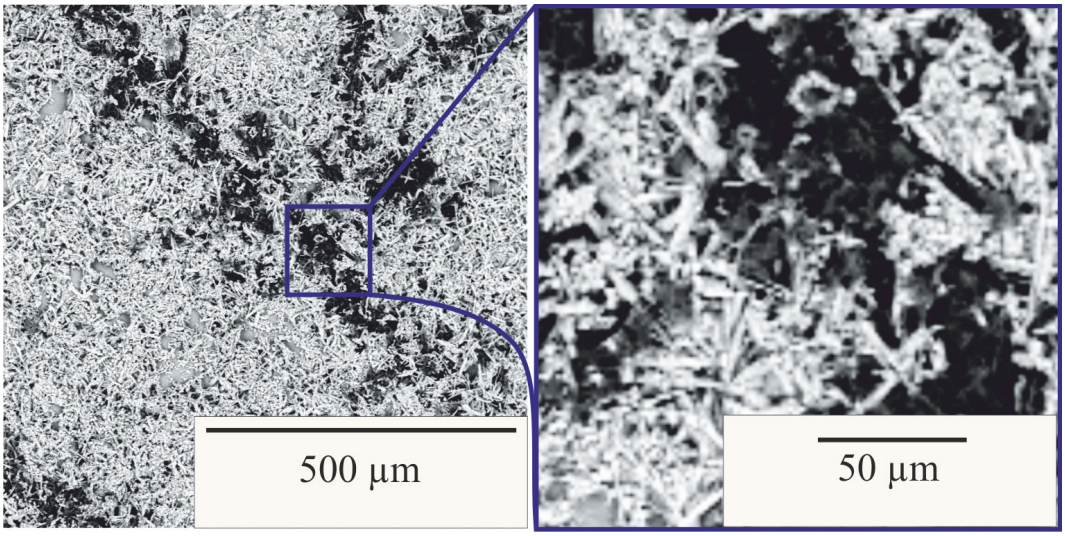

Figure 4.45: Backscattering electrons microscopy of a high oxalic excess sample in diols. The darker areas correspond to low molecular weight atoms whereas the light areas indicate high molecular weight species.

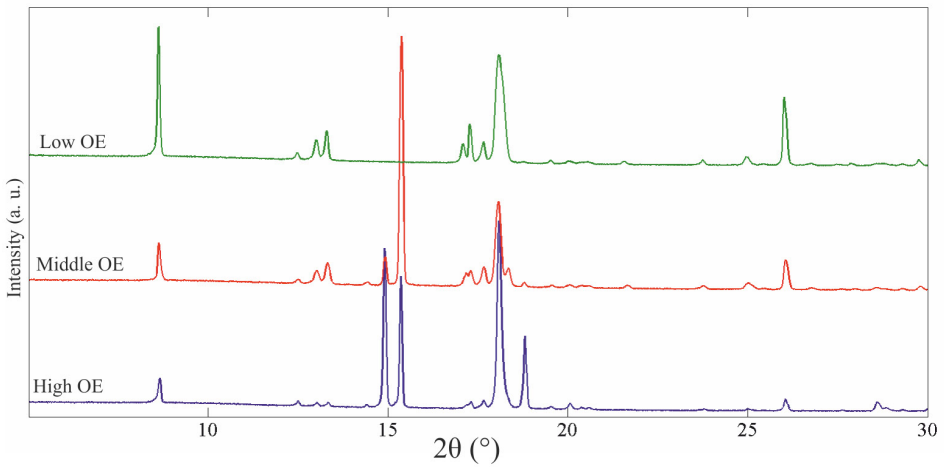

Figure 4.46: XRD patterns of the precipitates issued from the different precipitation regimes obtained with 50% water 50% diols mixture for oxalic excess of 0.2M (upper line), 0.7M (middle line) and 0.9M (lower line)).

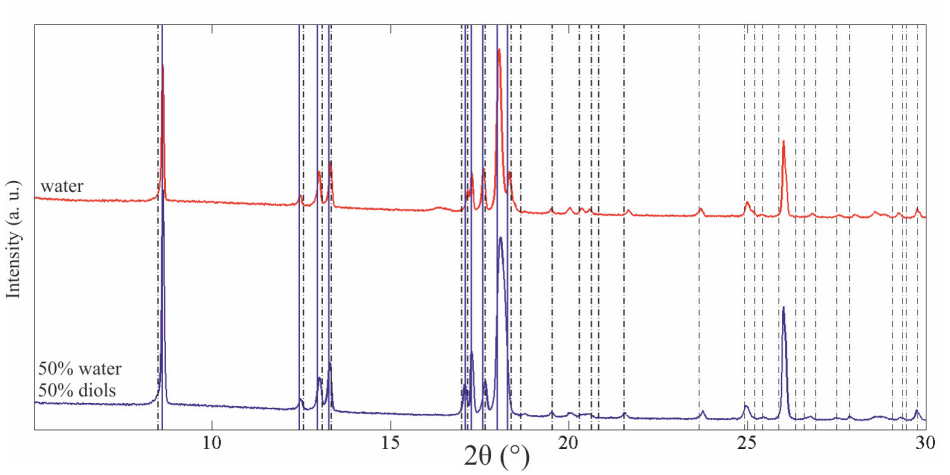

Figure 4.47: XRD patterns of precipitates obtained in pure water solvent (upper row) and in 50% wsater, 50 % diols medium (lower row) for an oxalic excess of 0.2M. The dotted and solid lines refer to the peak positions for the Ollendorf and our resolved structures respectively.

Small Angle X-Ray Scattering

SAXS experiments were performed to compare the surface over volume ratio of the needles and microflowers particles. In figure 4.48 are shown the SAXS patterns measured on needles, microflowers and a mixture of both (Fig:4.48a). In each case, the loglog plot at small q values is compared with a q^{-3} and q^{-4} profile (Fig:4.48b). Table 4.4 gathers the transmission coefficients, T, volume fractions, ϕ and power law exponents, x, determined for the three sample. The transmission coefficient is measured directly on the SAXS apparatus. The volume fraction is calculated from the transmission coefficient and the capillary inner diameter using equations 4.3 and 4.4.

$$e_x = \frac{ln(\frac{T_x}{T_{solvent}})}{\mu_{CeOx} - \mu_{solvent}} \tag{4.3}$$

where μ_{CeOx} =8.66 cm^{-1} and $\mu_{solvent}$ =1.21 cm^{-1} are the cerium oxalate and water linear attenuation coefficient at 0.71 Å and e_x is the sample thickness.

$$\phi = \frac{e_x}{d_i} \tag{4.4}$$

where d_i is the capillary inner diameter.

The power law was determined by fitting the $I = A * \exp q^{-x}$ function and the measured intensity for q between 0.2 and 1.1 nm through a mean square sum minimization.

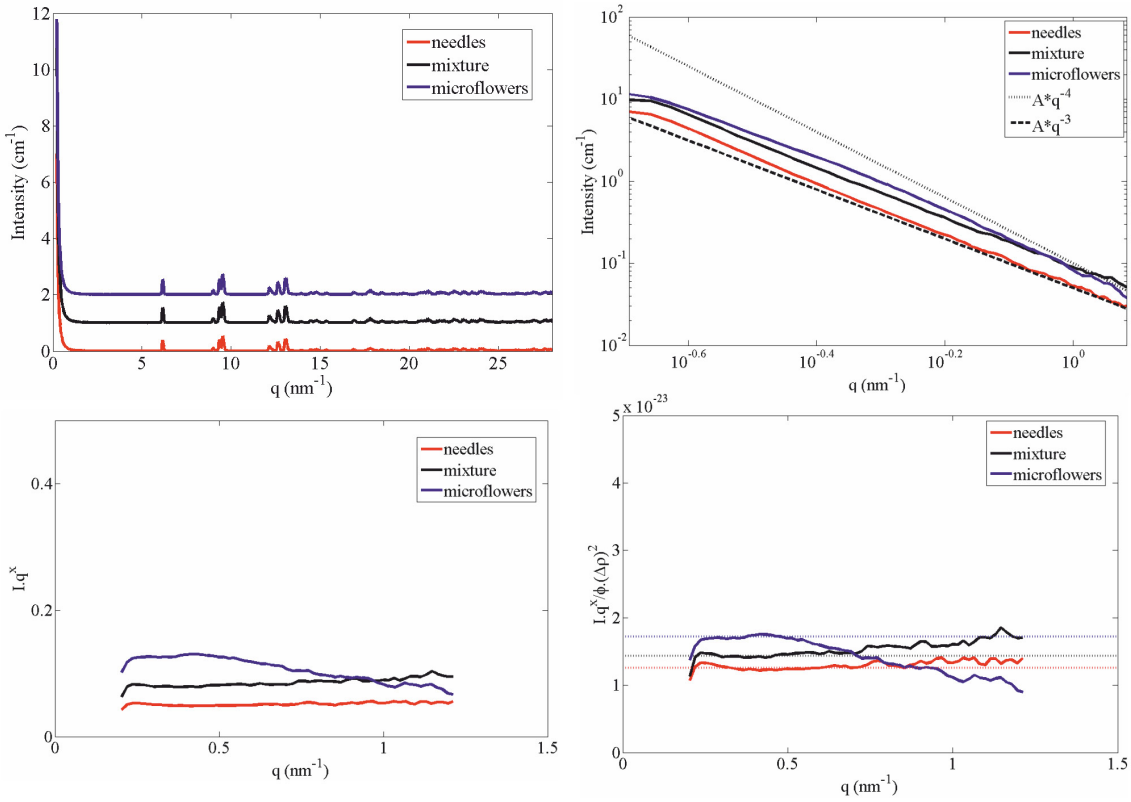

Figure 4.48: a) SAXS patterns of the three precipitation regims. b)Loglog representation of the small q values. c) and d) evaluation of the surfaces of volume ratios.

	T	ϕ	x
needles	0.51	0.40	3.2
mixture	0.42	0.56	3.2
microflowers	0.33	0.74	3.0

Table 4.4: Determination through the SAXS apparatus of the samples transmission, T, volume fraction, ϕ and power law, x.

The identical peak positions on the three SAXS patterns confirm that needles and microflowers are made from the same mineral. The scattering intensities decrease with the scattering vector with a power law close to 3. Such a tendency indicates a not well-defined interface between the scattering particles and the surrounding media. It is also the proof, that all the mineral investigated here have two big dimensions and a small one[99].

In 50% water and 50% propanediols solvent, precipitation patterns induced by sessile drop coalescence are stable over time. This enables to correlate the precipitate features to their location once the Marangoni flow vanished, even after the drying step. Weakly light scattering precipitation patterns, at low OE, are composed of submicrometer particles which evolve in microflowers-like precipitates by Ostwald ripening. Scattering light precipitation patterns, at high OE, are needle precursors which grow by the same mechanism. The XRD patterns of dried precipitates indicate an identical monoclinic crystal structure for the cerium oxalate obtained in both regimes. There are small differences between the lattice parameters of these cerium oxalate and the one resolved by Ollendorf.

4.4.3 Discussion about local environment effects

Fringes appear to be an alternation of particles with different optical properties. The weakly light scattering particles will evolve in microflowers through Ostwald ripening, whereas the strongly light scattering particles will grow as needles. The precipitation of needles or microflowers and their precursors are determined by the supersaturation conditions and the chemical environment during the nucleation, aggregation and growth of the precipitates. The morphologies and structure of the precipitates obtained are independent from the Marangoni flow direction.
Additional experiments with control reactants feed, should be considered to investigate further the influence of each step on the final features. One configuration could be to add a third drop during the coalescence of oxalic acid and cerium nitrate sessile drops with water solvent. The third one, containing additional reactants and diols, would be put into contact with the coalescing drops at a different moment (e.g 0s, 1s, 10s, 1min, 2min or 10min after two first drop contacts). These experiments aim to determine whether the initial submicrometer particles are the key to the final morphology or if the latter depends on the chemical environment during their growth. Moreover, the separated influences of 1,2 propanediol and 1,3 propanediols on the precipitate features was not investigated separately here. Indeed, due to their close chemical structures, it was assumed, at a first approximation, that they had identical effect on the precipitates. However, studies with different species of precipitates have concluded that the effect of each diol on the solid was different.

In the following, two experiments are presented. They are related to the local effect of the reactant transport on the precipitates.

Precipitates obtained in beakers

For comparison, the morphology of precipitates produced by mixing in a vial 50 µL of cerium nitrate solution at different concentrations with 50 µL of 1.1M oxalic acid were imaged by optical microscopy, once the precipitates growth completed. The mixing was performed by hand shaking. The solvent composition after mixing is 50% water, 25% 1,2-propanediol and 25% 1,3-propanediol. The evolution of the precipitate morphologies as a function of the oxalic excess is represented in figure 4.49. The percentages and curves are given as estimations.

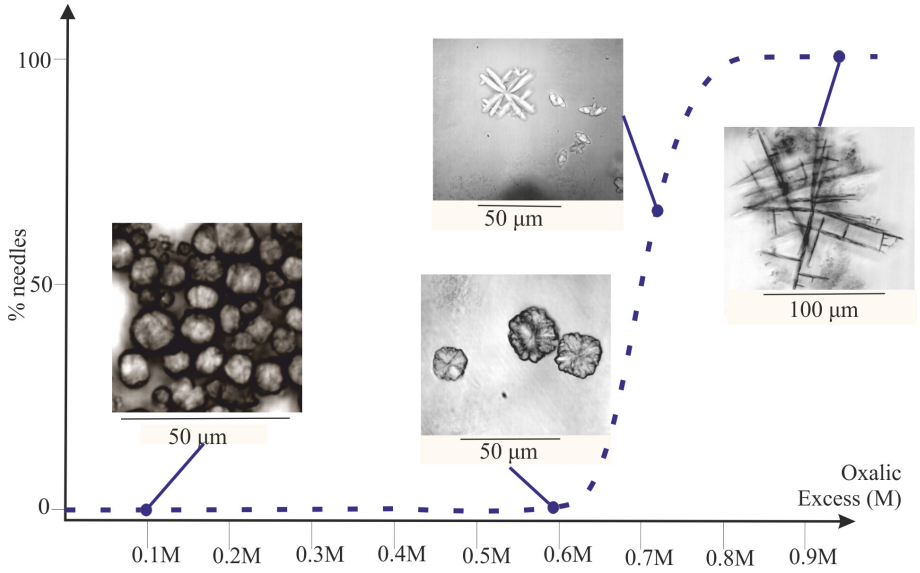

Figure 4.49: Precipitates obtained in beakers with hand mixing as a function of the oxalic excess. As in the case of coalescing drops, mainly microflowers are produced at low OE whereas needles are obtained at high OE.

At low oxalic excess, microflowers with an average diameter between 10 µm and 25 µm are produced. These diameters vary with the oxalic excess. The lower the oxalic excess, the smaller the precipitates. At high oxalic excess, needle-like particles precipitate with a length around 40 µm. The transition between both morphologies is observed for an oxalic excess of approximately 0.7M, for which precipitates with intermediate shape are observed.

These results validate, that microflowers are obtained due to the presence of propanediols in the solvent and are independent from the drop coalescence configuration. Moreover, this confirms that the final precipitate morphology is linked to the initial supersaturation conditions. The oxalic excess threshold, t_{mn} at the transition between nee-

dles and microflowers corresponds to the oxalic excess for which periodic precipitation patterns were obtained in solvent composed of 50% water, 25% 1,2-propanediol and 25% 1,3-propanediol. The mixing conditions of these experiments are not well defined. As a consequence, for the same initial conditions, variations in the size of the precipitates can be observed. Moreover, the easy implementation of these control experiments, and the homogeneity of the precipitate sizes and morphology, at fast mixing rate, inside a unique sample, make it particularly suitable to study the influence of the 1,2-propanediol compared to the 1,3-propanediols on t_{mn} and the precipitate morphologies.

High viscosity solvent

Figure 4.50 displays the morphologies of precipitates formed in 25% water, 75 % diols media for different oxalic excess, imaged by SEM.

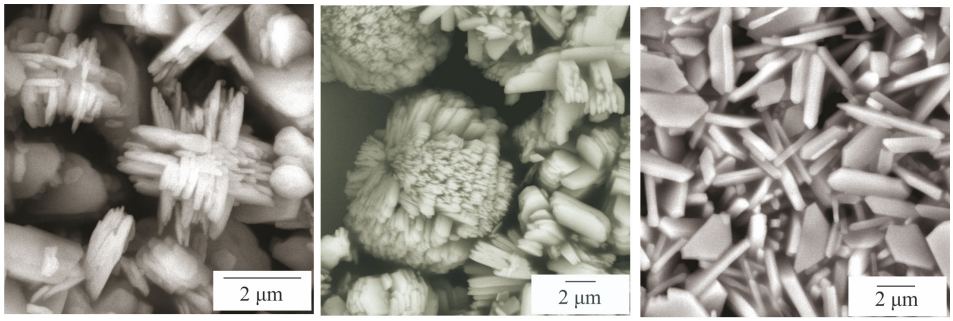

Figure 4.50: Morphologies of the cerium oxalate precipitates obtained in 25% water/ 75 % diols solvent at different oxalic excess

At high oxalic excess needles and slab are obtained with a typical length of 6 µm and width varying between 5 µm and below 1 µm. As for precipitates produced in 50% water, 50% diols medium, organized precipitates are obtained at low oxalic excess. Their shape is similar to the microflowers with a significantly smaller characteristic size around 8 µm. Moreover, the intermediate case exhibits both micoflowers and single slabs. In the intermediate oxalic excess SEM image of figure 4.50, a thick microflower is exhibited. It seems to be composed of several layers of superposed cross-like units. The morphologies exhibited by these precipitates appear to depend on the observation direction. However, as shown previously in 50% water / 50% diols media, cerium oxalate can precipitate under plenty of microflower like morphologies. Therefore, this

observation is not sufficient to affirm, that all microflowers obtained in high viscous media are thick.

The XRD patterns of precipitates produced in 25% water, 75% diols medium (not shown here), exhibit the same peaks as the ones precipitated in 100% water or 50% water/50% diols media.

4.4.4 Conclusions on precipitates features

All the obtained results indicate that the solid size and morphology depend of the local supersaturation ratio during the nucleation, aggregation and growth process, and by extension of the flows. The medium has a high impact on the precipitate morphologies and sizes. Indeed, needle-like precipitates are formed in purely aqueous solution, during the coalescence of sessile drops, independently from the precipitation pattern. On the contrary, both needles or microflowers can be produced when the precipitation media contained diols. At low oxalic excess, microflowers are in majority precipitates, whereas at high oxalic excess only needles are observed. Periodic patterns are composed of needle precursors, in the strongly light scattering regions, and of microflower precursors in the weakly light scattering domains. Moreover, the XRD pattern analyzes indicate similar crystal structure of the precipitates independently from the precipitation media and morphology. However, a more detailed analyze of the XRD pattern, and particularly of the peak width, could bring more imformations on the structure and agglomeration of both morphologies. Such analyses could not be performed hereby. Rietveld refinement on the XRD patterns yields a monoclinic structure with lattice parameters close to the ones exhibited by the structure resolved by Ollendorf for cerium oxalate decahydrated.

Confocal microscopy observations in 50% water 50% diols media reveals a growth by Ostwald ripening of the precipitates, regardless of their morphologies. This growth mechanism is probably independent from the precipitation solvent. Indeed, identical precipitation patterns, *i. e.* either strongly light scattering at high oxalic excess or weakly light scattering at low oxalic excess, are observed in 100% water, %50 water/50% diols and 25% water/75% diols medium. Two remaining open question are: what is the difference between submicrometer particles precipitated at different OE either in water or in mixture solvent ? Indeed, such results could indicate that the features of submicrometer particles, just as their optical properties, are independent from the chemical environment and only depend on the oxalic excess. Then, the morphology

difference would only be a result of the effect of the solvent during the growing step. In other words, weakly light scattering submicrometer particles obtained at low oxalic excess in 100 % water would lead to microflowers, if they were grown in 50% water /50% diols media. However, further experiments, as the one described in section 4.4.3, have to be carried on in order to have a closer look on the relation between the particle feature and the local environment.

4.5 Structured solvent

So far, this study focuses on the flow induced by the coalescence of drops and its effects on the oxalic precipitation of cerium nitrate. We have shown, that the Marangoni flow and the reactants mixing strongly influence the precipitation reaction, when two low contact angle sessile drops coalesce in a surrounding air media. Water/diols mixtures were used to decorrelate $\Delta\gamma$, from the sursaturation ratio.

Researches about ternary systems reveal that the use of structured solvent modifies the activity of chemical components (See Sec:2.3.3). Structured solvents, also called pre-Ouzo effect, refers to monophasic water/hydrotrope/oil mixtures at a composition near the phase separation boundary. Recent studies have shown, that the formation of nanoscopic size oil rich domains, with diffuse interfaces, induces a modification of the activity coefficients in the pre-Ouzo region of the phase diagramm. Hereby, such systems are applied in order to modify, in a non quantitative way, the activity coefficients of the reactive species and thus the supersaturation ratio relevant for the precipitation reaction. This section gathers preliminary results on the cerium oxalate obtained during the coalescence of drops with structured solution as solvent.

4.5.1 Temperature dependence of the ternary phase diagram

The phase diagram of the ternary system is temperature dependent. Hence, in the case of water/1,2-propanediol/n-octanol, the miscibility increases with temperature (in other words mixtures which separate at a given temperature may be stable at a higher temperature). This property was used to prepare solvent mixtures in the pre-Ouzo region of the phase diagram, at 25 °C. For this purpose, solutions were prepared at 25 °C before being phase separated at 5 °C by centrifugation. The heavier phase thus obtained, the water rich solution, is in the pre-ouzo region of the phase diagram.

Figure 4.51 illustrates the phase diagram of water/1,2-propanediols/n-octanol mixtures at 5 °C and 25 °C, and the final composition of the solvent in the pre-Ouzo region of the phase diagram at 25 °C (blue point). For curiosity purpose, we have tested the four possible configurations regarding the reactants dissolved either in the water-rich or oil-rich as prepared solvent (See below Fig:4.53).

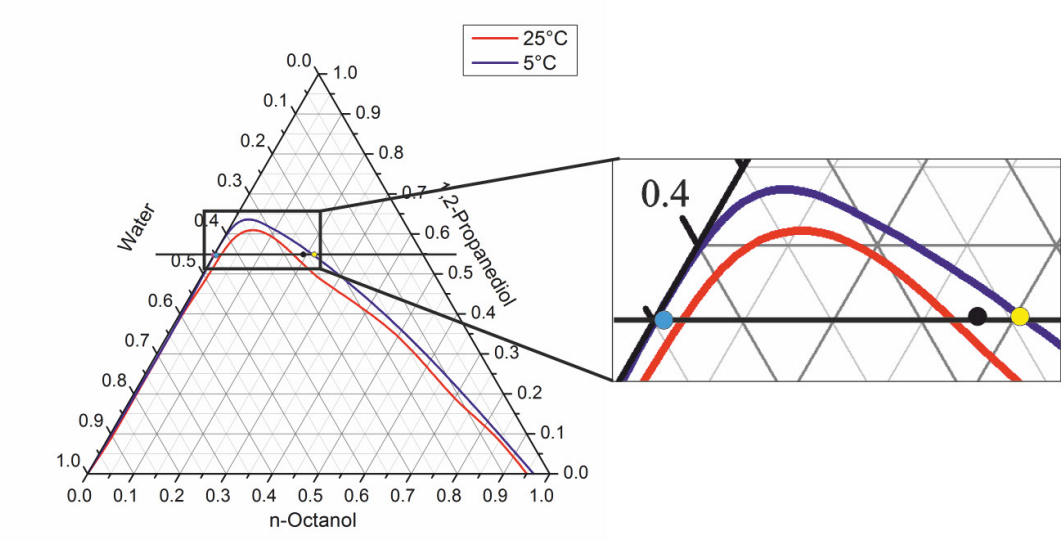

Figure 4.51: Ternary phase diagram of the water/1,2-propanediol/n-octanol system measured at 5 °C in blue and 25 °C in red. Insert: Zoom in the region of interest highlighting the composition of the structured solvent (black: initial mixture before phase separation, blue: water rich domain, yellow: oil rich domain).

4.5.2 Precipitation pattern, morphologies and structure in ternary solvent

First, the investigation on structured solvent were carried out at the OE value leading to periodic precipitation in the case of binary solvent (*i.e.* $[C_2H_2O_4]$=1.1M; $[Ce(NO_3)_3]$=0.45M; OE=0.43M). Figure 4.52 shows the periodic pattern obtained in the binary mixture 45% water and 55% 1,2-propanediol. This composition corresponds to the intersection of the water/diols side of the phase diagram and the demixing line of the ternary preparation. The precipitation regimes and the corresponding precipitate morphologies observed in the ternary solvent are shown on Figure 4.53. In each case, the Marangoni flow is directed from the cerium nitrate drop to the oxalic acid one (*i.e.* reverse Marangoni flow). Although at the same OE fringes are formed in binary mixtures, none of the precipitate issued from ternary mixture exhibits periodicity. Instead, a homogeneous strongly light-scattering precipitate is formed when cerium nitrate is dissolved in the water-rich phase (cases a and b). This pattern is identical to the one obtained in binary mixtures at high OE . Conversely, precipitation of a large weakly light-scattering domain results from a configuration, where cerium nitrate is dissolved in the oil-rich phase (case c and d). This pattern is very similar the pattern obtained in binary mixtures at low OE. We note, that the precipitate pattern is independent of the solvent, in which oxalic acid is

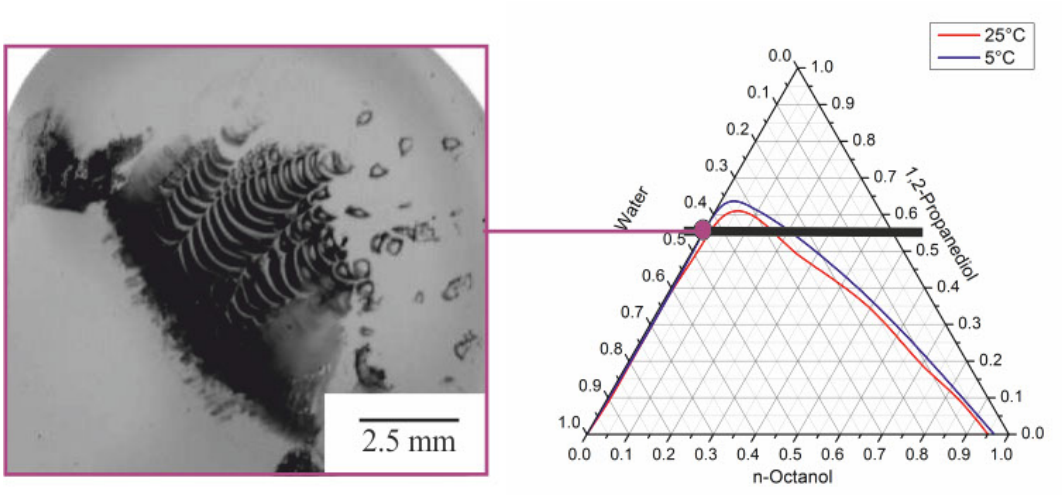

Figure 4.52: Periodic pattern obtained for OE=0.43M and a binary mixture as solvent(45% water and 55% 1,2-propanediol).

dissolved.

Friberg et al. [100] have shown that the hydrotrope plays the role of the "surfactant" in the so-called surfactant-free microemulsions (SFME). Thus, in pre-Ouzo aggregates, the diol acts similarly as a co-solvent between water and octanol. As a result, the diol activity is reduced by the presence of octanol aggregates [101, 102]. This has two consequencse:

- The solutes present either as nanoparticles or ion pair, would have to partition between the octanol rich aggregates and the structured water-rich phase. The equilibrium goes along the well-documented log-p scale of hydrophilicity [103].
- On the surface of the particles growing, the competitive adsorption isotherms will be modified. In binary solvent, we have seen that either needle or microflower-like particles precipitate. This is the basis of the enhanced enzymatic activity of SFME, known since nearly a century, and described in detail by Khmelnitsky et al. [104].

The oscillation between needle and microflowers is presumably controlled by the surface adsorption influencing the rate of crystal growth. Therefore, it is expected, that using a ternary structured solvent would change deeply the morphology of the precipitates. In the present state of theory, prediction is not possible, therefore we investigate this phenomenon by keeping everything constant as much as possible, and test the effect of presence or absence of pre-ouzo type aggregates.

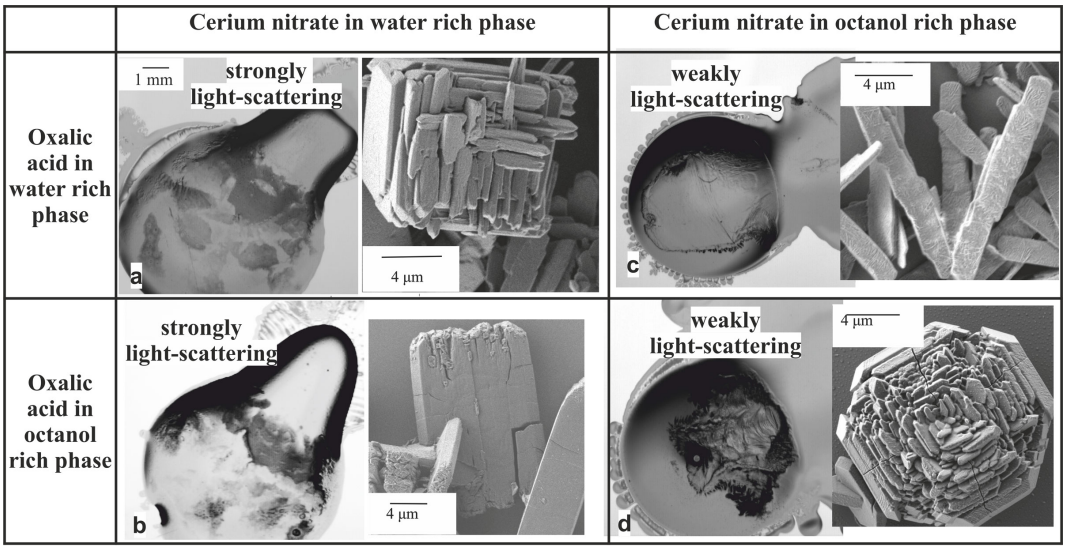

Figure 4.53: Cerium oxalate morphologies obtained in the different solvents for OE=0.43M and corresponding pattern observed by OM. Cases a,b: a large light scattering precipitate is formed, when the cerium nitrate in dissolved in the water rich-phase. Cases c, d) weakly light-scattering patterns issued from systems for which the cerium nitrate is dissolved in the oil-rich phase.

Regarding the particle morphology, the results exhibited in Figure4.53 show that elongated particles are formed when both reactants are dissolved in different solvent composition (Fig:4.53 cases b and c). More precisely, slabs are observed, when cerium nitrate only is dissolved in the solution containing pre-ouzo aggregates. Needles, which are very similar to the ones obtained in binary mixture at high OE, precipitate, when oxalic acid only is dissolved in the solution containing pre-ouzo aggregates. In these two cases, the solvents of the two drops are not miscible and a phase separation may occur.

When the two reactants are dissolved in identical solvent (cases a and d), organized structures are formed. In both cases, the particles look like well-organized needles or slab arrangements. The most astonishing point of the results is that elongated and organized structures are found both in strongly light scattering and weakly light scattering precipitation patterns. However, these results are only preliminary, and additional experiments are needed to investigate further the effect of structured solvent on the precipitation.

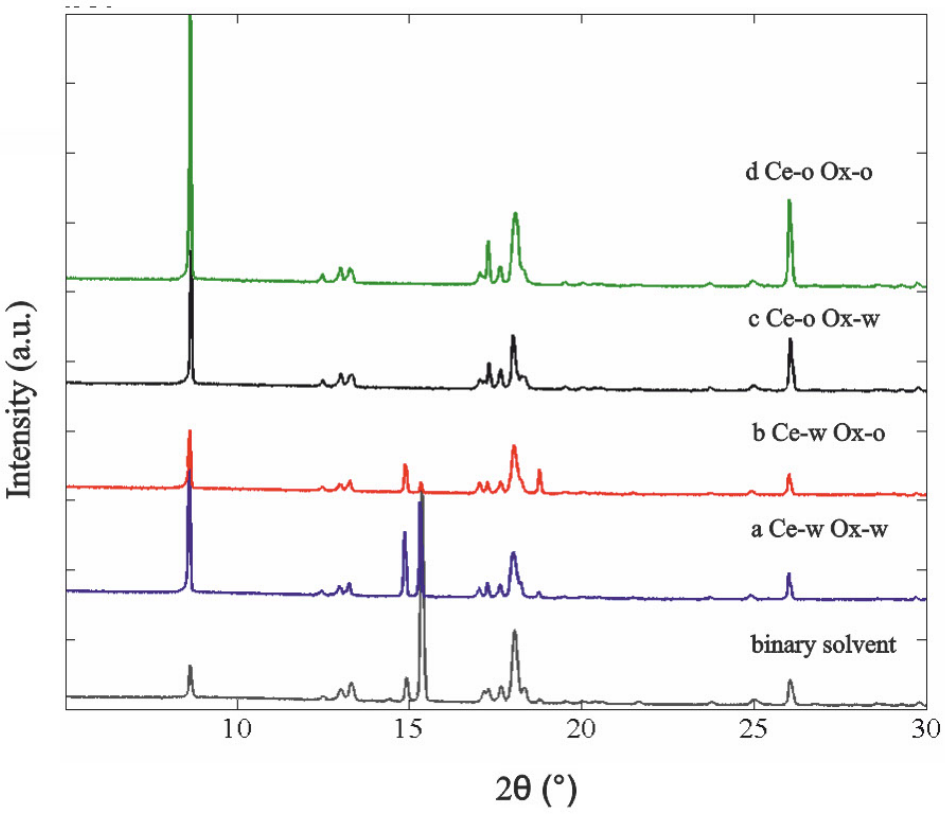

Figure 4.54: XRD pattern of the precipitates issued from binary mixture (lower row) and ternary solvent for OE=0.43M.

4.5.3 Crystal structures

The crystalline structure of the particles issued from ternary solvents were investigated by XRD (See Fig:4.54). The peak positions of the XRD patterns are identical to the ones of particles precipitated in water or binary mixtures. The peaks characteristic of the presence of dried oxalic acid (*i.e;* 2θ =14.9°, 15.3° and 18.8°) are exhibited by the pattern of both particles issued from binary mixtures and ternary mixtures with cerium nitrate dissolved in the water-rich phase (case a and b). These peaks are not observed on the XRD patterns of particles issued from ternary mixtures with cerium nitrate dissolved in the oil-rich phase (case c and d).

4.5.4 Short conclusion on ternary solvent

The preliminary experiments demonstrate, that ternary solvent leads to a modification of both the precipitation patterns and the cerium oxalate particle morphologies. In bi-

nary mixture, the investigated OE leads to a periodic precipitation pattern. In ternary solvent a shift toward the high OE (strongly light-scattering pattern) is achieved when cerium nitrate is dissolved in the water-rich phase. Conversely, the dissolution of cerium nitrate in the oil-rich phase leads to patterns identical to the ones obtained at low OE in binary mixture (weakly light-scattering particles).

Besides, the particle morphologies differ from the ones obtained in binary mixtures. New well-organized particles precipitate, if the reactants are dissolved in the same solvents. These particles, with an overall square shape, look like arrangements of needles and slabs. The crystal structure remains the same regardless of the solvent used.

CHAPTER 5

CONCLUSION AND OUTLOOKS

It is generally accepted that the flow and mixing conditions are relevant parameters regarding chemical reaction products. They are of major importance in the cases of crystallization and precipitation processes and affect the properties of the obtained particles (*e.g.* size and morphology). The link between mixing and precipitate properties is still poorly understood although it is very relevant economically for numerous industrial processes.

In this study, we investigated the interplay between a precipitation reaction and hydrodynamic conditions. For this purpose, several configurations of drop/drop coalescence were applied. The main experiments consist in bringing into contact these two drops with one drop containing oxalic acid and the second one containing cerium nitrate. Oxalic acid and cerium nitrate react and form insoluble cerium oxalate. When the two drops contact each other, they may coalesce. The coalescence behaviour will affect the precipitation reaction and vice versa. Two configurations of coalescing drops have been investigated, namely high-contact angle sessile drops in viscous liquid ("spherical" drops) and low contact angle sessile drops in air. The latter configuration has been investigated more thoroughly, in particular the impact of the liquid properties and of the chemical composition on the precipitation and the coalescence behaviour will affect the precipitation reaction and vice versa.

The study first focuses on the coalescence of "spherical" drops immersed in a liquid medium. In this configuration, it is found that, as soon as the two drops come into contact by their liquid/liquid interfaces, a liquid bridge is created between them. Pre-

cipitation occurs right away in this liquid bridge. The result is the formation of a solid precipitate barrier between the two drop volumes. This prevents further mixing of the liquids and hinders the precipitation reaction. Because of the hindered precipitation reaction and the poor mixing of both liquids in this configuration it has not been investigated in more details.

In the second, main part, of the thesis the drop/drop coalescence and precipitation behaviour have been investigated with sessile drops. Due to the surface tension difference, a Marangoni flow may be induced between the two drops. This affects the coalescence and precipitation behaviours.
Previous studies with miscible and non-reacting liquids have shown, that, in air, this Marangoni flow may even be strong enough to delay temporally the coalescence. We investigate in this thesis the effect of a precipitation reaction on the coalescence of sessile drops in air. We observed four coalescence behaviours (compared to two in the case without reaction), namely (1) barrier precipitation, (2) complete coalescence with Marangoni flow, (3) partial coalescence with Marangoni flow, and (4) non-coalescence. In case (1) and (4) the mixing is very weak. Therefore, here we focus on the case of partial and complete coalescence with a Marangoni flow, for which the mixing is substantial. In these cases, precipitate is continuously formed in the contact region between the two drops. It is then pushed away by the Marangoni flow from the neck to the high surface tension drop.

The precipitate generated during the complete and partial coalescence with Marangoni flow has been investigated for three different solvent compositions (100% water, 50% water/ 50% diols and 25% water/ 75% diols mixtures) and for varying reactant concentrations. Thus, the solvent viscosity, a first control parameter, has been varied between 1 mPa s and 15 mPa s. For the two solvents with diols, a second control parameter, the surface tension difference between the two drops has been adjusted independently from the reactant concentrations. The reactant concentration has been quantified by the oxalic acid excess, OE, the third control parameter. At high OE, in all three solvent cases, a large homogeneous domain, which strongly scatters light, is formed above the high surface tension drop. These precipitates are needle-like cerium oxalate with sizes varying between 25 to 4 µm. At low OE, weakly light-scattering precipitate particles emerge. The morphologies of these particles depend on the solvent. In water, they are small needles, whereas in water/diols mixtures cerium oxalate particles look like microflowers. At intermediate OE, fascinating periodic precipitation patterns are

formed. These patterns consist in alternating strongly and weakly light-scattering precipitates. In the case of diol mixture, the fringes are alternation of needles and microflower precipitate domains. These periodic patterns are formed presumably due to a convection/diffusion/reaction process.
It has been shown, that the three precipitation patterns (weakly light-scattering, strongly light-scattering and periodic pattern) are independent from the Marangoni flow direction. XRD analysis reveals that the structure of these precipitates, with different morphologies, are identical.
The free acidity inside the reactive drops has not been investigated in this study. However, this parameter could be related to the precipitates morphologies. Thus, a systematic investigation of the precipitate morphologies as a function of the solution free acidity would enrich this study.
In the last part of this thesis, a modification of the reactant activities and the chemical reaction is proposed and preliminary experiments are presented. The use of water/diols/octanol solvent, which composition corresponds to the pre-Ouzo part of the phase diagram, leads to the precipitation of cerium oxalate with various exotic morphologies.

Up to now, the details of the process leading to the periodic precipitation remain unknown, because we do not know the local concentration yet. To gain more inside, it would be helpful to gather more data about the evolution of the average periodic pattern wavelength with the solvent viscosity. The relation between λ and η is presumably the key to a better understanding of the mechanisms at the origin of the periodic precipitation. It would be very interesting if other systems than cerium oxalate, would lead to similar behaviour including fringe formation. To verify the universality of the processes, the selected chemical system must form two different products. Preferably these two products should be distinguishable by OM. Another open question is still the relation between the morphologies of the precipitates and the diols. Last but not least, it would be interesting to investigate the coalescence and precipitation behaviour of sessile drops in liquid media. This configuration is closer to the industrial process.

Acknowledgements

This work was realized in the framework of a collaboration project between the French Commission for Nuclear and Alternative Energy (CEA Marcoule, France), the Max Planck Institute of Colloids and Interfaces (MPIKG Potsdam-Golm, Germany), and the Marcoule Institute of Separation Chemistry (ICSM Marcoule, France). Equivalent time has been spent in both countries.

I am deeply grateful to Prof. Thomas Zemb and Prof. Helmuth Möhwald, first, for giving me the opportunity to perform this study under their supervision, and then for their constant support and advices during this PhD. Special thanks to Thomas Zemb for his support in the development of my future projects. I would like to thank Hans Riegler for the fruitful, numerous discussions on coalescence and precipitation among other topics. I have both developed my critical spirit and learnt to consider facts from different perspectives at his side. This work would not have been the same without the supervision of Dr. Sophie Charton. Her endless help, support and her great advices enabled me to overcome the most difficult tasks of this project. It was a real pleasure to work with all of you and to mix your different expertises and point of views. I would like to thank Prof. J-C. Valmalette and Prof. G. Brezesinski for accepting to review this thesis and Prof. J-F. Dufrêche and Prof. H-J. Bart for being part of the jury committee.

This collaboration project has been a great opportunity for me to meet people with various backgrounds and origins from whom I have learnt a lot scientifically and personally. Regarding the German side, my first thanks go to my group partners among them Rodrigo, José, Chenyu, Ferenc, Hubert and Guoxiang. Special thanks go to Virginie, with whom it was a pleasure to work in the lab and support each other in the wild German jungle, to Dr. Stefan Karpitschka (alias Senior) for the time he spent to guide me during the first months of this PhD and the teaching of a so-true German song and to Stephan (alias Junior) for his help with technical issues, specially with the "Artung

Französen sind in der Nähe" computer and for finally asking for hugs. I owe many thanks to Stefanie Riedel and Sebastian Podszus for helping me with German administration and traditions, increasing my everyday happiness, teaching catch-up German sentences, laughing at French accent and being my German family. Thank you to Bahareh and Afroditi for being so generous in their friendships (and for giving me a roof when I needed one). It was a pleasure to meet so many people at MPIKG, among them Bat-el, Janos, Rémi, Sacha, Thomas, Marcos, Martin, Laurent, Tim, Marc, Menny, Reinhild, Caro, Aurelio, Tom, Basti, Levan, Jan, Vasil, Sonja, Jonas, Heidehiko, Amy, Rugby and many others. Thank you for all the hugs and love I have received from all of you. I am indebted to Florian for the English checking of a great part of this thesis and his constant support even from far away. Outside the MPIKG, living in Germany was quite an adventure. Thank you to Rico, Miriam, Antonin, my different flatmates and my impro-partners to have walked on my side during that time.

En ce qui concerne la partie française de cette collaboration, je remercie l'ensemble des permanents du LGCI pour leur accueil chaleureux ainsi que leur aide précieuse tout au long de ce projet. Je suis particulièrement reconnaissante envers Hervé Roussel et Fabrice Lamadie pour leurs nombreux conseils et idées. Merci à Tojonirina Randriamanantena pour son soutien constant, notamment durant les périodes de doute. Ce fut un plaisir de croiser ou recroiser le chemin de Diane, Jean-François, Marion, Moussa, Damien, Selim, Benji, Maximilien et Matthias. Merci à Lucie, Loren, Adeline et Romain pour avoir apporté quotidiennement un brin de soleil à la maison. Ce fut bien chouette!

Aurélie, Marine, Emma, Clément, Maxime il n' y a pas de mot pour exprimer l'importance que vous avez à mes yeux. Merci pour votre amitié sans failles depuis toutes ces années. Sophie, Nico, Vincent, Eloi (j'ai hâte de continuer la tournée des places en C), Romain, Florentina, Maria, Manue, Noémie, Cadémis, Fanny, Mélina et Débohra merci pour tous les bons moments passés à vos côtés, pour les tonnes de souvenirs recoltés et accrochés. Cette période aurait été beaucoup moins heureuse sans le soutiens de ma famille, merci à eux. Merci à Alex et aux pandinios pour les nombreuses cartes postales toutes plus touchantes les unes que les autes. Je remercie également mon frère, Fabien, et mes parents de m'avoir toujours soutenus et encouragés dans mes projets même lorsque ces derniers m'éloignent d'eux. Pauline merci milles fois. Merci de m'avoir guidée pour devenir ce que je suis, d'avoir été un parfait modèle lors de notre enfance. Merci d'être présente encore aujourd'hui pour partager les bon moments et

pour me réconforter dans les moins bons.

Bibliography

[1] M. Kind. Colloidal aspects of precipitation processes. Chemical Engeneering Science, 57:4287–4293, 2002. http://www.sciencedirect.com/science/article/pii/S0009250902003457.

[2] S. R. Chemburkar, J. Bauer, K. Deming, H. Spiwek, K. Patel, J. Morris, R. Henry, S. Spanton, W. Dziki, W. Porter, J. Quick, P. Bauer, J. Donaubauer, B.A. Naryanan, M. Soldani, D. Riley, and K. McFarland. Dealing with the impact of ritonavir polymorphs on the late stages of drug process development. Organic research Process and Development, 4:413–417, 2000. http://pubs.acs.org/doi/abs/10.1021/op000023y.

[3] LO. Suber, I. Sondi, E. Matijevic, and D. V. Goia. Preparation and the mechanisms of formation of silver particles of different morphologies in homogeneous solutions. Journal of Colloid and Interface Science, 288:489–495, 2005. http://www.sciencedirect.com/science/article/pii/S0021979705002778.

[4] Y. Sun and Y. Xia. Shape-controlled synthesis of gold and silver nanoparticles. Science, 298:2176–2179, 2002. http://science.sciencemag.org/content/298/5601/2176.

[5] G. Borda, J. Duhamet, F. Gandi, and J.Y. Lanoe. Solute precipitation method and device, 08 2008. https://www.google.com/patents/US8431097.

[6] S. Charton, A. Kacem, A. Amokrane, G. Borda, F. Puel, and J.-P. Klein. Actinides oxalate precipitation in emulsion modeling: From the drop scale to the industrial process. Chemical Engineering Research and Design, 91:660–669, 2013. http://www.sciencedirect.com/science/article/pii/S0263876213000439.

[7] J. S. Eow and M. Ghadiri. Electrostatic enhancement of coalescence of water droplets in oil: a review of the technology. Chemical Engineering Journal, 85:357–368, 2002. http://www.sciencedirect.com/science/article/pii/S1385894701002509.

[8] J. Kamp and M Kraume. Influence of drop size and superimposed mass transfer on coalescence in liquid/liquid dispersions - test cell design for single drop inves-

tigations. Chemical Engineering Research and Design, 92:635–643, 2014. http://www.sciencedirect.com/science/article/pii/S0263876213005388.

[9] A. C. Ihnen, A. M. Petrock, T. Chou, B. E. Fuchs, and W. Y. Lee. Organic nanocomposite structure tailored by controlling droplet coalescence during inkjet printing. ACS Appl. Mater. Interfaces, 4:4691–4699, 2012. http://pubs.acs.org/doi/abs/10.1021/am301050n.

[10] M. Fricke and K. Sundmacher. Emulsion-assisted nanoparticle precipitation: Time scale analysis and dynamic simulation. Industrial and Engineering Chemistry Research, 51:1579–1591, 2012. http://pubs.acs.org/doi/abs/10.1021/ie2006164.

[11] C. Andrieu, D. A. Beysens, V. S. Nikolayev, and Y. Pomeau. Coalescence of sessile drops. Journal of Fluid Mechanics, 453:428–438, 2003. http://journals.cambridge.org/action/displayAbstract?fromPage=online&aid=99037&fileId=S0022112001007121.

[12] F Blanchette. Simulation of mixing within drops due to surface tension variations. Physical Review Letter, 105:074501, 2010. http://journals.aps.org/prl/abstract/10.1103/PhysRevLett.105.074501.

[13] C. T. Bartlett, G. A. Genero, and J. C. Bird. Coalescence and break-up of nearly inviscid conical droplets. Journal of Fluid Mechanics, 763:369–385, 2015. http://journals.cambridge.org/action/displayAbstract?fromPage=online&aid=9478823&fileId=S0022112014006648.

[14] W. D. Ristenpart, P. M. M Calla, R. V. Roy, and H. A. Stone. Coalescence of spreading droplets on a wettable substrate. Physical Review Letters, 97:064501, 2006. http://journals.aps.org/prl/abstract/10.1103/PhysRevLett.97.064501.

[15] M. Sellier and E. Trelluyer. Modelling the coalescence of sessile droplets. Biomicrofluidics, 3:022412, 2009. http://www.ncbi.nlm.nih.gov/pmc/articles/PMC2717581/.

[16] S. Karpitschka and H. Riegler. Quantitative experimental study on the transition between fast and delayed coalescence of sessile droplets with different but completely miscible liquids. Langmuir, 14:11823—11829, 2010. http://pubs.acs.org/doi/abs/10.1021/la1007457.

[17] S. Karpitschka and H. Riegler. Noncoalescence of sessile drops from different but miscible liquids: hydrodynamic analysis of the twin drop contour as a self-stabilizing traveling wave. Physical Review Letter, 109:066103, 2012. http://journals.aps.org/prl/abstract/10.1103/PhysRevLett.109.066103.

[18] S. Karpitschka and H. Riegler. Sharp transition between coalescence and non-coalescence of sessile drops. Journal of Fluid Mechanics, 743:

R1, 2014. http://journals.cambridge.org/action/displayAbstract?fromPage=online&aid=9191603&fileId=S0022112014000731.

[19] H. Riegler and P. Lazar. Delayed coalescence behavior of droplets with completely miscible liquids. Langmuir, 24(13):6395–6398, 2008. http://pubs.acs.org/doi/abs/10.1021/la800630w.

[20] S. Karpitschka, C. Hanske, A. Fery, and H. Riegler. Coalescence and noncoalescence of sessile drops: Impact of surface forces. Langmuir, 30:6826–6830, 2014. http://pubs.acs.org/doi/abs/10.1021/la500459v.

[21] H. Cölfen and M. Antonietti. Mesocrystals and Nonclassical Crystallization. John Wiley Sons, 2008.

[22] M. Fricke and D. Volkmer. Biomineralization I: Crystallization and Self-Organization Process, chapter 1, pages 4–6. Springer, 2007. http://www.springer.com/br/book/9783540463795.

[23] M. Volmer and A Weber. Nucleation in supersaturated products. Zeitschrift von Physikalische Chemie, 119:277–301, 1926.

[24] R. Becker and W. Döring. Kinetische behandlung der keimbildung in übersättigen dämpfen. Annalen der Physik, 24:719–752, 1935. http://onlinelibrary.wiley.com/doi/10.1002/andp.19354160806/abstract.

[25] J. Gibbs. On the equilibrium of heterogeneous substances, part i. Transactions of the Connecticutt Academy, 108:197–224, 1876. http://onlinelibrary.wiley.com/doi/10.1002/andp.19344130502/abstract.

[26] J. Gibbs. On the equilibrium of heterogeneous substances, part ii. Transactions of the Connecticutt Academy, 108:343–524, 1877.

[27] D. Gebauer, M. Kellermeier, J. D. Gale, L. Bergström, and H. Cölfen. Pre-nucleation clusters as solute precursors in crystallisation. The Royal Society of Chemistry, 43:2348–2371, 2014. http://pubs.rsc.org/en/content/articlelanding/2014/cs/c3cs60451a#!divAbstract.

[28] I. V. Markov. Crystal Growth For Beginners. World Scientific, 1995. http://www.worldscientific.com/worldscibooks/10.1142/5172.

[29] A. Berthoud. Formation of crystal faces. Journal of Chemical Physics, 10:624–635, 1912.

[30] J.J.P. Valeton. Viii. wachstum und auflösung der kristalle i. Zeitschrift für Kristallographie-Crystalline Materials, 59(1):135–169, 1923. http://www.degruyter.com/dg/viewarticle/j$002fzkri.1923.59.issue-1-6$002fzkri.1923.59.1.135$002fzkri.1923.59.1.135.xml.

[31] W. Kossel. Zur energetik von oberflächenvorgängen. Annalen der Physik, 21: 457–480, 1934.

[32] S. Veesler, F. Puel, and G. Fevotte. Polymorphism in processes of crystallisation in solution. STP Pharma pratiques, 13:1–29, 2003. http://sysweb.cinam.univ-mrs.fr/pro_perso/veesler/pdf/veesler.pdf.

[33] D. Larcher, G. Sudant, R. Patrice, and J.-M. Tarascon. Some insights on the use of polyols-based metal alkoxides powders as precursors for tailored metal-oxides particles. Chemical Materials, 15:3543–3551, 2003. http://pubs.acs.org/doi/abs/10.1021/cm030048m.

[34] W. Z. Ostwald. Studies on formation and transformation of solid materials. Zeitschrift von Physikalische Chemie, 22:289–330, 1897.

[35] J. M. Garcia-Ruiz, S. T. Hyde, A. M. Carnerup, A. G. Christy, M. J. Van Kranendonk, and N. J. Welham. Self-assembled silica-carbonate structures and detection of ancient microfossils. Science, 302:1194–1197, 2003. http://science.sciencemag.org/content/302/5648/1194.

[36] D. Gebauer, A. Völkel, and H. Cölfen. Stable prenucleation calcium carbonate clusters. Science, 322:1819–1822, 2008. http://science.sciencemag.org/content/322/5909/1819.

[37] A. Glasner. Speculations on a new mechanism of crystal growth from aqueous solutions. Isreal Journal of Chemistry, 7:633–648, 1969. http://onlinelibrary.wiley.com/doi/10.1002/ijch.196900084/abstract.

[38] H. Cölfen and S. Mann. Higher-order organization by mesoscale self-assembly and transformation of hybrid nanostructures. Angewandte Chemie, 42:2350–2365, 2003. http://onlinelibrary.wiley.com/doi/10.1002/anie.200200562/full.

[39] B. Judat and M. Kind. Morphology and internal structutre of barium sufate - derivation of a new growth mecanism. Journal of Colloids and Interfaces Science, 269:341–353, 2004. http://www.sciencedirect.com/science/article/pii/S0021979703007331.

[40] S. Mann. Biomineralization: principles and concepts in bioinorganic material chemistry, chapter 8. Oxford University Press, 2001.

[41] J. Romann, V. Chevallier, A. Merlen, and J.C. Valmalette. Self-organized assembly of copper oxalate nanocrystals. Journal of Physical chemistry C., 113: 5068—5074, 2009. http://pubs.acs.org/doi/abs/10.1021/jp805335f.

[42] B. Judat and M. Kind. Morphology and internal structure of barium sulfate—derivation of a new growth mechanism. Journal of Colloid and Interface Science, 269:341–353, 2004. http://www.sciencedirect.com/science/article/pii/S0021979703007331.

[43] A. Xie, L. Wei, S. Wang, X. Liu, J. Zhang, and Y. Yang. Template-free hydrothermal synthesis and CO oxidation properties of flower like CeO2 nanostructures. Materials Research Bulletin, 59:18–24, 2014. http://www.sciencedirect.com/science/article/pii/S0025540814003420.

[44] H. Imai. Self-Organized Formation of Hierarchical Structures, chapter 2, pages 47–58. Springer, 2007. http://link.springer.com/chapter/10.1007/128_054.

[45] S. Kinoshita. Pattern Formations and Oscillatory Phenomena, chapter 2, pages 62–118. Elservier, 2013. http://store.elsevier.com/Pattern-Formations-and-Oscillatory-Phenomena/isbn-9780123970145/.

[46] R. E. Liesgang. Über einige eigenschaften von gallerten. Naturwissenschaftiche Wochenschrift, 11:353–362, 1896.

[47] H. K. Henisch. Growth in Gel and Liesegang Ring, chapter 3, pages 48–82. Cambridge University Press, 1988. http://ebooks.cambridge.org/ebook.jsf?bid=CBO9780511525223.

[48] T. Wang, A-N. Xu, and H. Cölfen. Formation of self-organized dynamic structure patterns of barium carbonate crystals in polymer-controlled crystallization. Angewandlte Chemie, 45:4451–4455, 2006. http://onlinelibrary.wiley.com/doi/10.1002/anie.200601038/abstract.

[49] W. Ostwald. Lehrbuch der allgemeinen chemie. Zeitschrift für anorganische Chemie, 1, 1896. http://www.worldscientific.com/doi/pdf/10.1142/9789814271585_fmatter.

[50] A. Turing. The chemical basis of morphogenesis. Philosophical Transation of the Royal Society of London B, 238:37–72, 1952. http://hopf.chem.brandeis.edu/members_content/yanglingfa/pattern/Turing/The%20Chemical%20Basis%20of%20Morphogenesis.pdf.

[51] J. A. Venables and C. J. Harland. Electron back-scattering patterns- a new technique for obtaining crystallographic information in the scanning electron microscope. Philosophical Magazine, 27:1193–1200, 1973. http://www.tandfonline.com/doi/abs/10.1080/14786437308225827#.VrqA8vl95mM.

[52] L. Rongy. Influence of Marangoni and buoyancy convection on the propagation of reaction-diffusion fronts. PhD thesis, Université Libre de Bruxelles, 2008.

[53] M. A. Budroni, L. Rongy, and A. De Wit. Dynamics due to combined buoyancy and Marangoni-driven convective flows around autocatalytic fronts. Physical Chemistry Chemical Physics, 14:14619–14629, 2012. http://pubs.rsc.org/en/content/articlelanding/cp/2012/c2cp41962a#!divAbstract.

[54] G. Borda, E. Brackx, L. Boisset, and D. Duhamet, J. andd Ode. Use of a pulsed column contactor as a continuous oxalate precipitation reactor. Nuclear Engineering and Design, 241:809–814, 2011. http://www.sciencedirect.com/science/article/pii/S0029549311000094.

[55] Villermaux J. Génie de la réaction chimique. Lavoisier, 1985.

[56] W. Kunz. Specific Ion Effects, chapter 1, pages 21–23. World Scientific, 2011. http://www.worldscientific.com/doi/pdf/10.1142/9789814271585_fmatter.

[57] T. Young. An essay on the cohession of liquids. Philosophical Transation of the Royal Society of London B, 95:65–87, 1805. http://www.jstor.org/stable/107159?seq=1#page_scan_tab_contents.

[58] R. N. Wenzel. Surface roughness and contact angle. Journal of Physicak and Colloids Chemistry, 53:1466–1467, 1949. http://pubs.acs.org/doi/abs/10.1021/j150474a015.

[59] A. B. D. Cassie and S. Baxter. Wettability of porous surfaces. Transversal Faraday Society, 40:546–551, 1944. http://pubs.rsc.org/en/content/articlepdf/1944/tf/tf9444000546.

[60] S. Karpitschka. Dynamics of Liquid Interfaces with Compositional Gradients Sessile Drop Noncoalescence and Other Effects. PhD thesis, Postdam University, 2012.

[61] J. Thomson. On certain curious motions observable at the surfaces of wine and other alcoholic liquors. Philosophical Magazine, 10:330–333, 1855. http://www.tandfonline.com/doi/abs/10.1080/14786445508641982.

[62] A. F. M. Leenaars and J. A. M. Huethorst. Marangoni drying: a new extremely clean drying process. Langmuir, 6:1701–1703, 1990. http://pubs.acs.org/doi/abs/10.1021/la00101a014.

[63] D. G. A. L. Aarts, H. N. W. Lekkerkerker, H. Guo, G. H. Wegdam, and D. Bonn. Hydrodynamics of drplet coalescence. Physical Review Letter, 95:164503, 2005. http://journals.aps.org/prl/abstract/10.1103/PhysRevLett.95.164503.

[64] J. Eggers, J. R. Lister, and H. A. Stone. Coalescence of liquid drops. Journal of Fluid Mechanics, 401:293–310, 1999. http://journals.cambridge.org/download.php?file=%2FFLM%2FFLM401%2FS002211209900662Xa.pdf&code=23f8d918ec86c0083f42f347c677729f.

[65] M. Wu, T. Cubaud, and C.M. Ho. Scaling law in liquid drop coalescence driven by surface tension. Physics of Fluid, 16:51–54, 2004. http://scitation.aip.org/content/aip/journal/pof2/16/7/10.1063/1.1756928.

[66] L. Duchemin, J. Eggers, and C. Josserand. Inviscid coalescence of droplet. J. Fluid Mech., 487:293–310, 2003. http://journals.cambridge.org/action/displayAbstract?fromPage=online&aid=162929&fileId=S0022112003004646.

[67] N; J. Cira, A. Benusiglio, and M. Prakash. Vapour-mediated sensing and motility in two-component droplets. Nature, 519:446–450, 2015. http://www.nature.com/nature/journal/v519/n7544/full/nature14272.html.

[68] J. N. Israelachvili and B. W. Mitchell, D. J. amd Ninham. Theory of self-assembly of hydrocarbon amphiphiles into micelles and bilayers. Journal of the Chemical Society-Faraday Transaction, 72:1525–1568, 1976. http://pubs.rsc.org/en/content/articlepdf/1976/F2/F29767201525.

[69] R. Zana and M. J. Eljebari. Fluorescence probing investigation of the self-association of alcohols in aqueous solution. Journal of Physical Chemistry, 97:11134–11136, 1993. http://pubs.acs.org/doi/abs/10.1021/j100144a039.

[70] R. Zana. Aqueous surfactant-alcohol systems: a review. Advances in Colloids and Interface Science, 57:1–64, 1995. http://www.sciencedirect.com/science/article/pii/000186869500235I.

[71] G. D. Smith, C. E. Donelan, and R. E. Barden. Oil-continous microemulsions composed of hexane, water and 2-propanol. Journal of Colloids and Interface Science, 60 (3):488–496, 1977. http://www.sciencedirect.com/science/article/pii/0021979777903137.

[72] B. A. Keiser, D. Varie, R. E. Barden, and S. L. Holt. Detergentless water/oil microemulsions composed of hexane, water and 2-propanol. Journal of Physical Chemistry, 83 (10):1276–1280, 1979. http://pubs.acs.org/doi/abs/10.1021/j100473a008.

[73] N. F. Borys, S. L. Holt, and R. E. Barden. Detergentless water/oil microemulsions. iii. effect of koh on phase diagramm and effect of solvent composition on base hydrolysis of esters. Journal of Colloids and Interface Science, 71 (3):526–532, 1979. http://www.sciencedirect.com/science/article/pii/0021979779903278.

[74] S. Schöttl, D. Touraud, W. Kunz, T. Zemb, and D. Horinek. Consistent definitions of "the interface" in surfactant-free micellar aggregates. Colloids and Surfaces A: Physicochemical and Engineering Aspects, 480:222–227, 2015. http://www.sciencedirect.com/science/article/pii/S0927775714008772.

[75] O. Diat, M. L. Klossek, D. Touraud, B. Deme, I. Grillo, W. Kunz, and T. Zemb. Octanol-rich and water-rich domains in dynamic equilibrium in the pre-ouzo region of ternary systems containing a hydrotrope. Journal of applied

crystallography, 46:1665–1669, 2013. http://onlinelibrary.wiley.com/doi/10.1107/S002188981302606X/abstract.

[76] S. Schöttl, J. Marcus, O. Diat, D. Touraud, W. Kunz, T. zemb, and D. Horinek. Emergence of surfactant-free micelles from ternary solutions. Chemical sscience, 5:2949–2954, 2014. http://pubs.rsc.org/en/content/articlehtml/2014/sc/c4sc00153b.

[77] V. Tchakalova, T. Zemb, and D. Benczedi. Evaporation triggered self-assembly in aqueous fragance - ethanol mixtures and its impact on fragrance performance. Colloids and Surface A: Physicochemical and Engeneering Aspects, 460: 414–421, 2014. http://www.sciencedirect.com/science/article/pii/S0927775714000430.

[78] D. Chai, H. Lee, D. Jin Im, I. S. Kang, G. Lim, D. S. Kim, and K. H. Kang. Spontaneous electrical chemical charging of droplets by conventional pipetting. Scientific Reports, 3:2037, 2013. http://www.nature.com/articles/srep02037.

[79] H. An, G. Liu, and V. Craig. Wetting of nanophases: Nanobubbles, nanodroplets and micropancakes on hydrophobic surfaces. Advances in Colloid and Interface Science, 222:9–17, 2015. http://www.sciencedirect.com/science/article/pii/S0001868614002334.

[80] Y. Rotenberg, L. Boruvka, and A.W. Neumann. Determination of surface tension and contact angle from the shapes of axisymmetric fluid interfaces. Journal of Colloid and Interface Science, 93:169–183, 1983. http://www.sciencedirect.com/science/article/pii/002197978390396X.

[81] C. W. Davies. Interpretation of activity measurements. Journal of American Ceramic Society, 34:804–805, 1938. http://pubs.rsc.org/en/content/articlepdf/1938/tf/tf9383400804.

[82] S. Lalleman, M. Bertrand, E; Plassari, C. Sorel, and P. Moisy. Determination of the bromley contributions to estimate the activity coefficient of neodymium electrolytes. Chemical Engineer Science, 77:185–189, 2012. http://www.sciencedirect.com/science/article/pii/S0009250912000978.

[83] R. T. Eiswirth, H.-J. Bart, A. A. Ganguli, and E. Y. Kenig. Experimental and numerical investigation of binary coalescence: liquid bridge building and internal flow fields. Physics of fluids, 24:062108, 2012. http://scitation.aip.org/content/aip/journal/pof2/24/6/10.1063/1.4729791.

[84] V. Lombardi, C. Adduce, G. Sciortino, and M. La Rocca. Gravity driven current during coalescence of two sessile drops. Physics of fluids, 27: 016602, 2015. http://scitation.aip.org/content/aip/journal/pof2/27/2/10.1063/1.4907725.

[85] A. S. Myerson. Handbook of Industrial Crystallization second Edition, chapter 6, pages 141–152. Boston Butterworth-Heinemann, 2002. http://www.sciencedirect.com/science/book/9780750670128.

[86] A-P. Hyvärinen, H. Lihavainen, A. Gaman, L. Vairila, H. Ojala, M. Kulmala, and Y. Viisanen. Surface tensions and densities of oxalic, malonic, succininc, maleic, malic and cis-pionic acids. Journal of Chemical and Engineering Data, 51:255–260, 2006. http://pubs.acs.org/doi/abs/10.1021/je050366x.

[87] F. Lieblig. Master thesis. PhD thesis, University Potsdam, 2014.

[88] M. Jehannin, S. Karpitschka, S. Charton, T. Zemb, H. Möhwald, and H. Riegler. Periodic precipitation patterns during coalescence of reacting sessile droplets. Langmuir, 31:11484—11490, 2015. http://pubs.acs.org/doi/abs/10.1021/acs.langmuir.5b02482.

[89] E. M. Nicola, M. Or-Guil, W. Wolf, and Bär M. Drifting pattern domains in a reaction-diffusion system with nonlocal coupling. Physical Review E, 65: 055101, 2002. http://journals.aps.org/pre/pdf/10.1103/PhysRevE.65.055101.

[90] R. K. Pai, K. Jansson, and N. Hedin. Transport-mediated control of particles of calcium carbonate. Crystal Growth and Design, 9:4581–4583, 2009. http://pubs.acs.org/doi/abs/10.1021/cg900009j.

[91] J. Romann, V. Chevallier, A. Merlen, and J-C. Valmette. Self-organized assembly of copper oxalate nanocrystals. Journal of Physical Chemistry C., 113:5068–5074, 2009. http://pubs.acs.org/doi/abs/10.1021/jp805335f.

[92] J. Romann, J-C. Valmette, V. Chevallier, and A. Merlen. Surface interactions between molecules and nanocrystrals in copper oxalate nanostructures. Journal of Physical Chemistry C., 114:10677–10682, 2010. http://pubs.acs.org/doi/abs/10.1021/jp9082344.

[93] National Bureau of Stadards (US). Monography 25, Volume 13, p. 35, 1976.

[94] W. Ollendorf and F. Weigel. The crystal structure of some lanthanide oxalate decahydrates, ln2(c2o4)3·10h2o, with ln = la, ce, pr, and nd. Inorganic Nuclear Chemistry Letters, 5:263–269, 1969. http://www.sciencedirect.com/science/article/pii/0020165069801960.

[95] M. V. John and M. A. Ittyachen. Studies on Ce2(C2O4)3.nH2O crystals grown in hydro-silica gel. Bulletin of Materials Science, 21(5):387–391, 1998. http://link.springer.com/article/10.1007%2FBF02744923.

[96] L. Liu, W.and Feng, C. Zhang, H. Yang, J. Guo, X. Liu, X. Zhang, and Y. Yang. A facile hydrothermal synthesis of 3D flowerlike CeO2 via a cerium oxalate precursor. Journal of Material Chemistry A, 1:6942–6948, 2013. http://pubs.rsc.org/en/content/articlehtml/2013/ta/c3ta10487g.

[97] J. Wei, Z. Yang, H. Yang, T. Sun, and Y. Yang. A mild solution strategy for the synthesis of mesoporous CeO2 nanoflowers derived from Ce(HCOO)3. CrystEngComm, 13:4950–4955, 2011. http://pubs.rsc.org/en/content/articlehtml/2011/ce/c1ce05324h.

[98] L-S. Zong, J-S. Hu, A-M. Cao, Q. Liu, W-G. Song, and L-J. Wan. 3D flowerlike ceria micro/nanocomposite structure and its application for water treatment and CO removal. Chemical Materials, 19:1648–1655, 2007. http://pubs.acs.org/doi/abs/10.1021/cm062471b.

[99] M. Morvan, D. Espinat, J. Lambard, and T. Zemb. Ultrasmall- and small-angle x-ray scattering of smectite clay suspensions. Colloids and Surface A: Phisicochemical and Engineering Aspects, 93:193–203, 2003. http://www.sciencedirect.com/science/article/pii/092777579302656Y.

[100] S.E. Friberg, H. Hasinovic, Q. Yin, Z. Zhang, and R. Patel. The system water–ethanol–didodecyldimethylammonium bromide. phase equilibria and vapor pressures. Colloids and Surface A: Physicochemical and Engeneering Aspects, 15:145–156, 1999. http://www.sciencedirect.com/science/article/pii/S0927775799000667.

[101] A. Arce, A. Blanco, P. Souza, and I. Vidal. Liquid-liquid equilibria of water + methanol+ 1-octanol and water + ethanol + 1-octanol at various temperature. Journal of Chemical Engeneering Data, 39:378–380, 1994. http://pubs.acs.org/doi/abs/10.1021/je00014a042.

[102] A. Arce, J. Martinez-Ageitos, and A. Soto. Vle for water + ethanol +1-octanol mixtures. experimental measurments and correlation. Fluid Phase Equilibrium, 122:117–129, 1996. http://www.sciencedirect.com/science/article/pii/0378381296030415.

[103] N. Bodor, Z. Gabanyi, and C.-K. Wong. A new method for the estimation of partition coefficient. Journal of American Chemical Society, 111:3783–3786, 1989. http://pubs.acs.org/doi/abs/10.1021/ja00193a003.

[104] Y. L. Khmelnitsky, R. Hilhorst, and C. Veeger. Detergentless microemulsions as media for enzymatic reactions. European Journal of Biochemistry, 176:265–271, 1988. http://pubs.acs.org/doi/abs/10.1021/j100339a065.